INFORMATION TO USERS

This material was produced from a microfilm copy of the original document. While the most advanced technological means to photograph and reproduce this document have been used, the quality is heavily dependent upon the quality of the original submitted.

The following explanation of techniques is provided to help you understand markings or patterns which may appear on this reproduction.

1. The sign or "target" for pages apparently lacking from the document photographed is "Missing Page(s)". If it was possible to obtain the missing page(s) or section, they are spliced into the film along with adjacent pages. This may have necessitated cutting thru an image and duplicating adjacent pages to insure you complete continuity.

2. When an image on the film is obliterated with a large round black mark, it is an indication that the photographer suspected that the copy may have moved during exposure and thus cause a blurred image. You will find a good image of the page in the adjacent frame.

3. When a map, drawing or chart, etc., was part of the material being photographed the photographer followed a definite method in "sectioning" the material. It is customary to begin photoing at the upper left hand corner of a large sheet and to continue photoing from left to right in equal sections with a small overlap. If necessary, sectioning is continued again — beginning below the first row and continuing on until complete.

4. The majority of users indicate that the textual content is of greatest value, however, a somewhat higher quality reproduction could be made from "photographs" if essential to the understanding of the dissertation. Silver prints of "photographs" may be ordered at additional charge by writing the Order Department, giving the catalog number, title, author and specific pages you wish reproduced.

5. PLEASE NOTE: Some pages may have indistinct print. Filmed as received.

Xerox University Microfilms
300 North Zeeb Road
Ann Arbor, Michigan 48106

76-19,220

PRATHUANGSIT, Dhavajjai, 1950-
INELASTIC HYSTERESIS BEHAVIOR OF AXIALLY LOADED STEEL MEMBERS WITH ROTATIONAL END RESTRAINTS.

The University of Michigan, Ph.D., 1976
Engineering, civil

Xerox University Microfilms, Ann Arbor, Michigan 48106

INELASTIC HYSTERESIS BEHAVIOR OF AXIALLY LOADED STEEL MEMBERS WITH ROTATIONAL END RESTRAINTS

by

Dhavajjai Prathuangsit

A dissertation submitted in partial fulfillment
of the requirements for the degree of
Doctor of Philosophy
(Civil Engineering)
in The University of Michigan
1976

Doctoral Committee:

Associate Professor Subhash C. Goel, Co-Chairman
Professor Robert D. Hanson, Co-Chairman
Professor William J. Anderson
Associate Professor Movses J. Kaldjian
Professor Ivor K. McIvor

ACKNOWLEDGEMENTS

The author wishes to express his deepest gratitude to Professors Subhash C. Goel and Robert D. Hanson, Co-Chairmen of his doctoral committee for their invaluable guidance, assistance, and encouragement throughout the discourse of this dissertation. The author also wishes to express his indebtedness to all other members of his doctoral committee for their interest and assistance.

This dissertation is part of a research project sponsored by the National Science Foundation through Grant NSF-AEN7400930 which is directed by Professor Goel. The author was also the recipient of a Rackham Predoctoral Fellowship from The University of Michigan during the course of this research. The financial support from both institutes is sincerely appreciated.

Mr. Mark Butterfield assisted in drawing the graphs.

TABLE OF CONTENTS

		Page
ACKNOWLEDGEMENTS		ii
LIST OF TABLES		vii
LIST OF FIGURES		viii
NOTATION		xii
CHAPTER		
I.	INTRODUCTION	1
II.	ANALYTICAL SOLUTION	9
2.1	Initial Imperfection in the Form of Initial Plastic Rotation Angles	11
2.2	Physical Behavior of the Member Under Cyclic Loading	19
2.3	Model 1: Hysteresis Behavior with Exact Expression for Curvature	24
2.4	Model 2: Hysteresis Behavior with Approximate Expression for Curvature	25
2.5	Method of Solution for Model 2	30
2.6	Special Cases and Some Significant Properties of the Hysteresis Behavior	32
III.	PARAMETRIC STUDY	36
3.1	Influence of the Connection Flexural Strength	39
3.2	Influence of the Connection Flexural Stiffness	50
3.3	Influence of the Member Slenderness Ratio (L/r)	54
3.4	Influence of the Member Cross-Sectional Properties	63

TABLE OF CONTENTS (continued)

		Page
3.5	Influence of Simultaneous Variation of Several Parameters	66
3.6	Conclusions	71
IV.	SEMI-GRAPHICAL CONSTRUCTION OF THE HYSTERESIS CURVES	72
4.1	The Member with Balanced Strength Connections	75
4.1.1.	The Balanced Strength Ratio	75
4.1.2.	The Maximum Compressive Load	77
4.1.3.	The Double Plastic Rotation Region	78
4.1.4.	Slope of the E-Region Curve	80
4.1.5.	Construction of the Hysteresis Curve of a Member with Balanced Strength Connections	81
4.2	The Member with Smaller than Balanced Strength Connections	91
4.2.1.	The Compressive Load at the Occurrence of the First and the Second Plastification Along the Compression Envelope Curve	91
4.2.2.	The Slope and Length of the E-Region Curve	94
4.2.3.	The Slope of the Tension Induced Single Plastic Rotation Region	97
4.2.4.	Physical Constraints of the CIP Region Reversing from the TIP Region	99
4.2.5.	Construction of the Hysteresis Curve for the Member with Smaller than Balanced Strength Connections	101
4.3.	The Member with Greater than Balanced Strength Connections	108

TABLE OF CONTENTS (continued)

Page

4.3.1. The Compressive Load at the Occurrence of the First and the Second Plastification along the Compression Envelope Curve 108

4.3.2. The Slope and the Length of the E Region 109

4.3.3. The Tension Induced Single Plastic Rotation Region 109

4.3.4. Physical Constraints of the CIP Region Reversing from the TIP Region 111

4.3.5. Construction of the Hysteresis Curves for the Members with Greater than Balanced Strength Connections 111

4.4 Conclusions 115

V. APPLICATIONS OF RESULTS 119

5.1. Compressive Load Capacity 120

5.2. Member Energy Dissipation 124

5.3. Angles of Rotation at Midspan and at the Ends 132

5.4. Conclusions 136

VI. SUMMARY AND CONCLUSIONS 138

APPENDIX A - MODEL 1: HYSTERESIS BEHAVIOR WITH EXACT EXPRESSION FOR CURVATURE 143

A.1. Compressive Loading 144

A.1.1. Case I: - Inflection Point Within the Member Length 146

A.1.2. Case II: - Inflection Point Outside the Member Length 152

A.2. Zero Load Configuration 156

A.3. Tensile Loading 158

TABLE OF CONTENTS (concluded)

		Page
A.3.1.	Case I: - No Inflection Point	160
A.3.2.	Case II: - Inflection Point Outside the Member Length	162
A.3.3.	Case III: - Inflection Point Within the Member Length	166
A.4.	Other Possible Equilibrium Configurations	170
REFERENCES		174

LIST OF TABLES

Table	Title	Page
3.1	Properties of Members	40-41
3.2	Properties of Wide Flange Cross Sections	42
4.1	Properties of Members	74

LIST OF FIGURES

Figure	Title	Page
2.1	Member with End Restraints	10
2.2	Member with Initial Imperfection	12
2.3	Axial Load-Centerline Deflection for a Column with kL/r = 90	14
2.4	Axial Load-Centerline Deflection for a Column with kL/r = 54	15
2.5	Comparison of the Maximum Compressive Load	18
2.6	Typical Normalized Axial Load-Axial Displacement Hysteresis Loop	20
2.7	Member Equilibrium Configuration Under the Applied Load	21-22
2.8	Half Member Under the Applied Load	26
3.1	Influence of Connection Flexural Strength on the Hysteresis Behavior	44
3.2	Influence of Connection Flexural Strength on the Hysteresis Behavior	48
3.3	Influence of Connection Flexural Stiffness on the Hysteresis Behavior	51
3.4	Influence of Connection Flexural Stiffness on the Hysteresis Behavior	52
3.5	Influence of Slenderness Ratio on the Hysteresis Behavior	55
3.6	Influence of Slenderness Ratio on the Hysteresis Behavior	56
3.7	Comparison of the DP regions of Pin-Ended Members with Different L/r	58
3.8	Drop in Compressive Load and Rate of Change of AISC Plastic Design Column Strength	61
3.9	Influence of Cross-Sectional Properties on the Hysteresis Behavior	64

LIST OF FIGURES (continued)

Figure	Title	Page
3.10	Influence of Axis of Bending on the Hysteresis Behavior	67
3.11	Influence of Effective Slenderness Ratio on the Hysteresis Behavior	69
3.12	Influence of Effective Slenderness Ratio on the Hysteresis Behavior	70
4.1	Balanced Strength Ratio for Various Member Slenderness Ratios	76
4.2a	Slope of the Elastic Region on the Compression Side of the Normalized Hysteresis Loop	82
4.2b	Slope of the Elastic Region on the Tension Side of the Normalized Hysteresis Loop	83
4.3	Hysteresis Curve for a Member with Balanced Strength Connections Using Semi-Graphical Construction	85
4.4	The Initial Elastic Region	86
4.5	Comparison of the Graphical and the Analytical Hysteresis Curves for L/r = 60	89
4.6	Comparison of the Graphical and the Analytical Hysteresis Curves for L/r = 200	90
4.7	Compressive Load at the Occurrence of the Connection Plastic Hinges on the Envelope Curve	93
4.8	Compressive Load at the Occurrence of the Midspan Plastic Hinge at the End of the Envelope CISP Region	95
4.9	Physical Constraints of the Hysteresis Curve of a Member with Smaller than Balanced Strength Connections	100
4.10	Hysteresis Curve for a Member with Smaller than Balanced Strength Connections Using Semi-Graphical Construction	102

LIST OF FIGURES (continued)

Figure	Title	Page
4.11	Comparison of the Graphical and the Analytical Hysteresis Curves for L/r = 60	106
4.12	Comparison of the Graphical and the Analytical Hysteresis Curves for L/r = 200	107
4.13	Hysteresis Curve for a Member with Greater than Balanced Strength Connections Using Semi-Graphical Construction	112
4.14	Comparison of the Graphical and the Analytical Hysteresis Curves for L/r = 60	116
4.15	Comparison of the Graphical and the Analytical Hysteresis Curves for L/r = 200	117
5.1	Normalized Compressive Load Capacity of W 8x31 Members with L/r = 60	121
5.2	Normalized Compressive Load Capacity of W 8x31 Members with L/r = 200	122
5.3	Normalized Dissipated Energy of W 8x31 Members with L/r = 60	125
5.4	Normalized Dissipated Energy of W 8x31 Members with L/r = 200	126
5.5	Dissipated Energy of the Hysteresis Loop for $\Delta/\Delta_y = 5.0$	127
5.6	Comparisons of the Normalized Dissipated Energy	129
5.7	Dissipated Energy for W 8x31 Pin-Ended Members	131
5.8	Angles of Rotation at the Ends of W 8x31 Members at $\Delta/\Delta_y = 12.0$	133
5.9	Angles of Rotation at Midspan of W 8x31 Members at $\Delta/\Delta_y = 12.0$	134

LIST OF FIGURES (concluded)

Figure	Title	Page
A.1	Member Subjected to Compressive Loading	145
A.2	Half Member with Inflection Point Outside Its Length	154
A.3	Zero Load Configuration of the Half Member	157
A.4	Member Subjected to Tensile Loading	159
A.5	Half Member with Inflection Point Outside Its Length	163
A.6	Half Member with Inflection Point Within Its Length	167
A.7	Additional Member Equilibrium Configurations	171
A.8	Equilibrium Configurations of the Member with Connections that Have Smaller Flexural Strength than the Member	172

NOTATION

A	Cross-sectional area
A_w	Cross-sectional area of the web
C_c	Limiting effective slenderness ratio defined by equation (2.1e)
E	Young's modulus of elasticity
$E(\ )$	Complete elliptic integral of the second kind
$E(\ ,\ )$	Elliptic integral of the second kind
$F(\ )$	Complete elliptic integral of the first kind
$F(\ ,\ )$	Elliptic integral of the first kind
I	Moment of inertia
K	Axial load factor
L	Member length
M	Bending moment at a cross section
M_p	Plastic moment
M_{pc}	Plastic moment modified by the axial force, equation (2.10)
M_{pcc}	Modified plastic moment of the connection
M_{pcm}	Modified plastic moment of the member
M_1	Bending moment at the member end
M_2	Bending moment at midspan
P	Applied axial force
P_{cr}	Theoretical buckling load of a perfect member, equation (3.1)
P_{max}	Compressive load capacity, equation (2.1a)
P_{rl}	Approximate compressive load at the occurrence of plastic hinges at the connections, equations (4.3a and b)

P_{r2}	Approximate compressive load at the occurrence of plastic hinge at midspan, equation (4.4)
P_y	Axial yield load
$\overline{P}$	Absolute difference between the load at the occurrence of the midspan plastic hinge and the load on the tension envelope curve at the same Δ/Δ_y
R	Ratio of the connection flexural strength to the member flexural strength
R_b	Ratio of the balanced connection flexural strength to the member flexural strength
S	Deformed member length
T	Applied axial tensile force
U	Parameter, equation (3.3)
V	Parameter, equation (3.3)
X_m	Half distance between supports
Y_m	Lateral deflection at midspan
Y_β	Lateral deflection at the inflection point
Z	Plastic section modulus
a	Stiffness coefficient, equations (2.2 and 2.3)
b	Stiffness coefficient, equations (2.2 and 2.3)
b_f	Width of the flange
c	Distance from neutral axis to the extreme fiber in compression
c_1	Length coefficient used for semi-graphical construction, equation (4.5b)
c_2	Length coefficient used for semi-graphical construction, equation (4.5c)
c_3	Length coefficient used for semi-graphical construction, equation (4.5d)

d	Depth of the cross section
d_1	Length coefficient used for semi-graphical construction, equation (4.6b)
d_2	Length coefficient used for semi-graphical construction, equation (4.6c)
e	Initial eccentricity
k	Effective length coefficient
k_Θ	Rotational stiffness of the end spring
ℓ	Deformed half-member length
ℓ_c	Length of the elastic post-compression induced plastic rotation region of the normalized hysteresis curve, equation (4.5a)
ℓ_t	Length of the elastic post-tension induced plastic rotation region of the normalized hysteresis curve, equation (4.6a)
r	Radius of gyration
s	Deformed length coordinate
t_f	Thickness of the flange
t_w	Thickness of the web
x	Coordinate in orthogonal coordinate system
y	Coordinate in orthogonal coordinate system
Δ	Relative end displacement
Δ_y	Axial yield deformation
$\overline{\Delta}$	Distance along the Δ axis of the hysteresis curve between the points of plastification at midspan and at the ends
Θ	Angle between the tangent of the elastic curve and a line through the member ends
Θ_e	Elastic rotation angle at the end

NOTATION (concluded)

Θ_p	Initial plastic rotation angles
Θ_0	Angle between the tangent at the member end and a line through the member ends
Θ_1	Angle between the tangent at the member end and the chord of the deformed half member
Θ_2	Angle between the tangent at the member midspan and the chord of the deformed half member
Θ_{1p}	Plastic rotation angle at the end
Θ_{2p}	Plastic rotation angle at midspan
ϕ	Curvature
α	Axial load factor used for defining a and b
β	Angle between the tangent at the inflection point and a line through the member ends
μ	Connection parameter defined by equation (3.1), $\mu k = \frac{\pi}{2}$
ξ	Variable of integration
ρ	Variable of integration
σ_a	Allowable compressive stress, equation (2.1b)
σ_{max}	Maximum compressive stress, equation (2.1c)
σ_y	Yield stress
ϕ	Variable of integration

CHAPTER I

INTRODUCTION

In 1956 Housner[1] introduced the concept of inelastic design of structures subjected to seismic excitation and demonstrated the ability of structures to dissipate energy through inelastic hysteretic deformation. Since then there have been many studies concerned with the inelastic dynamic response of structures[2-10]. In these studies, idealizations of the hysteresis behavior of structural members have been employed. In the late 1950's Berg[2], Newmark[3], and Penzien[4] employed the elasto-plastic type hysteretic model for the inelastic behavior. This was followed by the utilization of the bilinear hysteretic model by Iwan[5], Clough[6], and Giberson[7], and of the curvilinear (Ramberg-Osgood) hysteretic model by Jennings[8], Kaldjian and Fan[9], and Goel[10]. Most of these studies involved typical unbraced, moment-resisting type structures.

Different forms of framing for high-rise structures have been accepted for earthquake-resistant design including braced frames which can provide greater lateral stiffness than moment-frame structures. In spite of their widespread use, few inelastic studies have been made of the braced-frame structures due to the lack of knowledge

regarding the hysteresis behavior of the bracing members. Hanson and Fan[11], Workman[12], and Goel and Hanson[13] used the elasto-plastic behavior in tension only for bracing members. This approximation is justified only for the bracing members with large slenderness ratios since their compressive-load-capability is neglected entirely.

Experimental studies[14-17] have demonstrated that steel structural members subjected to reversed cyclic-bending exhibit stable hysteresis loops of curvilinear form. So they can be satisfactorily modeled by a Ramberg-Osgood, bilinear, or more simply an elasto-plastic form in moment-curvature terms. For slender members subjected to primarily axial forces, especially the bracing members in a frame, the hysteresis behavior can be anticipated to be different owing to the strong interaction of axial forces and the post-buckling deformations. Many studies[18-28] have been conducted to determine the ultimate strength of axially loaded pin-ended columns as well as the ultimate strength and rotational capacity of members subjected to uniaxial and biaxial bending in the presence of large axial compressive forces. These studies utilized one-directional loading without consideration of reversed cyclic loading.

Recent available information concerning the hysteresis behavior of axially loaded members subjected to reversed axial forces is limited to theoretical and experimental studies at the University of Michigan and in

Japan. Higginbotham and Hanson[29] and Nilforoushan[30] obtained analytical hysteresis behavior of such a member by utilizing the elasto-plastic moment-curvature relationships with the fully plastic moment modified in the presence of axial force. The end conditions were assumed to be ideally-pinned, fully-fixed, or fixed-free, and the members were assumed to buckle elastically at Euler load. Higginbotham and Hanson's theoretical study[29] was verified with small scale experiments by Kahn and Hanson[31]. In Japan, a number of analytical and experimental studies of inelastic hysteresis behavior of axially loaded members[32-39] have been conducted. In most of these analytical studies, the significant assumptions were essentially the same as those used by Higginbotham and Hanson[29] and Nilforoushan[30].

Recently Shibata[39] studied the effect of the "length of plastic hinge" in an axially loaded pin-ended member. He divided the central region of the member which is expected to plastify during post-buckling behavior into several layers. Each layer was given elasto-plastic stress-strain material characteristics. This model produced a curvilinear moment-curvature relationship modified due to the presence of axial force. This model predicts the net change in column length which is the residual plastic deformation of the member subjected to inelastic post-buckling deformations. This phenomenon was observed in experimental studies[31, 36].

In these previous analytical studies of the hysteresis behavior of axially loaded members, the members are assumed to become unstable when the compressive load reaches either the Euler buckling load or the compression yield load. The end conditions are also assumed to be ideally-pinned, fully-fixed, or fixed-free. It is evident the realistic so-called axial-force-carrying members do not resist load in an ideal axial action. Such members which are mainly the bracing members in buildings and the truss members always have some bending action. This action arises because the members are not ideally pin-connected to the joints or other members. The flexural rigidity at the member ends provides the secondary load-resisting mechanism in bending which accounts for some share of the load resistance. Available studies[40-42] of trusses with rigid connections neglecting the interaction between the axial and bending effects have revealed that the maximum bending stress is generally less than 25 percent of the axial stress. The secondary stress may become very large when many stocky bars are connected at any one joint of the truss.

In addition to the restrained rotation, typical primarily axial-force-carrying members such as bracing members may also exhibit a transitional load-deflection characteristic due to imperfections in member straightness and axial load application. Proper consideration of these effects must be included in the analysis in order to

develop a thorough understanding of the hysteresis behavior of such members. Only with this knowledge a more reliable dynamic analysis as well as a more economical dynamic design of framed structures can be ensured.

To directly analyze the behavior of the bracing members in a real structure subjected to arbitrary combined cyclic bending and axial forces will be extremely complicated, if not impossible. However, for a bracing member that is connected to stiff joints, the rotation of the connections can be large compared with the rotation of the joints. In such cases if the joints are fixed or their rotation can be neglected, it is possible to model the rotational end restraints of a member due to the flexural rigidity of the connections by the rotational end springs. Hence, the physical model used in this dissertation is the axially loaded steel member with rotational end springs. The springs develop end moments which are directly proportional to the end rotation angles and in opposite direction to the rotation. The moment and end rotation angle can be viewed as the moment and rotation of the connection. The springs are also assumed to be symmetric since the connections of a bracing member are practically similar at both ends. The rotational end springs may also be used to simulate the rotational end restraints of an axially loaded member due to other connected members in a real structure.

The theoretical development of the inelastic

hysteresis behavior of this physical model is presented in Chapter II. The analytical solution for the member equilibrium configuration under the applied load using the exact expression for curvature and using the plastic hinge concept taking into account the axial force effect (referred to as Model 1) involves elliptic integrals of the first and second kinds. The resulting equations can be solved only by iterative procedures. Owing to the many sets of governing equations and to the iterative procedure required to solve each set of equations, it is impractical to use this solution for a complete study of the member behavior. Consequently, the complete governing equations and the corresponding methods of solution were not developed for all stages of member behavior.

An alternative solution (referred to as Model 2) is developed by utilizing an approximate expression for curvature as well as approximations in the geometry of the deformed member. The resulting equations possess a closed-form solution which is excellently suitable for the succeeding parametric study. In both models, initial imperfections of the member were introduced as plastic rotation angles at midspan and at the ends to simulate the effects of initial crookedness, residual stresses, and eccentricity of the applied load of a real member. Also a correlation of each branch of the hysteresis curve with the member physical behavior is presented in Chapter II.

Chapter III consists of the parametric study of the

hysteresis behavior. The parameters of interest are the connection flexural strength, the connection flexual stiffness, the member slenderness ratio, and the member cross-sectional properties. The concept of the balanced connection strength, which is defined as the connection flexural strength that causes plastic hinges to occur simultaneously at midspan and at the ends, is introduced. The member with balanced strength connections has several desirable characteristics as described throughout this dissertation.

The information obtained in Chapter III is used to develop a procedure for a semi-graphical construction of the hysteresis curves as described in Chapter IV. This method provides a simple means for obtaining an approximate member hysteresis curve. The various graphs and charts as well as equations presented in Chapter IV can be used to evaluate the influences of different parameters both qualitatively and quantitatively. The members are sub-divided according to their connection flexural strengths as the smaller than balanced strength, the balanced strength and the greater than balanced strength members for discussion of the member behavior characteristics.

Practical application of hysteresis behavior of the model used in this study is included in Chapter V. The goal is to establish member and connection properties that will optimize the compressive load capacity and the energy dissipation of the member for a given length requirement.

The significance of the balanced strength system is vividly illustrated. Also, the rotation angles at midspan and at the member ends are presented to give estimates of the flexural ductility required during a large axial displacement hysteretic cycle.

The analytical program of investigation and its results are used to advance the conclusions given in Chapter VI.

CHAPTER II

ANALYTICAL SOLUTION

In this chapter, the method of analysis of the inelastic hysteresis behavior of axially loaded steel members with general end restraints is presented. Symmetrical springs with rotational stiffness k_θ are used to represent the rotational end restraints while the variable active force is axial tension and compression. This physical model is shown in Figure 2.1. The rotational end restraints could be thought of as a property of semirigid connections or a simulation of the actual restraint due to connections with other structural members.

The significant assumptions employed in this study are:

(1) The member has an elastic-perfectly plastic stress-strain relationship which means that the member undergoes a change in length under constant axial load of magnitude equal to the yield strength.

(2) The member has an elastic-perfectly plastic moment-curvature relationship with the fully plastic moment modified to account for the axial force. This assumption is widely accepted, and it simplifies the mathematics of the solution.

(3) The member is uniform throughout its length with similar connections at both ends.

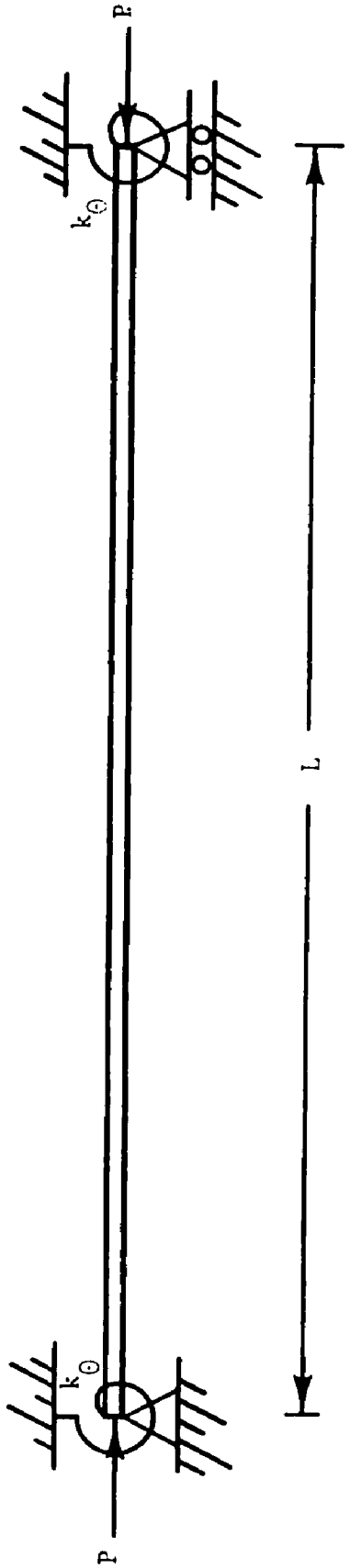


Figure 2.1 Member with End Restraints

(4) The connection (the rotational end spring) has an elastic-perfectly plastic moment-rotation relationship with the fully plastic moment modified to account for the axial force. This assumption conforms with (1) and simplifies the mathematics of the solution.

(5) The member is supported laterally along its length in such a way that no out-of-plane buckling can occur. Local buckling is also assumed not to occur within the range of deformation of the member in this study.

(6) Shear deformation is neglected since it is small compared to bending deformation for the sizes and lengths of the members used herein.

(7) Equal initial plastic rotation angles (θ_p) exist at the member midspan and at the connections as shown in Figure 2.2. The details of this initial imperfection are discussed in Section 2.1.

2.1. Initial Imperfection in the Form of Initial Plastic Rotation Angles

A mathematical member which satisfies the foregoing assumptions except assumption (7) and which is initially perfectly straight and free from residual stress will either buckle elastically at the theoretical buckling load or just shorten elastically until yielding occurs at the axial yield load when loaded in compression. A real member possesses some initial crookedness as well as patterns of residual stress. Due to these imperfections and due to unavoidable

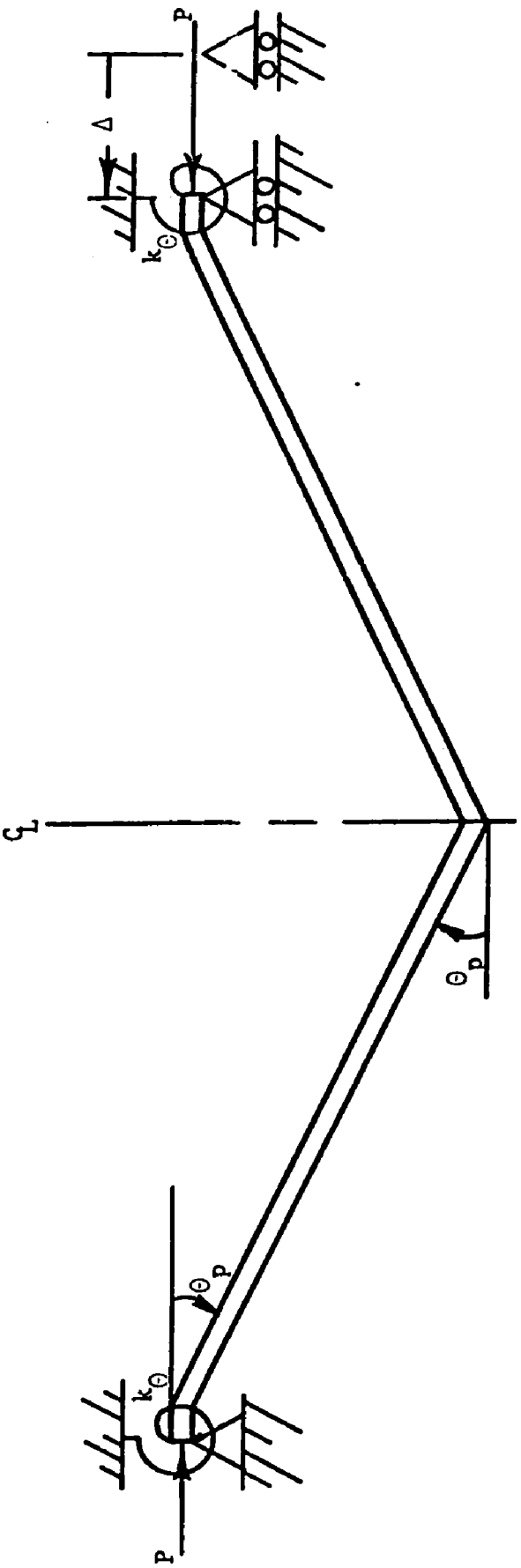


Figure 2.2 Member with Initial Imperfection

eccentricity of the applied load, this real member will buckle before its load reaches the theoretical buckling load. It also shows a transitional load-deflection behavior instead of instantaneous elastic buckling or compression yielding.

To account for these imperfections, equal initial plastic rotation angles θ_p are introduced at the connections and at the member midspan as shown in Figure 2.2. The initial plastic rotation angles are selected partly because they can be included in the method of analysis conveniently and partly because the mathematical member with these plastic rotation angles displays characteristics similar to those of a real member. It is evident from Figure 2.3 that the introduction of the initial plastic rotation angles results in a transitional load-deflection behavior which does not conform exactly with the corresponding experimental results. For a short member which mathematically does not buckle because the theoretical buckling load is higher than the member axial yield load, introduction of the initial plastic rotation angles results in the load-deflection behavior shown in Figure 2.4.

The experimental result in Figure 2.3 was taken from McFalls and Tall[20]. This 12 H 79 pin-ended member was a welded column manufactured from flame-cut plates with $L/r = 90$ (where L is the member length and r is the member radius of gyration about the axis of buckling) and with initial centerline eccentricity of 0.005 inch. The given value of the member axial yield strength σ_y from the tension coupon test was 36.7 ksi whereas no value was given for the modulus

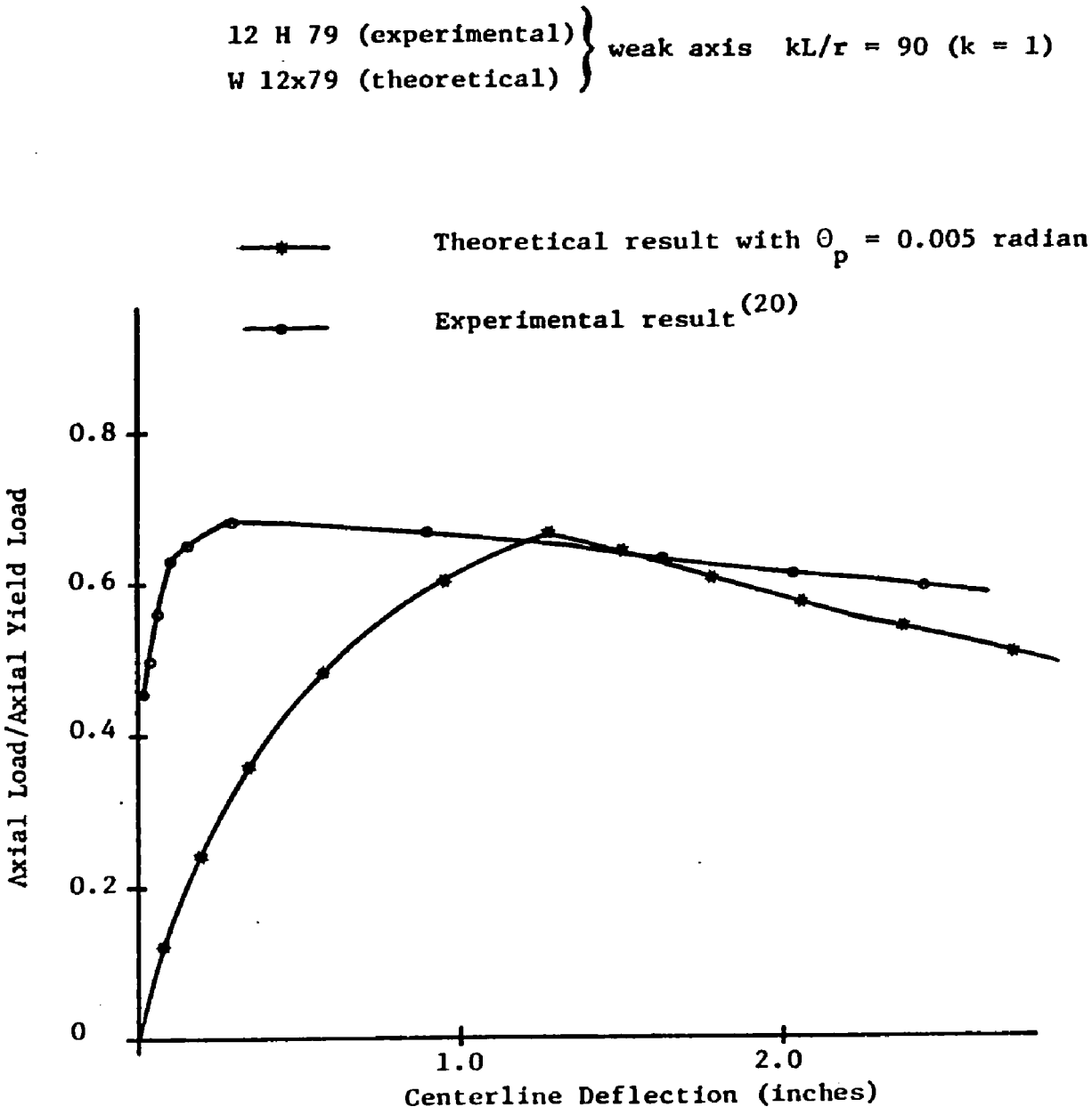


Figure 2.3 Axial Load-Centerline Deflection for a Column with kL/r = 90

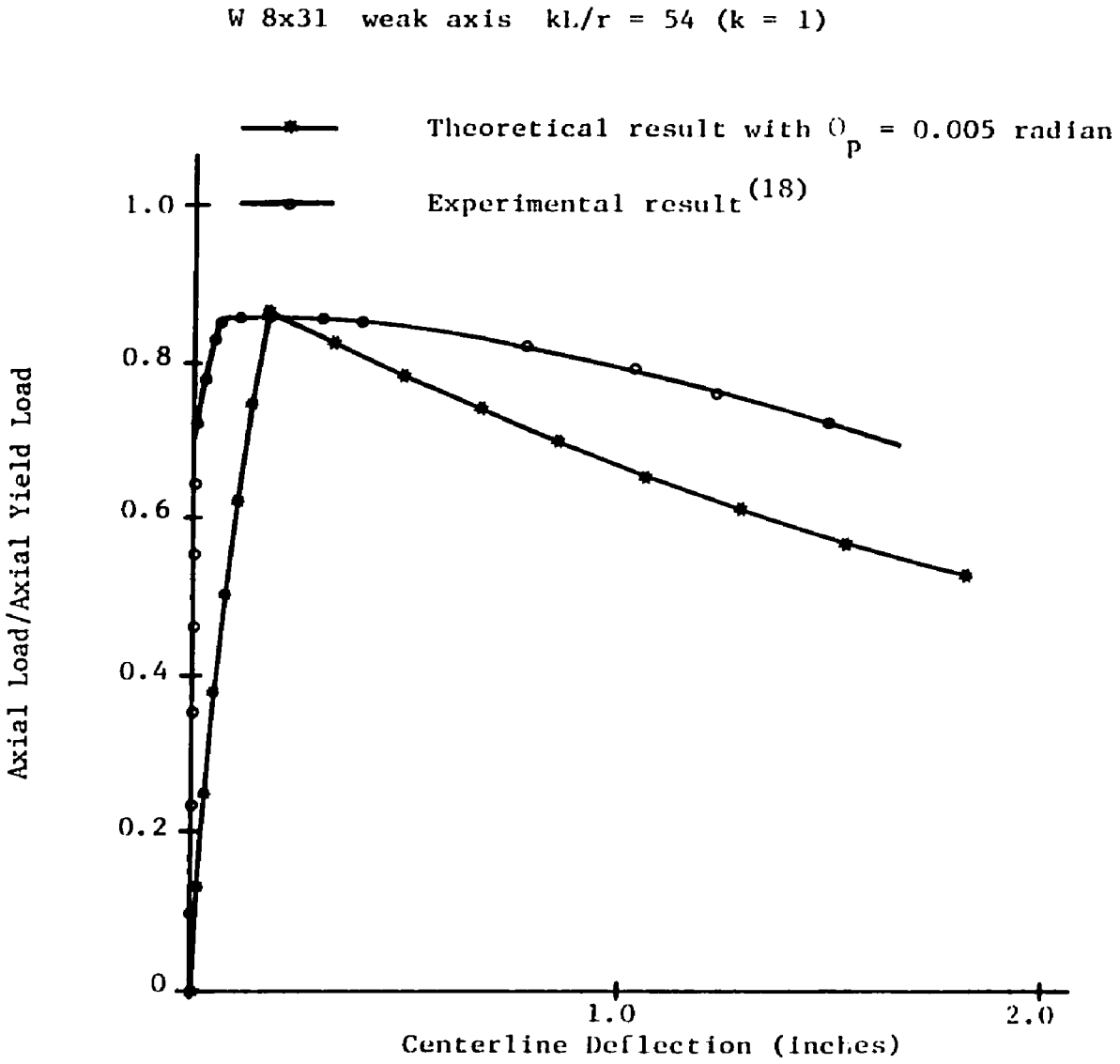


Figure 2.4 Axial Load-Centerline Deflection for a Column with kl/r = 54

of elasticity. However, the Young's modulus of elasticity E of 29000 ksi is estimated from the given load-strain plot of the corresponding stub-column test. The theoretical result in Figure 2.3 is the load-centerline deflection curve of a W 12x79 pin-ended member with σ_y = 36.7 ksi, E = 29000 ksi, and Θ_p = 0.005 radian (to be discussed in the next paragraph). The experimental result in Figure 2.4 was taken from Feder and Lee[18]. This W 8x31 pin-ended member was made of A-242 steel. The average value of several tension coupon tests for E and σ_y were 31300 ksi and 54.5 ksi, respectively. The maximum value of ec/r^2, where e is the initial eccentricity and c is the distance from neutral axis to the extreme fiber in compression, was observed to be 0.073. So the theoretical curve is that for a W 8x31 pin-ended member with E = 31300 ksi, σ_y = 54.5 ksi, and Θ_p = 0.005 radian.

The magnitude of Θ_p was selected on the basis of the agreement of the theoretical maximum compressive load carried by the member with the load capacity of the same member obtained from the AISC column design formula[43] times 1.7. This standard compressive load capacity is

$$P_{max} = \sigma_{max} A \tag{2.1a}$$

with

$$\sigma_{max} = 1.7\, \sigma_a \tag{2.1b}$$

where

$$\sigma_a = \frac{\sigma_y \left[1 - \frac{\left(\frac{kL}{r}\right)^2}{2\, C_c^2}\right]}{F.S.} \tag{2.1c}$$

$$F.S. = \frac{5}{3} + \frac{3\left(\frac{kL}{r}\right)}{8C_c} - \frac{\left(\frac{kL}{r}\right)^3}{8C_c^3} \qquad (2.1d)$$

and

$$C_c = \sqrt{\frac{2\pi^2 E}{\sigma_y}} \qquad (2.1e)$$

for $kL/r \leq C_c$. And

$$\sigma_a = \frac{12\pi^2 E}{23\left(\frac{kL}{r}\right)^2} \qquad (2.1f)$$

for $kL/r \geq C_c$.

P_{max} = compressive load capacity

σ_{max} = maximum compressive stress

A = member cross-sectional area

σ_a = allowable compressive stress

and

k = effective length coefficient

The factor of safety used in this AISC formula ranges from 1.67 for $kL/r = 0$ to 1.92 for $kL/r \geq C_c$, and the value of 1.7 was selected to be consistent with the AISC plastic design criteria.

The reason for choosing the AISC column design formula as the standard values is because it gives the average result of a large number of tests conducted under various member conditions; thereby, it renders a representative column strength. Figure 2.5 compares the theoretical maximum compressive loads of W 8x31 members with the modified AISC formula capacities at various effective slenderness ratios and magnitudes of Θ_p.

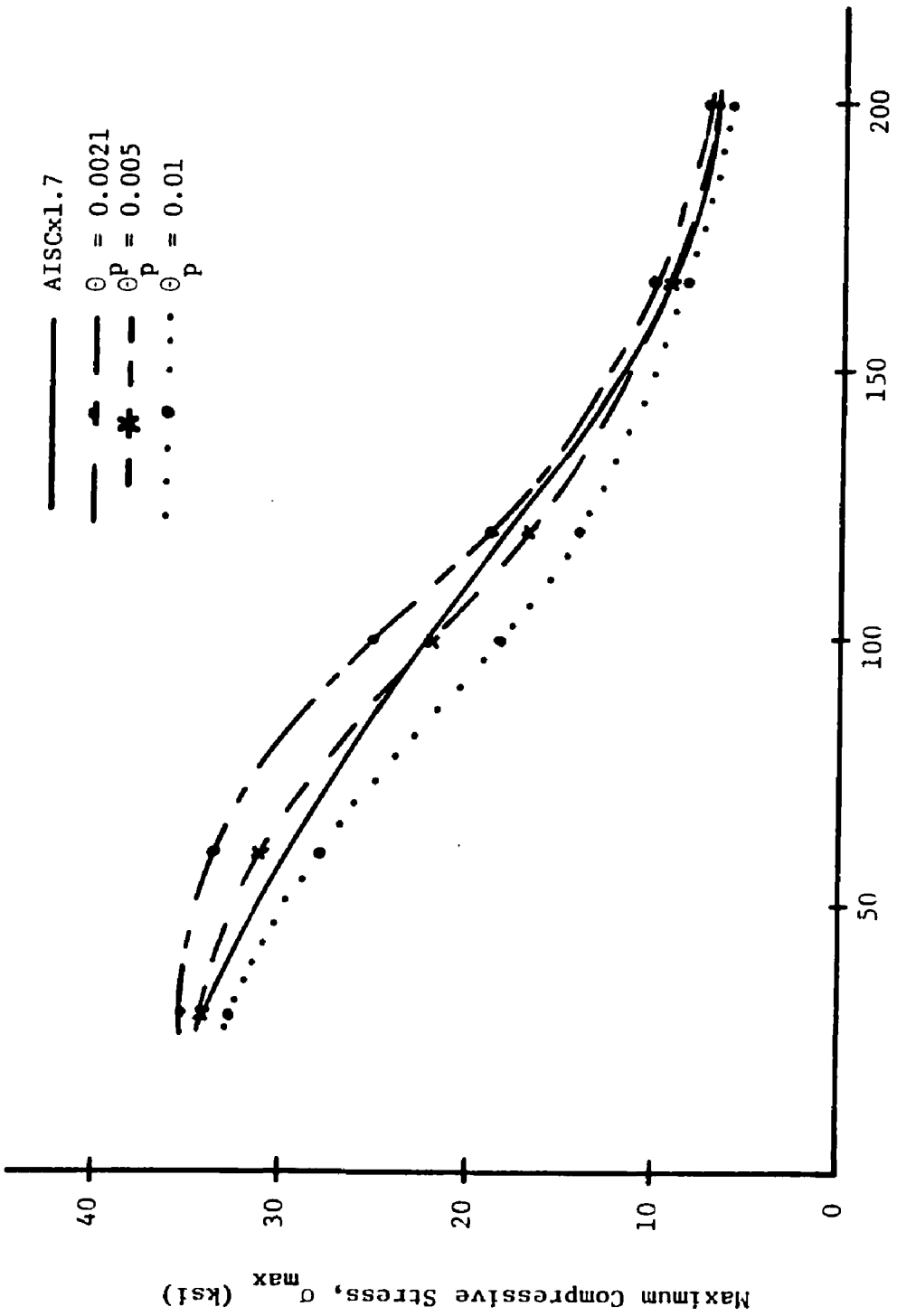


Figure 2.5 Comparison of the Maximum Compressive Load

It is evident that satisfactory agreement is obtained with θ_p = 0.005 radian for kL/r in the practical design range from 30-200. It should be mentioned that the members utilized for generating the theoretical compressive loads in Figure 2.5 were pin-ended members. Owing to the lack of available experimental results for members with different end conditions, it seems logical to use θ_p = 0.005 radian for all the members in this study. This was done.

2.2. Physical Behavior of the Member Under Cyclic Loading

In a typical hysteresis cycle, the member starts with an initial deflected shape with initial plastic rotation angles (θ_p) as shown in Figure 2.2. The applied compressive load forces the member to deflect more and introduces bending deformations along the member. This initial elastic region where the member ends are forced to move together corresponds to curve A-B of Figure 2.6 and the corresponding member deflected configuration is shown in Figure 2.7a. Tensile load and separation of the member ends are shown as positive in Figure 2.6. This elastic behavior terminates at point B in Figure 2.6 when plastification develops either at the member midspan or at the member ends as the bending moments at these locations attain their modified plastic moment capacities. Plastification can develop at both locations simultaneously. It can be verified that the plastic hinges can occur only at the member midspan and at the member ends, either in the member or in the connections.

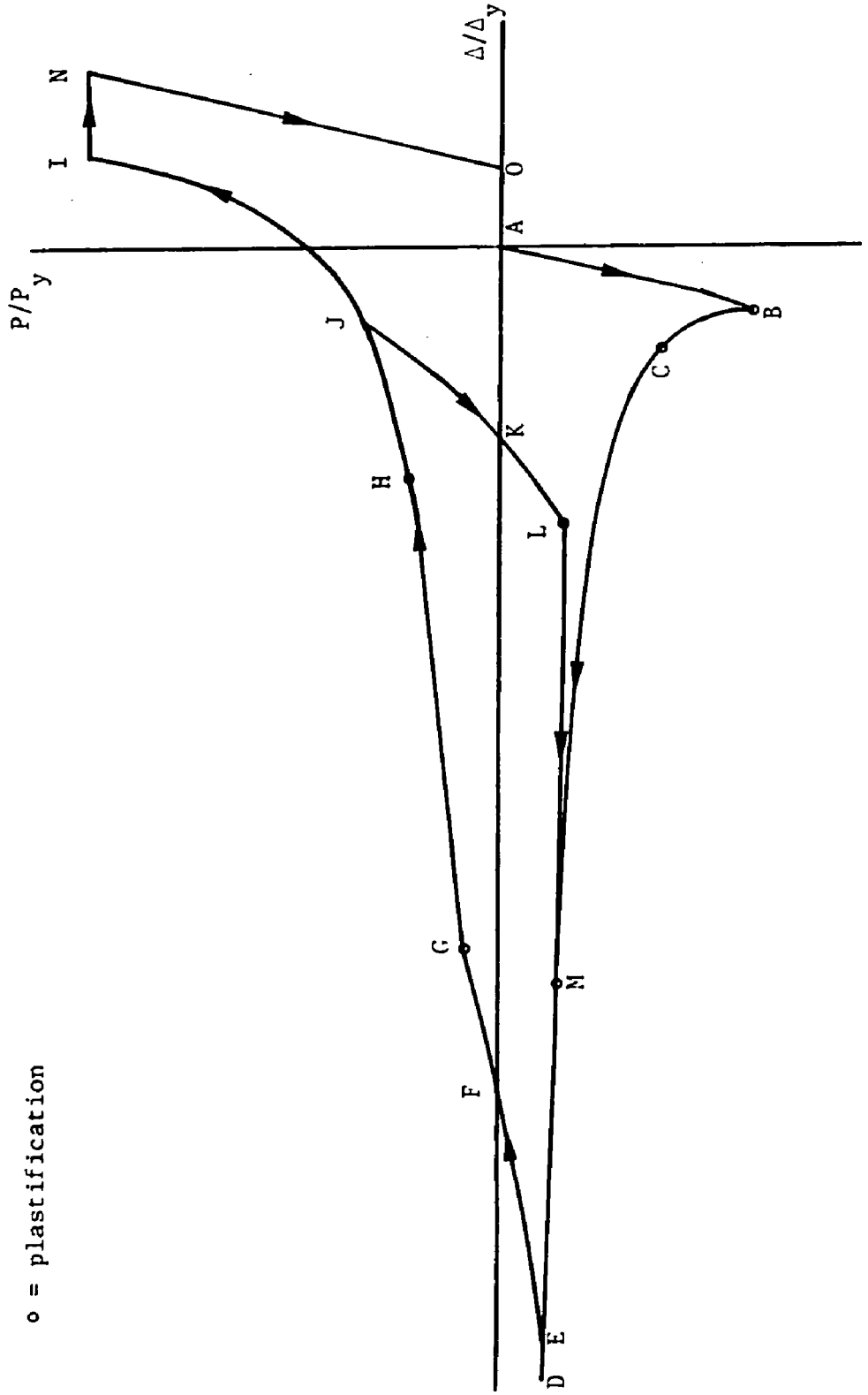
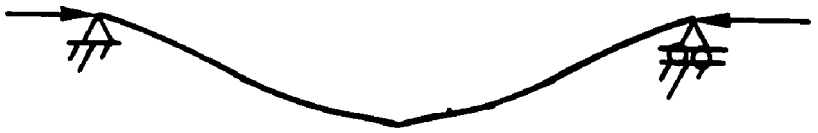
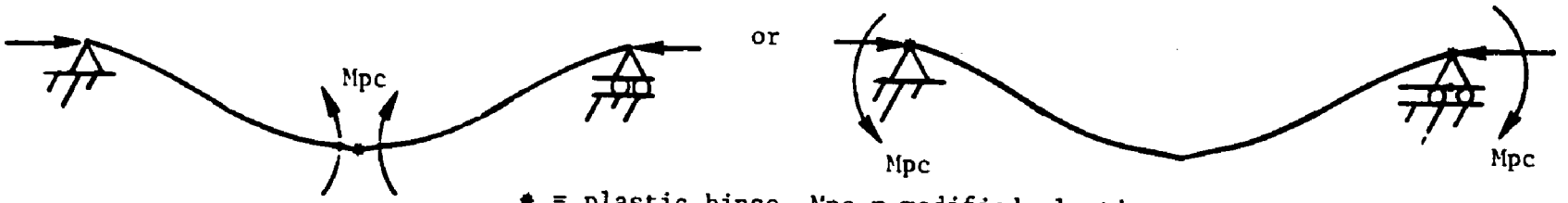


Figure 2.6 Typical Normalized Axial Load-Axial Displacement Hysteresis Loop

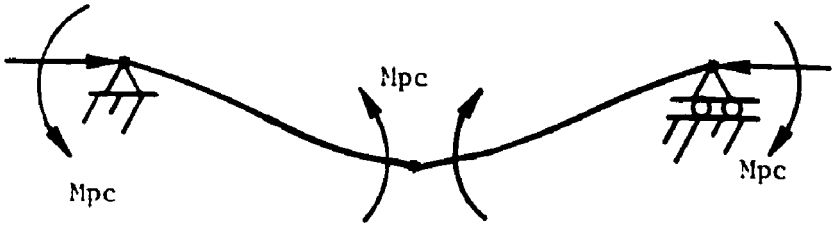


(a) Member Elastic Configuration Under Compressive Load



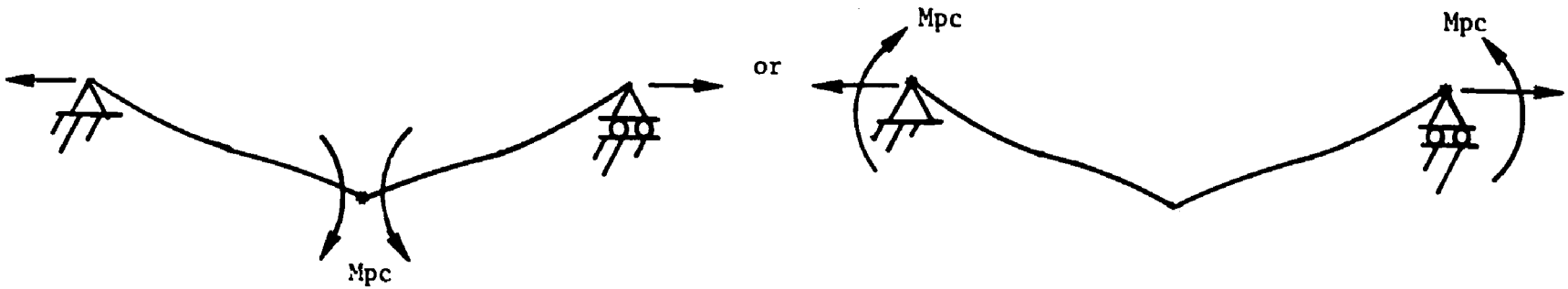
* = plastic hinge, Mpc = modified plastic moment

(b) Single Plastic Rotation Configuration Under Compressive Load

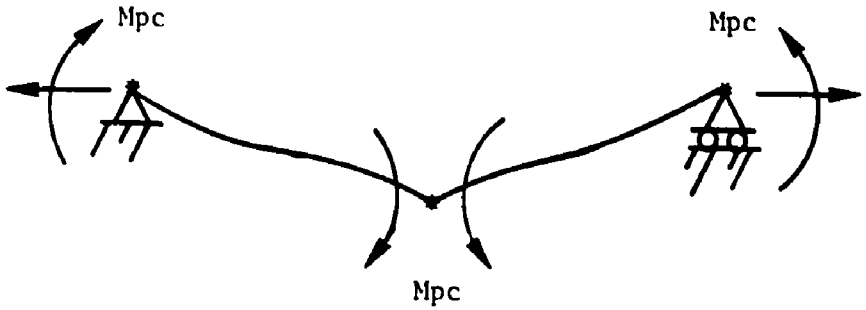


(c) Double Plastic Rotation Configuration Under Compressive Load

Figure 2.7 Member Equilibrium Configurations Under the Applied Load



(d) Single Plastic Rotation Configuration Under Tensile Load



(e) Double Plastic Rotation Configuration Under Tensile Load

Figure 2.7 Member Equilibrium Configurations Under the Applied Load (continued)

In the case where all the possible plastic hinges do not occur simultaneously, further movement of the ends together causes plastic rotation at the plastic hinge while the corresponding compressive load can either increase or decrease. This single plastic rotation region under compressive loading is shown as curve B-C in Figure 2.6, and the corresponding member deflected shape is shown in Figure 2.7b. At point C in Figure 2.6, plastification develops at the remaining plastic-hinge location. Further loading along the double plastic rotation region, curve C-D, results in decreasing compressive load. The corresponding deflected configuration is shown in Figure 2.7c. For convenience of discussions to follow, curve A-B-C-D of Figure 2.6 will be referred to as the compression envelope curve.

If the direction of the relative end displacement is reversed anywhere along the curve B-C-D, the plastic rotation ceases and the member behaves elastically again but with the residual plastic rotation angles developed before the reversal. Further separation of the ends results in the compressive load decreasing to zero magnitude followed by an increasing tensile load as shown by curve E-F-G. This elastic behavior terminates at point G where plastification reoccurs either at the midspan or at the ends.

Increase in magnitude of the tensile load forces plastic rotation to occur at the plastic hinge, but now this plastic rotation allows the member to straighten. This region is shown as curve G-H, and the corresponding deflected configuration is demonstrated in Figure 2.7d. At point H in

Figure 2.6, the second plastification develops at the remaining plastic-hinge location. Further increase in magnitude of the tensile load increases the separation of the member ends while the member undergoes double plastic rotation (curve H-I). The corresponding deflected shape of the member is shown in Figure 2.7e. The member becomes straight at point I in Figure 2.6 where the magnitude of the load is equal to the axial yield strength of the member. Curve I-N corresponds to the member yielding under constant axial tension yield load.

If the direction of the relative end displacement is reversed anywhere along curve G-H-I, elastic behavior prevails. Further movement of the ends together requires decreasing tensile load. Once the load decreases to zero magnitude followed by an increasing compressive load as shown by curve K-L-M-D, the member is governed by the same behavior as previously encountered along curve A-B-C-D.

2.3. Model 1: Hysteresis Behavior with Exact Expression for Curvature

The exact expression for curvature ($\Phi = \frac{d\theta}{ds}$) together with the assumptions introduced at the beginning of this chapter are used to derive the governing equation for the member behavior under cyclic loading. The details of this derivation and the method of solution are given in Appendix A. This model renders the governing equations which involve elliptic integrals and therefore needs an iterative type

solution. The problems in both the computing time and effort make it impractical to use this model for parametric study solutions. Thus, a computer program has not been developed to generate the complete hysteresis loop. Instead an alternative Model 2 which introduces further simplifications is presented.

2.4. Model 2: Hysteresis Behavior with Approximate Expression for Curvature

In this model, the approximate expression for curvature ($\Phi = \frac{d^2y}{dx^2}$) is used in addition to the previously stated assumptions for deriving the governing equations for the equilibrium configuration of the member by satisfying all the relevant compatibility and stress-strain relationships. Additional assumptions of the member deformations under the applied load make it possible to have a closed-form solution.

The sign convention employed in this study is as shown in Figures 2.2 and 2.8. The sign convention for the load and the relative end displacement is opposite to that used in the plot. Applying the slope-deflection equations for the member under the application of axial load to the half member in Figure 2.8 yields

$$M_1 = a\theta_1 + b\theta_2 \qquad (2.2)$$

$$M_2 = b\theta_1 + a\theta_2 \qquad (2.3)$$

where a and b are the stiffness coefficients. The half member can be used for this development because of the symmetry of the member and end connections.

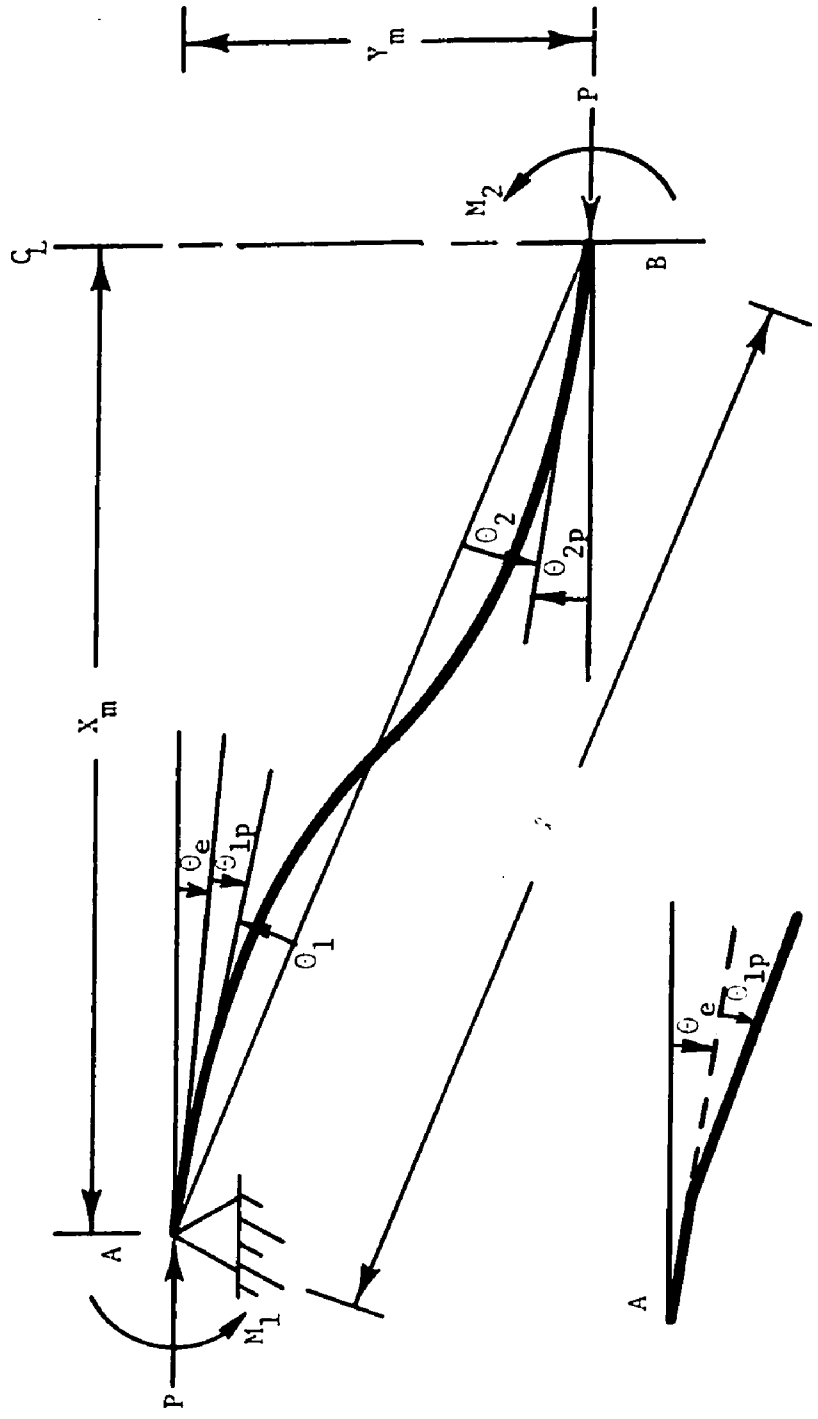


Figure 2.8 Half Member Under the Applied Load

Under Compressive Loading

$$a = \frac{\alpha(\sin\alpha - \alpha\cos\alpha)}{(2-2\cos\alpha - \alpha\sin\alpha)} \frac{EI}{\ell}$$

$$b = \frac{\alpha(\alpha - \sin\alpha)}{(2-2\cos\alpha - \alpha\sin\alpha)} \frac{EI}{\ell}$$

where

$$\alpha = \ell\sqrt{\frac{P}{EI}}$$

$$\ell = \frac{1}{2}\left(L - \frac{PL}{AE}\right)$$

I = member moment of inertia

Under Tension Loading

$$a = \frac{\alpha(\alpha\cosh\alpha - \sinh\alpha)}{(2-2\cosh\alpha + \alpha\sinh\alpha)} \frac{EI}{\ell}$$

$$b = \frac{\alpha(\sinh\alpha - \alpha)}{(2-2\cosh\alpha + \alpha\sinh\alpha)} \frac{EI}{\ell}$$

where

$$\alpha = \ell\sqrt{\frac{|P|}{EI}}$$

and

$$\ell = \frac{1}{2}\left(L - \frac{PL}{AE}\right)$$

The rotational-stiffness property of the connection gives

$$M_1 = k_\Theta \Theta_e \qquad (2.4)$$

Moment equilibrium of the half member in Figure 2.8 yields

$$M_1 + M_2 = PY_m \qquad (2.5)$$

The relation

$$\Theta_1 + \Theta_{1p} + \Theta_e = \Theta_2 + \Theta_{2p} \qquad (2.6)$$

can also be obtained from the geometry of the member in Figure 2.8. By assuming that the half-member chord length AB is equal to the deformed half-member length ℓ, and that the sine of the angle between chord AB and the horizontal axis is equal to the angle itself, the relation

$$\theta_1 + \theta_{1p} + \theta_e = \frac{Y_m}{\ell} \tag{2.7}$$

can be derived.

In this research, one of the parametric studies is the variation of the connection flexural strength while the connection flexural stiffness and the member properties are kept constant. The connection employed in the study always has lower or, at most, equal flexural strength to the member. This is because any increase in the connection flexural strength over the member flexural strength results in member end yielding and does not influence the end hysteresis behavior. Hence the conditions for plastification are

$$M_1 = M_{pcc} \tag{2.8}$$

if plastic hinges occur at the connections, and

$$M_2 = M_{pcm} \tag{2.9}$$

if plastic hinge occurs at midspan where[44]

$$M_{pc} = \pm M_p \left[1 - \left(\frac{P}{P_y}\right)^2\right] \tag{2.10a}$$

for rectangular cross sections and wide flange cross sections subjected to bending about the weak axis, and

$$M_{pc} = \pm M_p \left[1 - \frac{A^2}{4t_w Z}\left(\frac{P}{P_y}\right)^2\right] \left(0 < \frac{|P|}{P_y} < \frac{A_w}{A}\right) \tag{2.10b}$$

$$M_{pc} = \pm M_p \left\{ \frac{A}{2Z} \left[d\left(1-\frac{|P|}{P_y}\right) - \frac{A}{2b_f}\left(1-\frac{|P|}{P_y}\right)^2 \right] \right\}$$

$$\left(\frac{A_w}{A} < \frac{|P|}{P_y} < 1\right) \qquad (2.10c)$$

for wide flange cross sections subjected to bending about the strong axis. M_{pc} is positive when plastic rotation occurs under compressive loading and negative when plastic rotation occurs under tensile loading. In these equations

M_{pc} = modified plastic moment

M_{pcc} = M_{pc} of the connection

M_{pcm} = M_{pc} of the member

P_y = axial yield load = $\sigma_y A$

M_p = plastic moment = $\sigma_y Z$

Z = plastic section modulus

A_w = cross-sectional area of the web

t_w = thickness of the web

b_f = width of the flange

and

d = depth of the section

Geometry of the member in Figure 2.8 also gives

$$X_m^2 = \ell^2 - Y_m^2 \qquad (2.11)$$

Finally the relative end displacement Δ can be obtained from

$$\Delta = L - 2X_m \qquad (2.12)$$

2.5. Method of Solution for Model 2

If P is treated as the independent variable (known value), a closed-form solution of equations (2.2) - (2.12) can be obtained for every possible case as follows:

a) When the member and the connections remain elastic, the unknown quantities are M_1, M_2, Θ_1, Θ_2, Θ_e, and y_m. So by solving equations (2.2) - (2.7), the following results are obtained:

$$\Theta_1 = \frac{[k_\Theta \Theta_{1p} (aC+bC-k_\Theta) + k_\Theta \Theta_{2p} (b-aC-bC)]}{[(a+b_\Theta)(b-aC-bC) - (b-k_\Theta)(a-aC-bC+k_\Theta)]}$$

and

$$\Theta_2 = \frac{[-k_\Theta \Theta_{1p} - \Theta_1 (a-aC-bC+k_\Theta)]}{(b-aC-bC)}$$

where

$$C = \frac{k_\Theta}{P\ell}$$

M_1 and M_2 can be found by substituting Θ_1 and Θ_2 in equations (2.2) and (2.3). Θ_e and Y_m can then be obtained by substituting M_1 and M_2 in equations (2.4) and (2.5). Equations (2.11) and (2.12) give the values of X_m and Δ, respectively.

b) When plastic rotation occurs at midspan only, M_2 is given by equation (2.9) while Θ_{2p} becomes an unknown. Solving equations (2.2) - (2.5) and (2.7) yields

$$\Theta_1 = \frac{[M_{pcm} (b-aC-bC) + ak_\Theta \Theta_{1p}]}{(aaC-aa-ak_\Theta-bbC+bb)}$$

and

$$\Theta_2 = \frac{M_{pcm} - b\Theta_1}{a}$$

Then M_1, Θ_e, Θ_{2p}, and Y_m can be found by back substitution of the appropriate quantities in equations (2.2), (2.4), (2.6), and (2.5), respectively. X_m and Δ can be obtained from equations (2.11) and (2.12).

c) When plastic rotation occurs at the member ends only, M_1 is given by equation (2.8) while Θ_{1p} becomes an unknown. Equations (2.2), (2.3), and (2.5)-(2.7) can be solved to give

$$\Theta_1 = \frac{[M_{pcc}\ (1-aD-bD) + b\Theta_{2p}]}{(bbD+a-aaD)}$$

and

$$\Theta_2 = \frac{M_{pcc} - a\Theta_1}{b}$$

where

$$D = \frac{1}{P_\ell}$$

M_2, Θ_e, Θ_{1p}, and Y_m can be obtained by substituting the appropriate values in equations (2.3), (2.4), (2.6), and (2.5), respectively. Then X_m and Δ can be obtained from equations (2.11) and (2.12).

d) When plastic rotation occurs at both the midspan and the ends, equations (2.8) and (2.9) give the values of M_1 and M_2, but both Θ_{1p} and Θ_{2p} are unknowns. The required quantities are Θ_1, Θ_2, Θ_e, Θ_{1p}, Θ_{2p}, and Y_m. Solving equations (2.2) and (2.3) gives

$$\Theta_1 = \frac{aM_{pcc} - bM_{pcm}}{aa-bb}$$

and

$$\theta_2 = \frac{M_{pcm} - b\theta_1}{a}$$

θ_e and Y_m can be obtained from equations (2.4) and (2.5), and then equations (2.7) and (2.6) can be used to solve for θ_{1p} and θ_{2p}, respectively. X_m and Δ are given by equations (2.11) and (2.12).

Hence the closed-form solutions, which are very efficient for computer programming, have been obtained for every branch of the hysteresis behavior. A computer program has been developed to automatically generate the entire hysteresis loop to aid in the parametric study reported in the next chapter. The output of this computer program is the hysteresis loop in terms of the normalized axial load-axial displacement ($P/P_y - \Delta/\Delta_y$), where $\Delta_y = \frac{P_y L}{AE}$ is the axial yield deformation. A typical curve is shown in Figure 2.6. To elucidate the pattern, the correspondence of each branch of the hysteresis loop with the member physical behavior was given in Section 2.2. Additional comments about special cases and some significant properties of the hysteresis behavior will be given in the next section.

2.6. Special Cases and Some Significant Properties of the Hysteresis Behavior

There are several special properties of the hysteresis behavior which arise from the extreme member and connection properties. There are also physical constraints of the hysteresis loop which are useful for the study in the

following chapters. These special cases are summarized in this section for a better understanding of the hysteresis behavior.

1) For a given set of other properties of the member and connection, there is a corresponding connection flexural strength defined here as the balanced connection strength or simply the balanced strength. The member with balanced strength connection and with the introduced initial plastic rotation angles plastifies at the ends and midspan simultaneously when loaded along the initial elastic region. This balanced strength is a very important parametric value regarding the hysteresis behavior of the member. The significance of the balanced strength connection will be discussed in the following chapters.

2) If the connections have very small flexural stiffness and great flexural strength, the member subjected to compressive load will plastify first at midspan. Then the member has to undergo large plastic rotation before the second plastification can develop at the member ends. This means point C of Figure 2.6 is at a large compressive Δ/Δ_y. In the extreme case where the connection has zero flexural stiffness and nonzero flexural strength, plastic hinges can not be formed at the member ends and the member behaves as a pin-ended member.

3) For the elastic post-compression induced plastic rotation behavior (curve E-G of Figure 2.6), plastic hinges of the member with very low connection flexural strength can

redevelop at the connections even when the member is still subjected to compressive load. So curve E-G is very short and terminates on the compression side. Analogous behavior holds true for the elastic post-tension induced plastic rotation behavior.

4) The termination point of the tension induced single plastic rotation region (point H of Figure 2.6) depends on the starting point of the preceding elastic region (point E). If point E is anywhere between points B and C, i.e., before the second plastification occurs, point H is very close to point I (tension yield point). More precisely the smaller the plastic rotation angles are when the member ends begin to separate, the closer the point of second re-plastification is to the tension yield point.

5) The termination point of the compression induced single plastic rotation region (point M) reversing from the tension induced single plastic rotation region (curve G-H) is the same point as the starting point of the elastic region (point E) which precedes this tension induced single plastic rotation region. So, if point J is anywhere along curve G-H, point M will coincide with point E because they correspond to the same member configuration with the same plastic rotation angles.

There is one inconsistency in the mathematical solution regarding the initial plastic rotation angles. The plastic rotation angles at midspan and at the ends can become less than 0.005 radian due to the tension induced plastic

rotation action. In this event, after the tensile load is reduced to zero magnitude, reapplication of the compressive load does not cause the member to retrace the behavior produced when the compressive load is applied in the initial cycle (curve A-B of Figure (2.6)). Instead, the member will sustain higher maximum compressive load because of the reduction in the initial imperfections. To avoid this inconsistency, whenever the plastic rotation angles are less than 0.005 radian due to the tension induced plastic rotation action, θ_p = 0.005 radian is assumed to be restored in the member at zero load prior to the next compressive-loading cycle.

CHAPTER III

PARAMETRIC STUDY

With the aid of the computer program developed in Chapter II to generate the complete hysteresis loop of Model 2, one is in a position to conduct the parametric study. This study is very important for an understanding of the influence of different parameters on the hysteresis behavior. Such a knowledge is necessary for evaluating the relative importance of each parameter and for establishing criteria for the optimization of the hysteresis behavior based on selected objective functions. The evaluation of the influence of the parameters on the hysteresis characteristics is carried out in this chapter whereas the criteria for optimization of the hysteresis behavior is derived in Chapter V.

In this chapter each of the main parameters, namely, the connection flexural strength, the connection flexural stiffness, the member slenderness ratio (L/r), and the member cross-sectional properties is varied independently to evaluate its effect on the hysteresis behavior. The variation of the hysteresis behavior resulting from simultaneous variation of several parameters is also evaluated.

For convenience, the following abbreviated names

will be used to identify the various regions of the hysteresis loop which were described in Chapter II:

IE = initial elastic

CISP = compression induced single plastic rotation

CIDP = compression induced double plastic rotation

CIP = compression induced plastic rotation = CISP or CIDP

ECIP = elastic post-compression induced plastic rotation

TISP = tension induced single plastic rotation

TIDP = tension induced double plastic rotation

TIP = tension induced plastic rotation = TISP or TIDP

ETIP = elastic post-tension induced plastic rotation

E = elastic = IE or ECIP or ETIP

SP = single plastic rotation = CISP or TISP

and DP = double plastic rotation = CIDP or TIDP

Another thing that should be mentioned here is that the slopes of the corresponding regions of the hysteresis loops (P/P_y - Δ/Δ_y plots) of various members with different member and connection properties are compared throughout this chapter. There will be several conclusions of the type that the corresponding regions of different hysteresis loops have some relationship among their slopes at the same Δ/Δ_y. When the regions are linear, this implies that the mentioned relation exists where these

regions or their extensions intersect the Δ/Δ_y axis at the same Δ/Δ_y. However, when the regions are curvilinear, this implies that the mentioned relation exists for the average slopes of the regions where these regions or their extensions intersect the Δ/Δ_y axis at the same Δ/Δ_y. Also, with regard to comparison of lengths of the corresponding regions of hysteresis loops, the term at the same Δ/Δ_y likewise implies that those regions or their extensions intersect the Δ/Δ_y axis at the same Δ/Δ_y.

It is to be mentioned also that the connection flexural stiffness parameter used in this study is defined to be μ, for which

$$\mu = \frac{L}{2} \left(\frac{P_{cr}}{EI}\right)^{\frac{1}{2}} \tag{3.1}$$

and

$$\frac{\tan\mu}{\mu} = \frac{-2EI}{k_\theta L} \qquad \left(\frac{\pi}{2} \leq \mu \leq \pi\right) \tag{3.2}$$

where P_{cr} is the theoretical buckling load of an initially perfectly straight member of length L, rotational end restraint stiffness k_θ, and member bending stiffness EI (Figure 2.1). This parameter μ and the effective length coefficient of the member k are related by the equation

$$\mu_i k_i = \mu_j k_j = \frac{\pi}{2} \tag{3.3}$$

where i and j indicate the different sets of values of μ and k. For a pin-ended member, the end rotational stiffness is zero whereas the corresponding values of μ and k are $\pi/2$ and 1. On the other hand, for a fixed-ended member,

the end rotational stiffness is ∞ while the corresponding values of μ and k are π and 1/2. So for the end rotational stiffness between zero and ∞, μ and k vary between $\frac{\pi}{2}$ and π and 1 and 1/2 respectively.

Finally, the flexural strength of the member or the connection is the plastic moment value of the member or the connection. The strength ratio R and the balanced strength ratio R_b are defined here as the ratio of the connection flexural strength to the member flexural strength and the ratio of the balanced connection strength (Section 2.6) to the member flexural strength, respectively. The significance of the balanced strength and the balanced strength ratio on the hysteresis behavior is described in Section 3.1. The properties of members used for the parametric study in this chapter are listed in Table 3.1, and the properties of the wide flange sections used for these members are given in Table 3.2.

3.1. Influence of the Connection Flexural Strength

The connections are assumed to have axial strength equal to the member axial strength throughout this study while the flexural strengths may be different. The connection flexural strength, which is called the connection strength, is an important parameter regarding the order of the locations of plastic-hinge formation. This aspect of plastic-hinge formation has direct influence on the maximum compressive load carried by the member, on the dissipated

TABLE 3.1. PROPERTIES OF MEMBERS

Member	L/r	kL/r	μ	L (in)	k_Θ (k-in/rad)	R	R_b	Shape	Figure
1	60	50	0.6π	120.6	1.127×10^4	1.0	0.25	W 8x31	3.1
2	60	50	0.6π	120.6	1.127×10^4	0.25	0.25	W 8x31	3.1
3	200	100	π	402	1.446×10^8	0.75	1.0	W 8x31	3.2
4	200	100	π	402	1.446×10^8	0.25	1.0	W 8x31	3.2
5	200	100	π	402	1.446×10^8	1.0	1.0	W 8x31	3.3,3.11 3.12
6	200	166.7	0.6π	402	3.382×10^3	1.0	0.297	W 8x31	3.3
7	60	30	π	120.6	5.783×10^8	0.5	1.0	W 8x31	3.4 3.5
8	60	50	0.6π	120.6	1.127×10^4	0.5	0.25	W 8x31	3.4 3.6
9	200	100	π	402	1.446×10^8	0.5	1.0	W 8x31	3.5
10	200	166.7	0.6π	402	3.382×10^3	0.5	0.297	W 8x31	3.6
11	200	125	0.8π	402	1.91×10^4	0.767	0.767	W 8x31	3.9
12	200	125	0.8π	208	6.985×10^3	0.762	0.762	W 14x22	3.9

TABLE 3.1. PROPERTIES OF MEMBERS (continued)

Member	L/r	kL/r	μ	L (in)	k_θ (K-in/rad)	R	R_b	Shape	Figure
13	200	200	0.5π	1164	0.0	0.0	0.0	W 12x190*	3.10
14	200	200	0.5π	650	0.0	0.0	0.0	W 12x190	3.10
15	120	100	0.6π	241.2	5.637×10^3	1.0	0.284	W 8x31	3.11
16	120	100	0.6π	241.2	5.637×10^3	0.25	0.284	W 8x31	3.12

Remarks: All members have E = 30,000 ksi

* strong-axis bending; the rest are subjected to weak-axis bending.

TABLE 3.2. PROPERTIES OF WIDE FLANGE CROSS SECTIONS

Section	A (in^2)	d (in)	b_f (in)	t_f (in)	t_w (in)	I (in^4)	Z (in^3)	r (in)	Axis of Bending
W 8x31	9.12	8.0	8.0	0.433	0.288	37.0	14.0	2.01	W.A.
W 14x22	6.49	13.72	5.0	0.335	0.23	7.0	4.39	1.04	W.A.
W 12x190	55.9	14.38	12.67	1.736	1.06	590	143	3.25	W.A.
W 12x190	55.9	14.38	12.67	1.736	1.06	1890	311	5.82	S.A.

energy of the hysteresis loop, and on the angles of plastic rotation at the plastic hinges. For these influences, which will be discussed in more detail in the subsequent chapters, special attention is paid to the order of the locations of plastic-hinge formation and to the concept of the balanced connection strength.

As previously described in Chapter II, for each set of other properties of the member and connection (with only one exception as described below), there is a corresponding connection strength called the balanced strength. The member with the balanced strength connections and with the introduced initial plastic rotation angles plastifies at midspan and at the ends simultaneously when loaded along the IE region. So the CIDP region of the member with balanced strength connections follows the IE region directly without the intermediate CISP region, Member 2 of Figure 3.1.

When the direction of the relative end displacement of the member with balanced strength connections is reversed anywhere along the CIDP region, the member behaves elastically until plastification redevelops in the reverse direction under tensile load. For a fixed-ended member ($\mu = \pi$), plastic hinges again occur at the member ends and midspan simultaneously. For a nonfixed-ended member, the member replastifies first at midspan followed by the TISP region until plastic hinges reoccur at the connections as shown in Figure 3.1 Member 2. This TISP region is a little

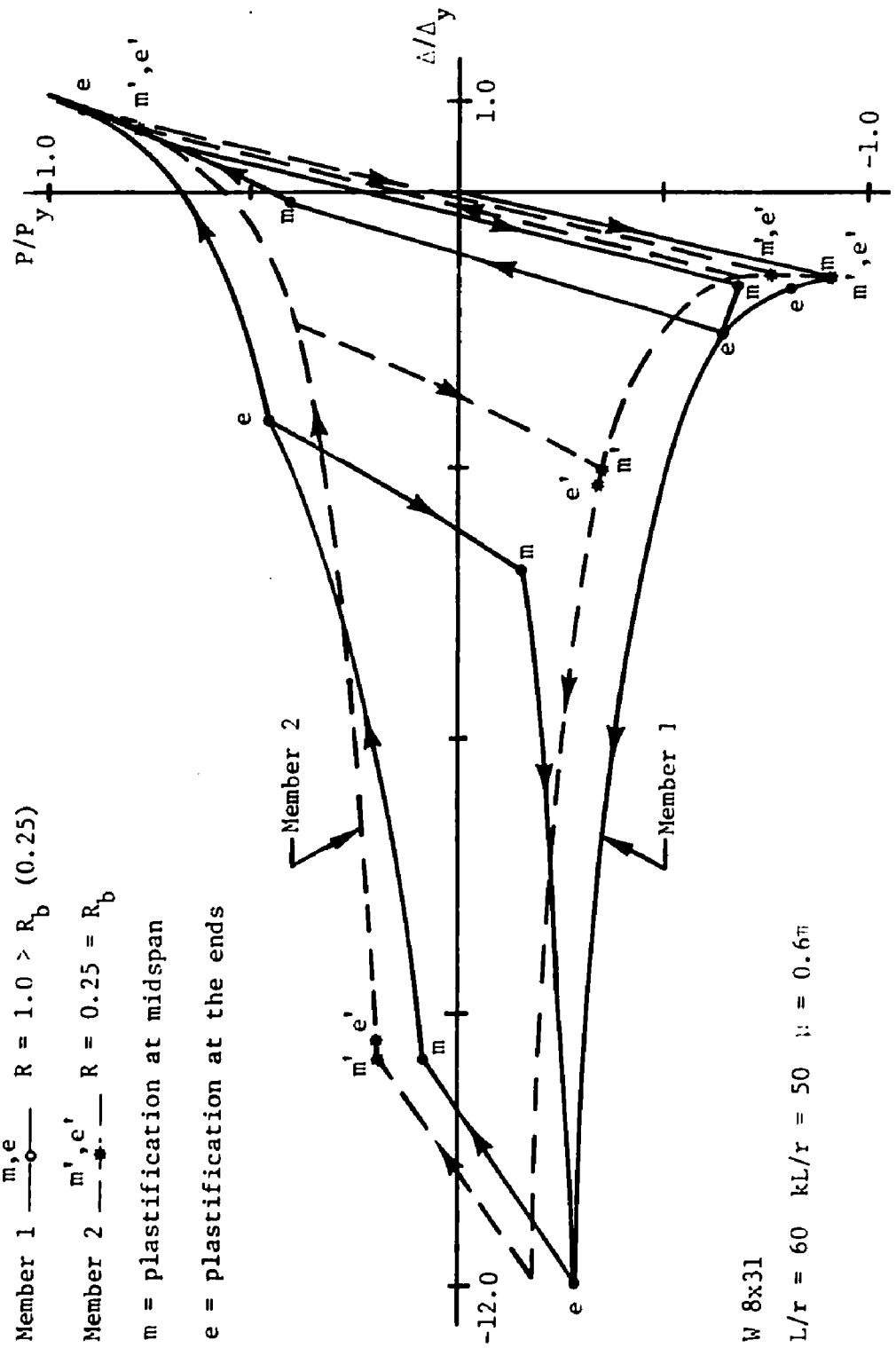


Figure 3.1 Influence of Connection Flexural Strength on the Hysteresis Behavior

longer for the member with smaller connection stiffness, but is practically the same curve as the TIDP region at the same Δ/Δ_y (tension envelope curve). The member exhibits analogous pattern of plastic-hinge formation as described above when the direction of the relative end displacement is reversed anywhere along the TIP region.

The only case that plastic hinges cannot occur simultaneously at the member ends and midspan at the termination of the IE region is the case of a pin-ended member ($\mu = \frac{\pi}{2}$). In this case, the value zero is assigned for the balanced connection strength. Mathematically there is no variation in the hysteresis behavior of a pin-ended member regardless of the value of its connection strength since no moment can be developed at the member ends. Conceptually, plastic hinges can occur at the connections immediately after loading for zero connection strength, but plastic hinges cannot develop at the connections for non-zero connection strength. Conversely, there is no variation in the hysteresis behavior of a member of zero connection strength regardless of the value of its connection flexural stiffness.

For the case where the connection strength is greater than the balanced strength, the member with the selected initial imperfection subjected to compressive load plastifies first at midspan (Figure 3.1 Member 1). So the IE region is followed by the CISP region with the

plastic rotation at midspan until plastification occurs at the member ends. If the end displacement is reversed anywhere along the CIP region, the member behaves elastically up to the reoccurrence of plastic hinge at midspan followed by the TISP region until plastification redevelops at the ends. Same order of plastic-hinge formation prevails for the reverse in direction of the end displacement anywhere along the TIP region.

The lengths of the corresponding E regions at the same Δ/Δ_y of the hysteresis loops of a member with varying connection strengths are approximately the same and equal to that at the same Δ/Δ_y of the hysteresis loop of this member with balanced strength connections (Figure 3.1). Except for members with very low slenderness ratio, maximum compressive load carried by this type of member corresponds to the point of occurrence of the plastic hinge at midspan on the IE region (member with L/r about 60 or less may produce maximum compressive load at the plastification at the ends at a slightly higher load than that of the plastification at midspan). So there is little or no change in the maximum compressive load carried by a member when the connection strength is varied provided that these strengths are equal to or greater than the balanced connection strength. The corresponding SP regions at the same Δ/Δ_y are longer for the member with greater connection strength since higher moment has to be generated to develop plastic hinges at member ends for the

member with greater connection strength.

Figure 3.2 shows the hysteresis loops of members with the connection strength that is smaller than the balanced connection strength. Reverse order of plastic-hinge formation to that of the former case prevails, i.e., plastification develops first at the connections and later at midspan. This is due to the reduction in the magnitude of moment required to plastify the connections from the balanced strength case. It should also be mentioned that if the connection strength is very close to the balanced strength, it is possible that plastification develops first at midspan along the ECIP or ETIP regions and then at the connections very shortly after. This behavior is the transition between the smaller than balanced strength and the balanced strength cases. The corresponding E regions at the same Δ/Δ_y are shorter for the member with smaller connection strength due to the reduction in the plastic moment magnitude of the connections. This also implies that the maximum compressive load sustained by a member of this type is lower for smaller connection strength. Also all the E regions of the member with zero strength connections have zero length.

Besides the above observations, other important conclusions from the comparison of the hysteresis loops in Figures 3.1 and 3.2 are that the slopes of the E regions at the same Δ/Δ_y of the hysteresis loops of members that

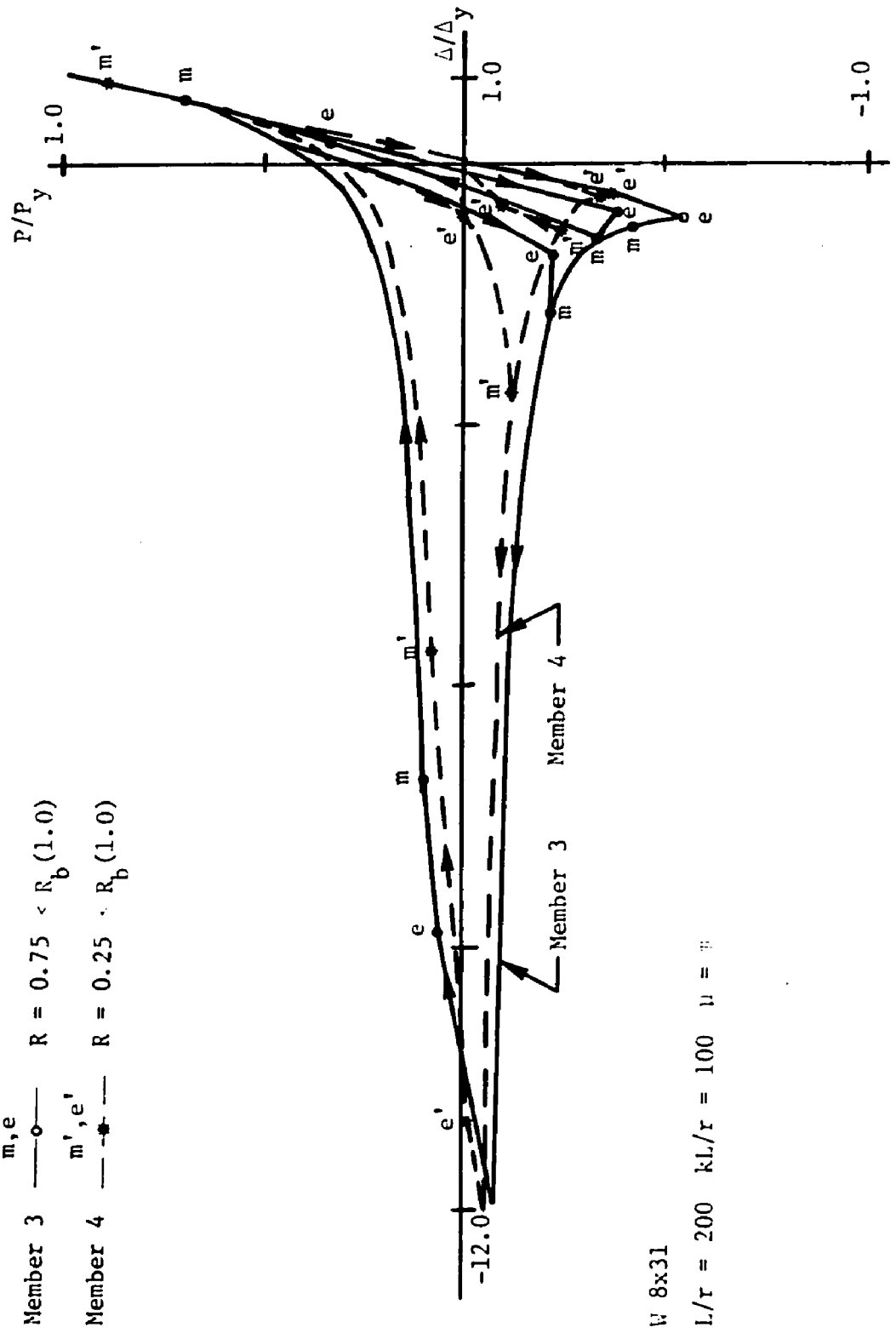


Figure 3.2 Influence of Connection Flexural Strength on the Hysteresis Behavior

differ only in the connection strength are virtually the same. The slopes of the ECIP and the ETIP regions at the same Δ/Δ_y of a member are approximately the same. This is also true for the rest of the parametric study. For the case where the connection strength is smaller than the balanced connection strength, the slopes of the TISP regions at the same Δ/Δ_y of the hysteresis loops of members that differ only in the connection strength are also approximately the same. With regard to the dissipated energy of the hysteresis loop, the member with greater connection strength sustains higher magnitude of load at the same Δ/Δ_y than the member with smaller connection strength along the corresponding DP regions. This characteristic is expected since higher connection strength corresponds to stronger member. Nevertheless, the percentage of increase in the magnitude of the sustained load is lower than the percentage of increase in the connection strength. The energy dissipation, however, depends on the characteristics of various regions and is less obvious for comparison. For the members with smaller than balanced strength connections it is evident that more energy is dissipated by the member with greater strength connections for the same interval of Δ/Δ_y of the hysteresis loops. For the members with greater than balanced strength connections, the variation in energy dissipation for the same interval of Δ/Δ_y of the hysteresis loops with respect to the variation in the

connection strength is less than the former case and not so obvious. The energy dissipation characteristic of the hysteresis loops will be investigated in more detail in Chapter V.

3.2. Influence of the Connection Flexural Stiffness

The connection flexural stiffness, henceforth called the connection stiffness, directly affects the balanced connection strength. It should be remembered that the connection stiffness was defined with the parameter μ in the introduction of this chapter. When the connection stiffness is π, the balanced strength ratio is equal to one since the fixed-ended member with equal connection and member flexural strength and with the introduced initial plastic rotation angles plastifies at the ends and midspan simultaneously. As the connection stiffness decreases, the balanced strength ratio decreases. The lower limit of the connection stiffness is $\frac{\pi}{2}$ while the corresponding balanced strength ratio is zero, which is the case of a pin-ended member.

Figures 3.3 and 3.4 illustrate the influence of the connection stiffness on the hysteresis behavior. When the connection stiffness is varied while all other properties of the member and the connection are kept constant, the slopes of the E regions at the same Δ/Δ_y are steeper for the hysteresis loop of the member with greater connection stiffness. This increase in the axial load-axial displace-

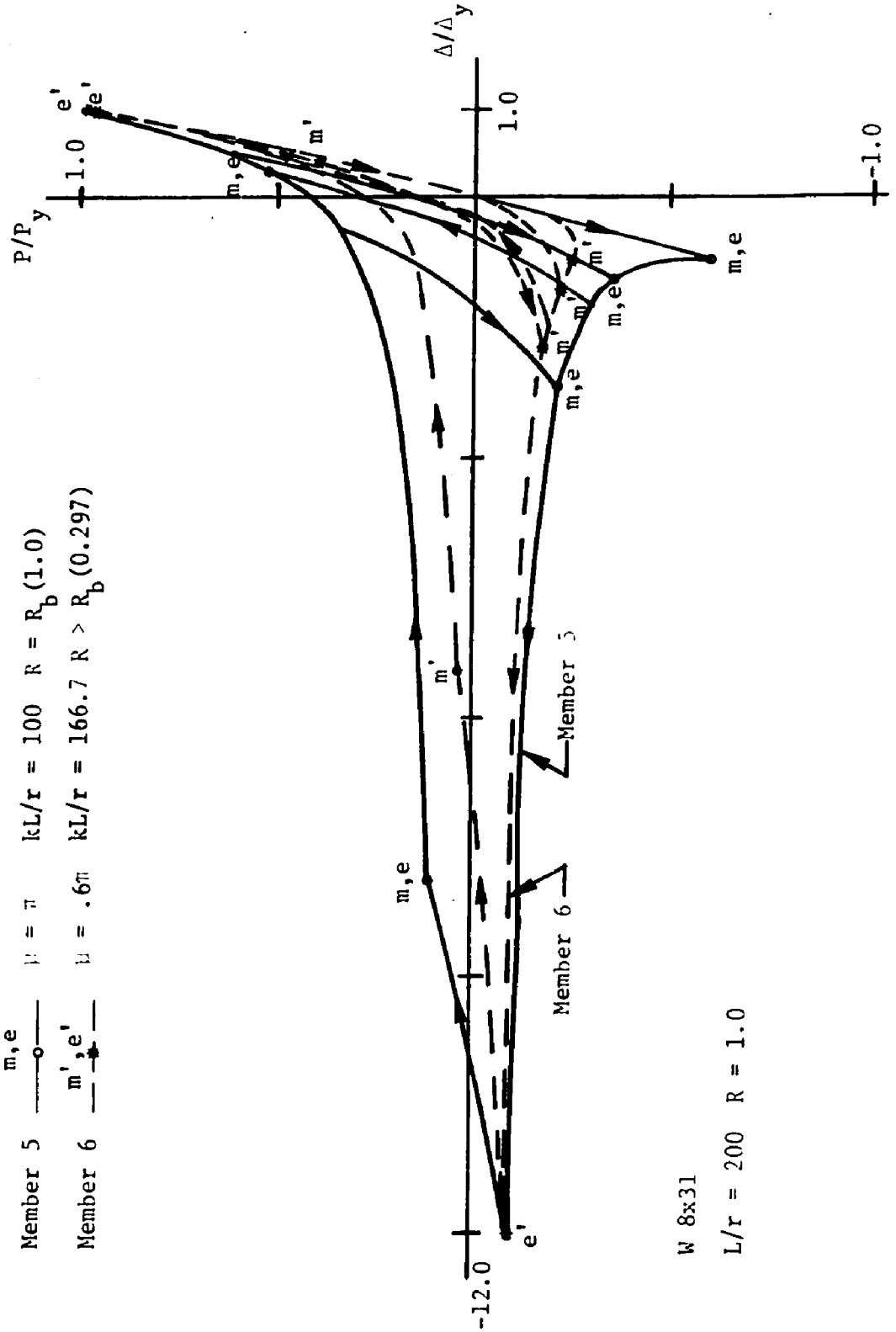


Figure 3.3 Influence of Connection Flexural Stiffness on the Hysteresis Behavior

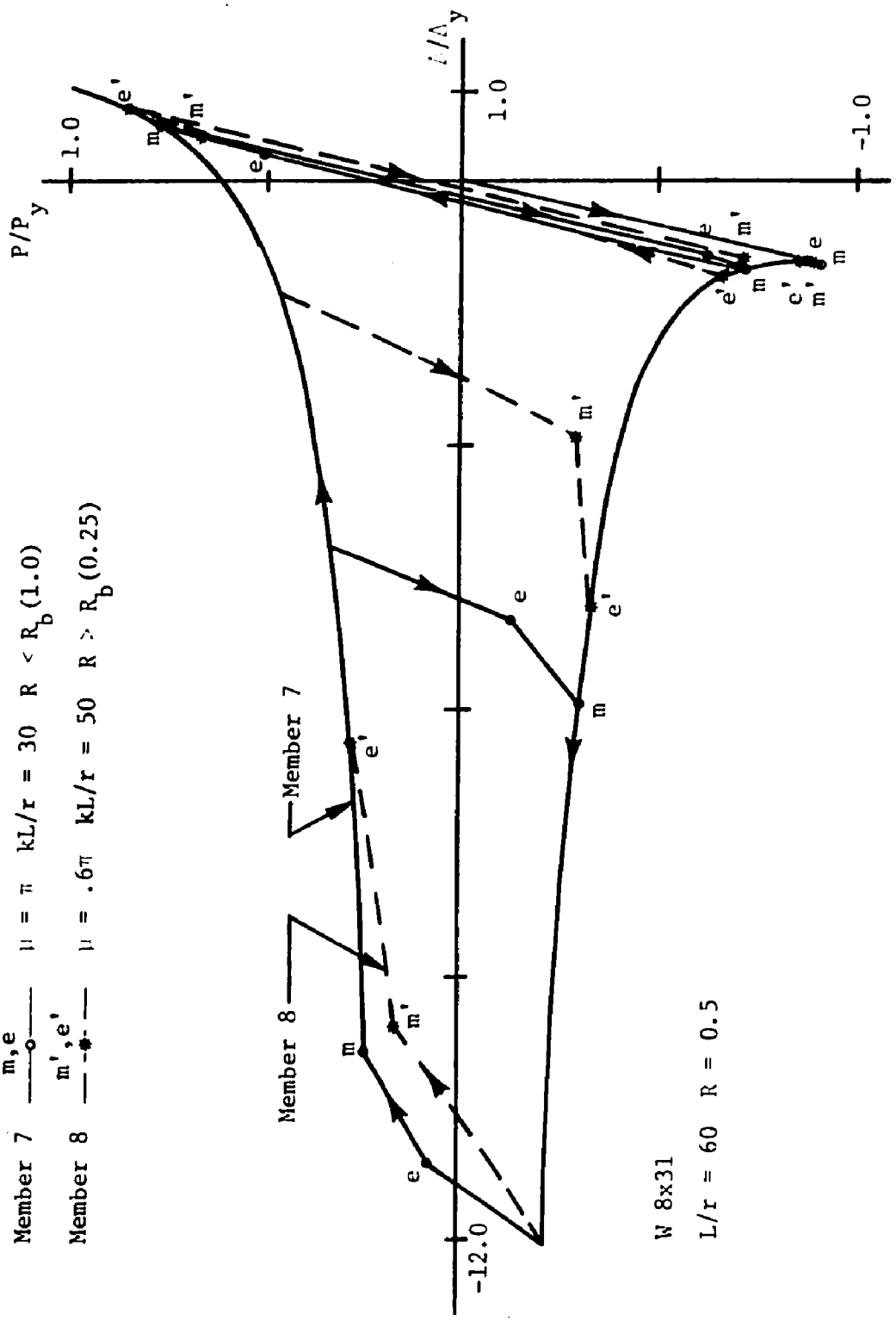


Figure 3.4 Influence of Connection Flexural Stiffness on the Hysteresis Behavior

ment stiffness is anticipated since physically a member is stiffer with stiffer connections. The magnitude of this difference in slope will be studied in the next chapter. Also, for a member with a specific set of properties, the variation in the connection stiffness alone can change the order of the plastic-hinge formation, i.e., can make the given connection strength greater or smaller than the balanced connection strength. This is because the variation in the connection stiffness changes the balanced connection strength as illustrated in Figure 3.4.

With regard to the compressive-load-carrying capacity of members that differ only in the connection stiffness, higher load can be carried by the member with greater connection stiffness. This characteristic can be expected since increasing the connection stiffness is the same as decreasing the effective length coefficient and, hence, reduces the effective slenderness ratio, kL/r, of the member. Nevertheless, the variation in the connection stiffness of a member does not change the load resisted by the member at the same Δ/Δ_y along the DP regions. Consequently, the compression envelope curves of the hysteresis loops of members that differ only in the connection stiffness are different only before the occurrence of the second plastification. However, this second plastification can take place at a very large Δ/Δ_y if the connection stiffness is very low. The general conclusion

about the dissipated energy is that for a fixed interval of Δ/Δ_y of the hysteresis loops, the member with greater connection stiffness dissipates more energy and the difference is mainly due to the contribution of the E and the SP regions.

3.3. Influence of the Member Slenderness Ratio (L/r)

As defined earlier in the introduction of this chapter, a constant connection stiffness, μ, for each slenderness ratio gives a constant effective length coefficient k (equation 3.3). The reason for fixing this effective length coefficient k is that it is widely accepted and is significant for design purposes.

It is evident from Figures 3.5 and 3.6 that the variation in the slenderness ratio alone does not significantly influence the hysteresis behavior regarding the order of plastic-hinge formation. This is because the balanced strength ratio is not so sensitive with the variation only in the member slenderness ratio for any fixed value of k (see Section 4.1.1).

For the E regions at the same Δ/Δ_y and the corresponding SP regions at the same Δ/Δ_y of the hysteresis loops of members with different slenderness ratios, the member with lower slenderness ratio displays steeper slope. This is consistent with the physical behavior that a shorter member is stiffer than a longer member with other properties being the same. The magnitude of the difference in these

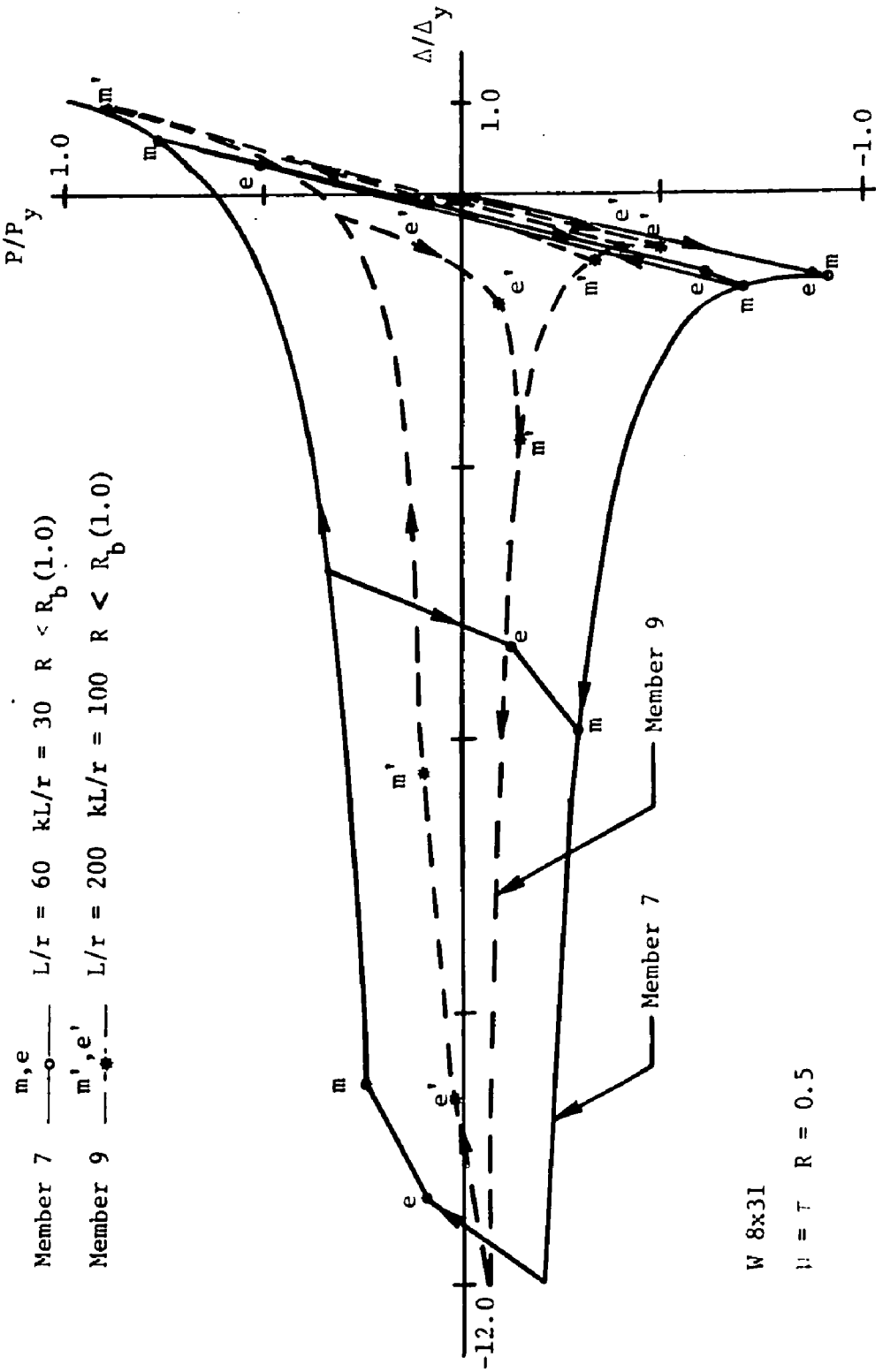


Figure 3.5 Influence of Slenderness Ratio on the Hysteresis Behavior

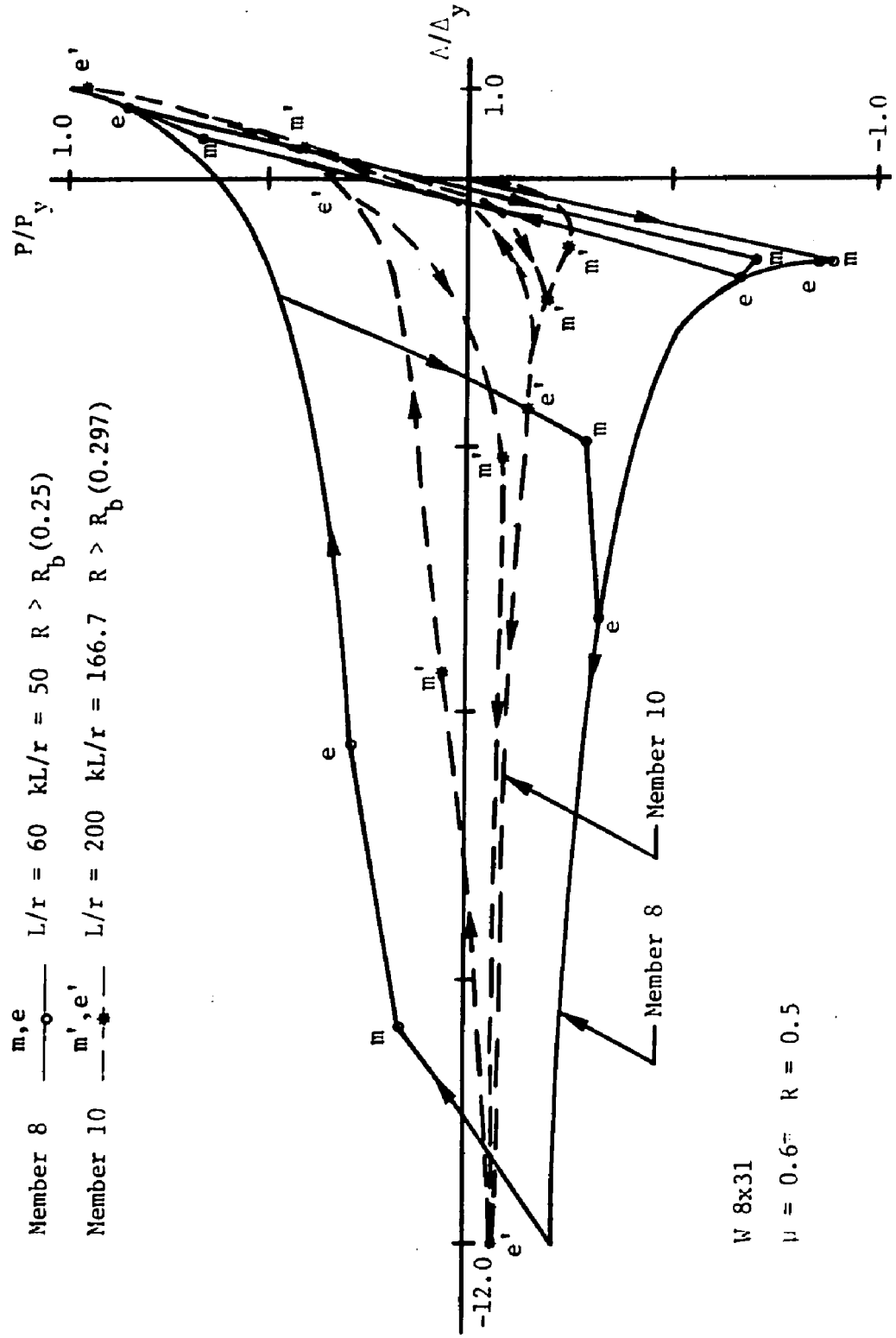


Figure 3.6 Influence of Slenderness Ratio on the Hysteresis Behavior

slopes will be studied in the next chapter. The maximum compressive load resisted by a shorter member is also, as expected, higher than that of the longer member.

For the corresponding DP regions of the different hysteresis loops, the shorter member sustains higher magnitude of load than the longer member at the same Δ/Δ_y. The percentage of difference in this magnitude of load is quite close to the percentage of difference in the lengths of the members. Thus, for the same range of Δ/Δ_y on the hysteresis loops of members of different lengths, more normalized energy is dissipated by a less slender member (area under the normalized hysteresis loop is the normalized energy dissipation).

Another interesting phenomenon that should be brought to attention here is the change in shapes of the DP regions after the occurrence of the second plastic hinge on the compression envelope curves of members with different slenderness ratios. Figure 3.7 shows the compression envelope curves of W 8x31 pin-ended members with L/r = 200, 60, 30, 15, and 1, respectively. It is evident that the beginning portion of the DP region is quite flat for L/r = 200 member. Then a reduction in L/r results in a more rapid loss of compressive load as demonstrated by L/r = 60. Further reduction in L/r results in a less rapid loss in compressive load until it becomes almost constant as L/r approaches zero. This phenomenon can be explained by

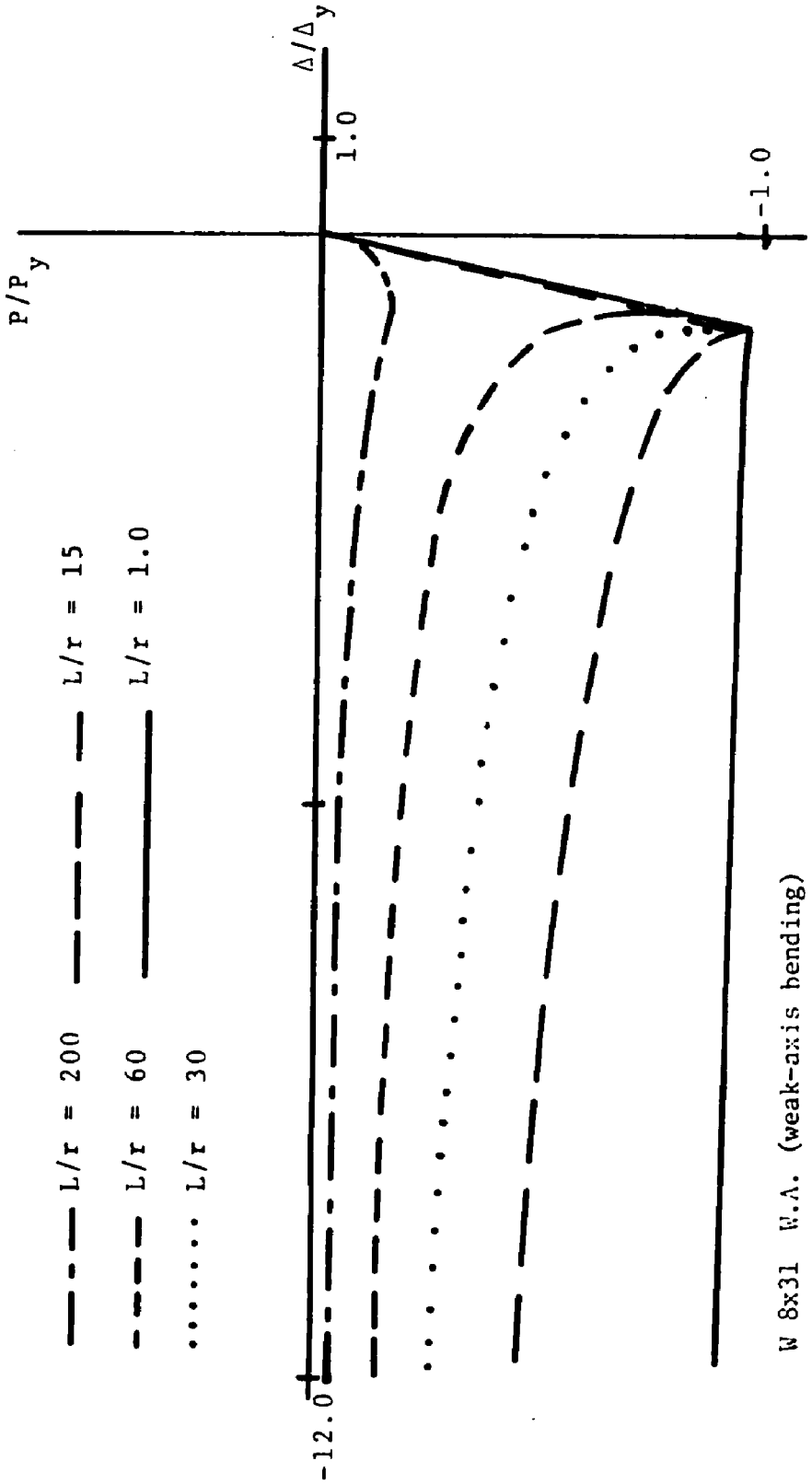


Figure 3.7 Comparison of the DP Regions of Pin-Ended Members with Different L/r

investigating the governing equation of the DP region.

The Δ/Δ_y of the DP region is given by the equation

$$\frac{\Delta}{\Delta_y} = \frac{2AE}{P_y L}\left[\frac{L}{2} - \sqrt{\left(\frac{L}{2} - \frac{PL}{2AE}\right)^2 - \left(\frac{M_{pcc} + M_{pcm}}{P}\right)^2}\right] \quad (4.1a)$$

The introduction and application of this equation will be given later in Section 4.1.3. The term $(\frac{L}{2} - \frac{PL}{2AE})$ is the deformed half length of the member which is assumed to be equal to the length of chord AB (Figure 2.8), and the term $(\frac{M_{pcc} + M_{pcm}}{P})$ is equal to Y_m. Differentiating equation (4.1a) with respect to P/P_y gives

$$\frac{d\ \frac{\Delta}{\Delta_y}}{d\ \frac{P}{P_y}} = \frac{(\frac{1}{2} - \frac{P}{2AE}) - U - V}{\frac{X_m}{L}} \quad (3.3)$$

where $$U = \frac{4AE\ (1 + R)^2 M_p\ M_{pcm}}{PL^2 P_y^2}$$

$$V = \frac{2AE\ (1 + R)^2\ M^2_{pcm}}{P^3 L^2}$$

and M_p = plastic moment of the member

The ratio of the deformed half length, $(\frac{1}{2} - \frac{P}{2AE})$, to the member length, and X_m/L are both approximately equal to 0.5 at the occurrence of the second plastic hinge for these members of different L/r. Therefore, the variations in shape of the DP-region starting portions are mainly due to the variations of U and V which indirectly reflect the rate of

change of Y_m with respect to P.

For a large L/r member, V has large value and is a dominant term while U has small value. This means that the slope of the hysteresis curve (P/P_y - Δ/Δ_y plot) at the DP-region beginning portion is negative and quite flat as shown by L/r = 200 member in Figure 3.7. Decrease in L/r reduces the values of both U and V until L/r is about 60. Then further decrease in L/r increases U while V continues reducing. For L/r between 100 and 15, both U and V are small which makes $\frac{d\frac{\Delta}{\Delta_y}}{d\frac{P}{P_y}}$ either a small negative or small positive value. This means that the loss in compressive load is rapid with small change in Δ/Δ_y. When L/r becomes very small, U assumes a very large value, and the corresponding slope is negative and very flat. This large U can be thought of as the geometric effect. All the conclusions are verified by the hysteresis curves shown in Figure 3.7.

Another way of showing the change in axial load for these members after the midspan plastic hinge has occurred is to show the magnitudes of the drop in compressive load from the maximum compressive load (at the occurrence of the midspan plastic hinge) to the load at some point on the DP region. For this purpose, the function $\frac{P_{max} - P_{(\Delta/\Delta_y=12)}}{P_y}$ for these members is plotted against L/r and shown as curve A in Figure 3.8. This curve indicates that this normalized

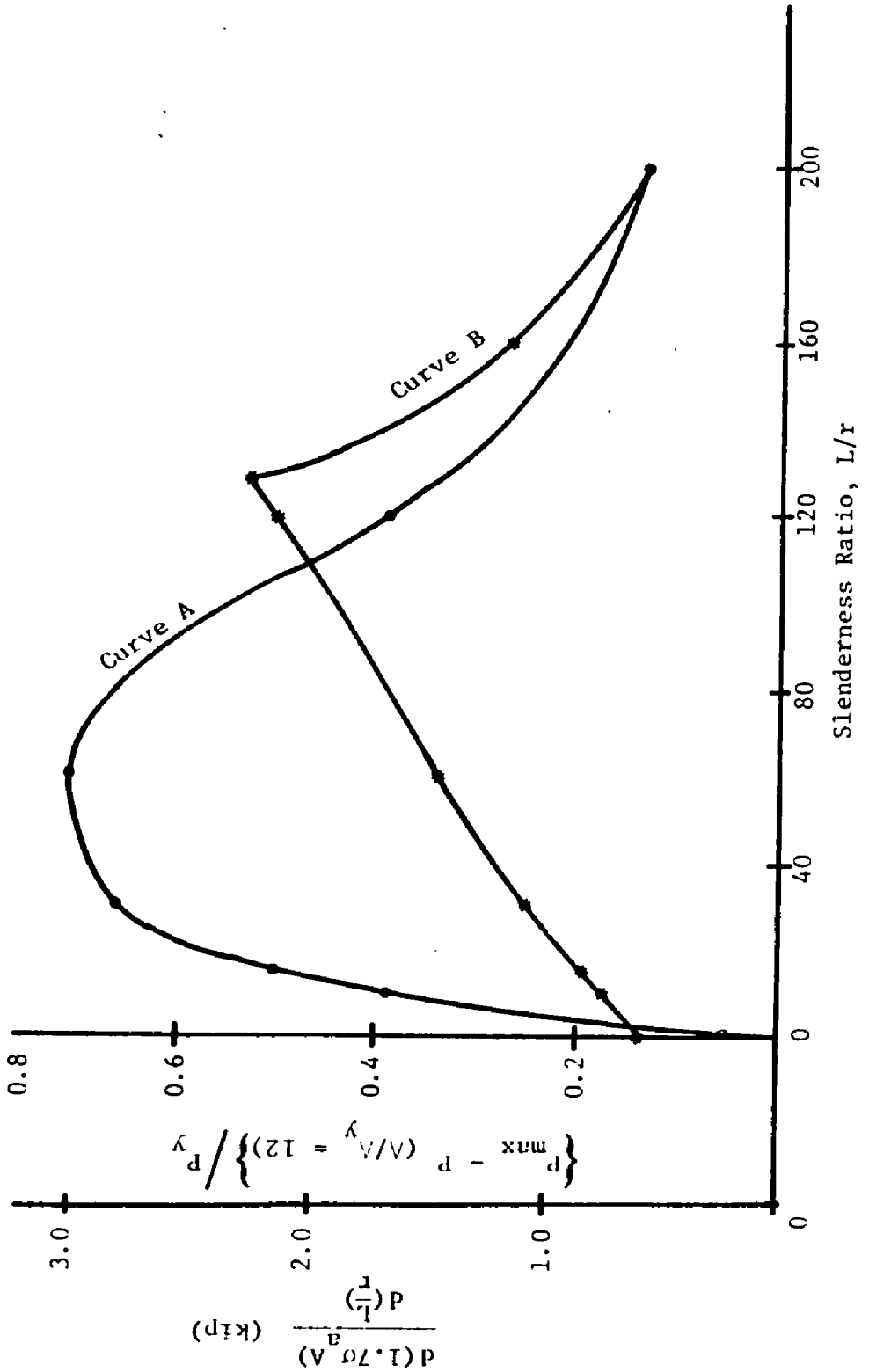


Figure 3.8 Drop in Compressive Load (Curve A) and Rate of Change of AISC Plastic Design Column Strength (Curve B)

drop in compressive load increases from almost zero for a very short member and reaches a maximum at L/r around 60. Then the drop starts decreasing as the slenderness increases.

Also in Figure 3.8, the absolute value of the rate of change of the AISC plastic design column strength[43] with respect to L/r, $\left| \frac{d(1.7\sigma_a A)}{d\left(\frac{L}{r}\right)} \right|$, is plotted against L/r and shown as curve B. This curve shows that, starting from a very short member, this magnitude increases with increasing L/r and reaches a maximum at L/r = 126.1 (for σ_y = 36 ksi, E = 29,200 ksi). Then it decreases as the slenderness increases. The L/r = 126.1 is the dividing value of the slenderness ratio between the elastic and the inelastic regions as defined by the AISC formulas.

It is evident from Figure 3.8 that both the drop (curve A) and the rate of change of axial compression strength (curve B) increase as L/r increases up to a value of L/r around 60. Then the drop starts decreasing while the rate of change of strength keeps on increasing with increase in L/r until L/r = 126.1 is reached. Thereafter, increase in L/r corresponds to decrease in both the drop and the rate of change of strength. From this, it may be observed that, for pin-ended members with L/r < 60, the inelastic behavior seems to dominate over the slenderness effect. For pin-ended members with L/r ranging from 60 to 126.1, the inelastic behavior and the slenderness effect

may be equally significant. And for pin-ended members with L/r > 126.1, the slenderness effect seems to dominate over the inelastic behavior. Hence, this information might allow one to divide the slenderness ratio of axially loaded pin-ended members into three regions, namely, small (L/r < 60), intermediate (60 < L/r < 126.1), and large (L/r > 126.1)

3.4. Influence of the Member Cross-Sectional Properties

In the preceding comparisons, only W 8x31 members which were constrained to bend about their weak axis were used. Consequently, it is natural to evaluate the effect on the hysteresis behavior of using members with different cross sectional properties as well as having the member buckle about the strong axis. To serve this purpose, additional weak-axis-bending hysteresis loops of the W 12x190 and the W 14x22 members and strong-axis-bending hysteresis loop of the W 12x190 member have been generated. The W 8x31 members were selected because axial compression test results for these members were available for comparison (Figure 2.4). The W 12x190 and W 14x22 members are selected to vary the cross-sectional properties from those of the W 8x31 members.

Figure 3.9 shows the comparison of the weak-axis-bending hysteresis loops of the W 8x31 and the W 14x22 members with the same slenderness ratio and the same

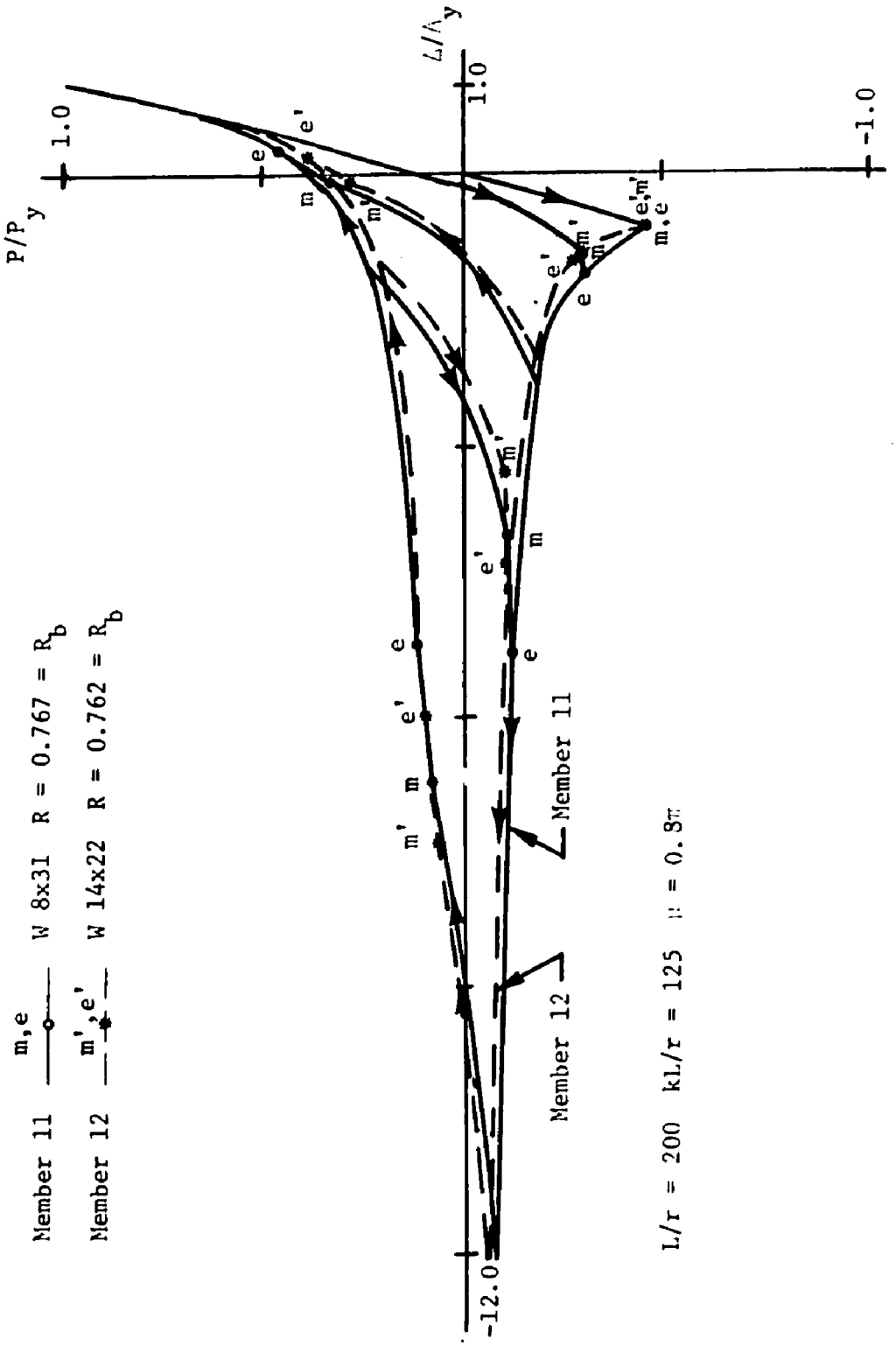


Figure 3.9 Influence of Cross-Sectional Properties on the Hysteresis Behavior

connection properties (same μ and R). Similar comparison of the weak-axis-bending hysteresis loops of the W 8x31 and the W 12x190 members with these same member and connection properties reveals virtually no difference and, therefore, is not shown here. Both hysteresis loops in Figure 3.9 show similar pattern of plastic-hinge formation. Along the corresponding DP regions at the same Δ/Δ_y, the hysteresis loop of the W 8x31 member shows higher magnitude of P/P_y than that of the W 14x22 member. It can be verified that along the corresponding DP regions, the member with greater Z/Ar value sustains higher magnitude of P/P_y than the member with smaller Z/Ar value at the same Δ/Δ_y. Physically Z/A represents the influence of the bending and axial strengths of the member and connection and r represents the influence of the member length on the magnitude of P/P_y. The weak axis Z/Ar values of W 8x31, W 12x190, and W 14x22 members are 0.764, 0.787, and 0.650, respectively which confirms the observed results about the relative magnitude of P/P_y of the corresponding DP regions. The slopes of the E regions at the same Δ/Δ_y and of the corresponding SP regions at the same Δ/Δ_y of the hysteresis loops of these members are practically the same. Also, there is virtually no difference in the maximum normalized compressive load (P/P_y) of both members in Figure 3.9. This equal compressive load capacity is expected since both members have the same kL/r.

With regard to the effect of bending about

different axes, the hysteresis loops of the weak- and the strong-axis-bending of the W 12x190 members were generated and are shown in Figure 3.10. Both members, having similar properties of the member and connections, show no difference in the order of plastic-hinge formation. However, along the corresponding DP regions at the same Δ/Δ_y, the strong-axis-bending member sustains higher magnitude of P/P_y. This again confirms the observation regarding the Z/Ar value because this value of 0.956 about the strong axis of W 12x190 member is higher than the corresponding value of 0.787 about the weak axis. Again, the slopes of the E regions at the same Δ/Δ_y and of the corresponding SP regions at the same Δ/Δ_y of both hysteresis loops differ only slightly. The difference in the normalized compressive load capacities of both members also is practically negligible.

From the above study, it can be concluded that, except for the variation in the magnitude of P/P_y of the DP region, the variation in the cross-sectional properties and the difference in the axis of bending without changing other member and connection properties do not significantly affect the hysteresis behavior.

3.5. Influence of Simultaneous Variation of Several Parameters

The preceding parametric studies involve variation

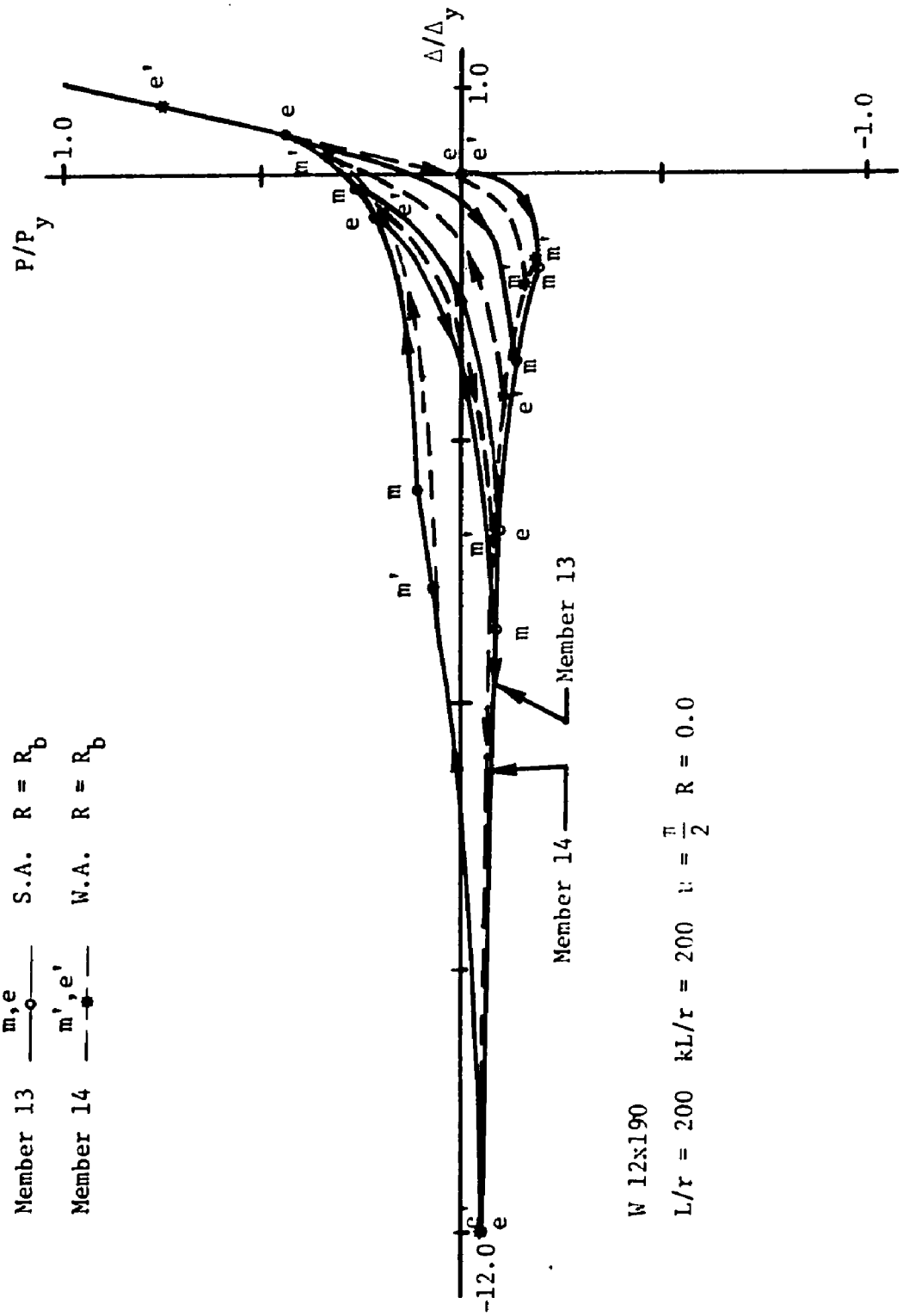


Figure 3.10 Influence of Axis of Bending on the Hysteresis Behavior

of only one parameter at a time. However, one would expect some relationship of the hysteresis behaviors of members that differ in more than one parametric property, for example, one would expect some resemblance in the hysteresis loops of different members that have the same effective slenderness ratio (kL/r). Such a study is conducted in this section.

Figure 3.11 shows the hysteresis loops of two W 8x31 members with the same kL/r as indicated. The slopes of the E regions of both members at the same Δ/Δ_y are practically the same. The longer member, which is a fixed-ended member with balanced strength connections, exhibits no SP region while the shorter member, having greater than balanced strength connections, shows the SP region. The maximum compressive loads of both members are almost equal. However, along the corresponding DP regions at the same Δ/Δ_y, the shorter member sustains higher magnitude of load than the longer member.

The above observation suggests that the corresponding DP regions of both hysteresis loops should be closer to each other if the connection strength of the shorter member is reduced to some extent. This idea is verified by the comparison of the hysteresis loops in Figure 3.12 for which the connection strength of the shorter member is reduced to be approximately equal to its balanced connection strength while there is no change in the properties of the longer member. As expected, the

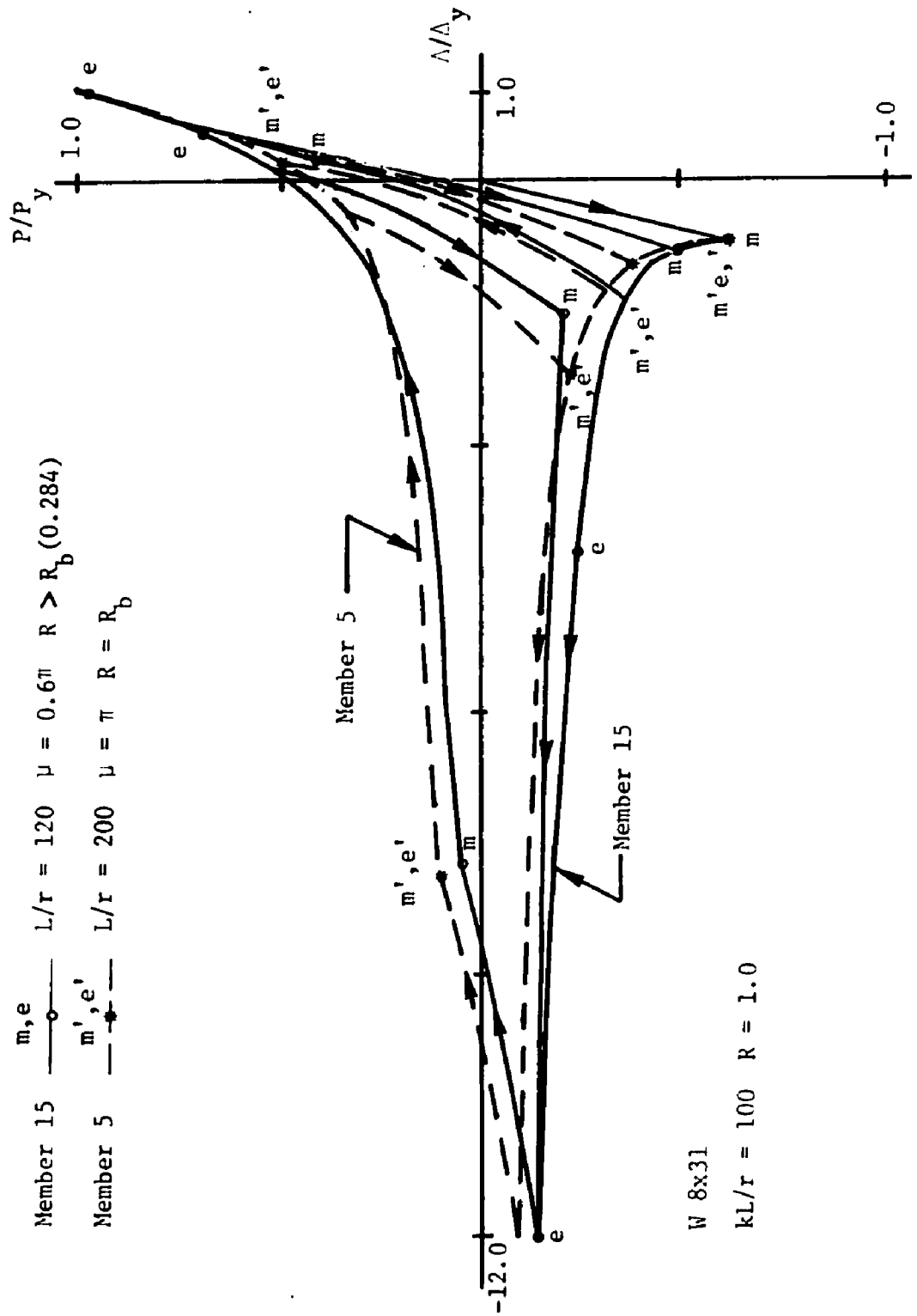


Figure 3.11 Influence of Effective Slenderness Ratio on the Hysteresis Behavior

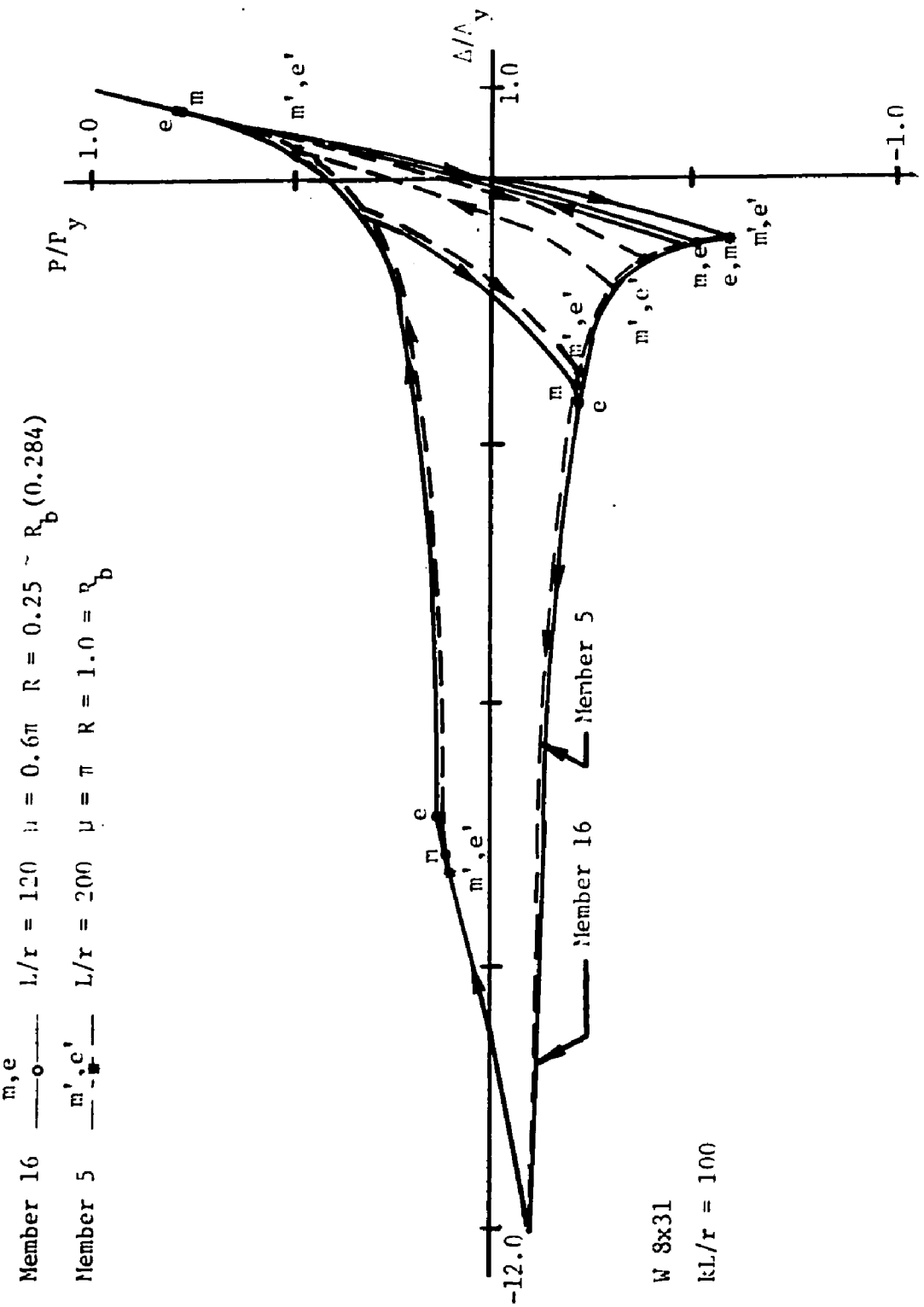


Figure 3.12 Influence of Effective Slenderness Ratio on the Hysteresis Behavior

corresponding DP regions of both hysteresis loops in Figure 3.12 are almost the same. The SP regions of the shorter member are also very short compared with those of Figure 3.11, and they are practically the same curve as the corresponding DP regions (envelope curves). The conclusions about the similarities in the slopes of the E regions and in the maximum compressive load carried by the member stated for Figure 3.11 also apply in this case.

This study indicates that there are only minor differences in the hysteresis loops of members with the same kL/r regardless of the values of k and L provided that the connection strength of each member is the balanced connection strength.

3.6. Conclusions

The introduction of this chapter presented several definitions and terms for the convenience of discussion in this dissertation. Sections 3.1 - 3.5 concluded the influence of different parameters on the hysteresis behavior qualitatively. Quantitative studies of the influence of these parameters and a semi-graphical construction of hysteresis curves will be developed in Chapter IV. It should be mentioned that changing the modulus of elasticity E from 30,000 to 29,000 ksi only changes the hysteresis-loop coordinates slightly without affecting the general hysteresis behavior shown here.

CHAPTER IV

SEMI-GRAPHICAL CONSTRUCTION OF THE HYSTERESIS CURVES

The qualitative study of the influence of different parameters on the hysteresis behavior was conducted in the previous chapter. Observations were made regarding the change in behavior of different regions of the hysteresis loop due to the variation of the parameters. In this chapter, that information is gathered and presented in a form suitable for introducing an empirical method of constructing the theoretical hysteresis curves. The members are subdivided into three groups on the basis of the connection strength. Group 1 consists of the members with balanced strength connections, Group 2 deals with the members with smaller than balanced strength connections, and Group 3 deals with the members with greater than balanced strength connections.

The semi-graphical construction of the hysteresis loop is intended to serve as a tool for generating approximate hysteresis curves without a computer and the program discussed in Chapter II. This method can be accomplished conveniently with a pocket calculator. The various observations and formulations introduced throughout this chapter also will provide an understanding of the parametric effects on the hysteresis behavior both qualitatively and quantita-

tively.

The sign convention used in this chapter is the same as that used in Chapter II. For the load, compression is positive, and, for the relative end displacement, shortening of the distance between the ends is positive. As in Chapter II, this sign convention is reversed in the hysteresis-loop plot to make it consistent with the usual plot sign convention. Also, for convenience of the discussions to follow, the CISP region of the hysteresis loop of a member loaded from the initial imperfection configuration is referred to as the envelope CISP region. Table 4.1 lists the properties of the members employed for study in this chapter. The properties of the wide flange cross section used for these members were given in Table 3.2. The member numbers are consistent with Table 3.1.

TABLE 4.1. PROPERTIES OF MEMBERS

Member	L/r	kL/r	μ	L (in)	k_Θ (k-in/rad)	R	R_b	Shape	Figure
1	60	50	0.6π	120.6	1.127×10^4	1.0	0.25	W 8x31	4.14
2,3*									
4	200	100	π	402	1.446×10^8	0.25	1.0	W 8x31	4.10
5	200	100	π	402	1.446×10^8	1.0	1.0	W 8x31	4.3
6-16*									
17	60	33.3	0.9π	120.6	1.602×10^5	0.826	0.826	W 8x31	4.5
18	200	125	0.8π	402	1.91×10^4	0.767	0.767	W 8x31	4.6
19	60	33.3	0.9π	120.6	1.602×10^5	0.25	0.826	W 8x31	4.11
20	200	153.8	0.65π	402	5.746×10^3	0.1	0.434	W 8x31	4.12
21	200	153.8	0.65π	402	5.746×10^3	1.0	0.434	W 8x31	4.13, 4.15

Remark: All members have E = 30,000 ksi and subjected to weak-axis bending.
*listed in Table 3.1.

4.1. The Member with Balanced Strength Connections

For each set of the other properties of the member and connection, there is one balanced connection strength. For the member with balanced strength connections (except for a pin-ended member), plastic hinges always occur at the midspan and at the ends simultaneously or not long after one another. The balanced strength connection case is, therefore, the boundary between the case where plastification occurs or reoccurs first at the member ends ($R < R_b$) and the case where plastic hinge occurs or reoccurs first at the midspan ($R > R_b$).

4.1.1. The Balanced Strength Ratio

The first thing that should be established in this section is the way to determine the balanced strength or equivalently, the balanced strength ratio. To directly compute the balanced strength ratio of a member with known member and connection properties by using the equations in Chapter II is very difficult without the aid of a computer. So the numerical data of the balanced strength ratio were obtained by using the computer program of Chapter II and presented by graphs as shown in Figure 4.1. The balanced strength ratio R_b is plotted against the connection stiffness parameter μ for discrete values of the slenderness ratio L/r for the weak-axis bending of W 8 x 31 members. The comparisons of these graphs and the corresponding graphs

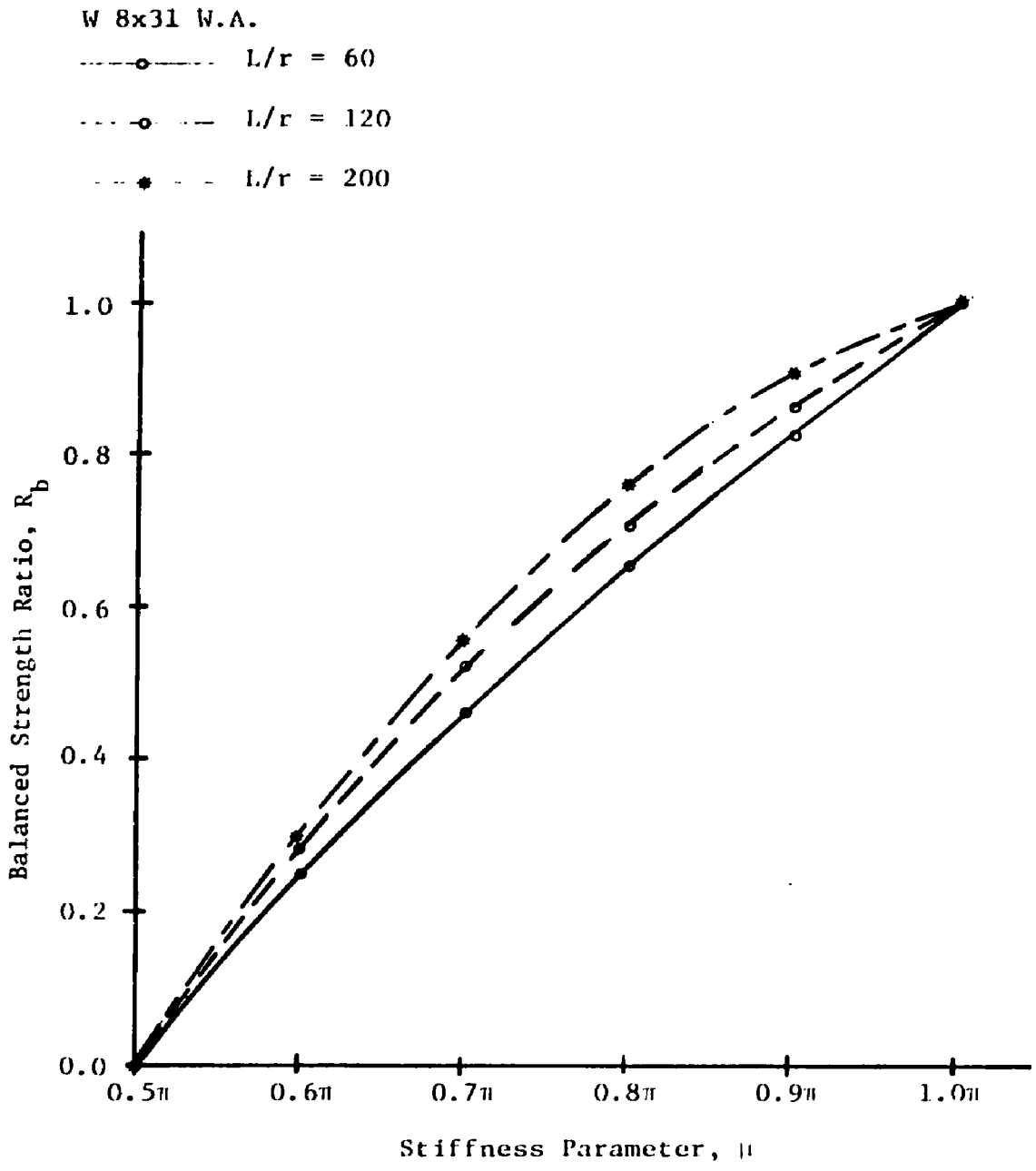


Figure 4.1 Balanced Strength Ratio for Various Member Slenderness Ratios

of the weak- and strong-axis bending of members using several different wide flange cross sections revealed differences of less than 2 percent and, therefore, is not shown here. So, for practical purposes, these graphs are recommended for the balanced strength ratio of all wide flange cross sections subjected to bending about either axis (L/r has more influence on the balanced strength ratio than cross-sectional properties).

When a member and its connection stiffness is selected, L/r and μ are fixed. These values can be used in Figure 4.1 to give the value of R_b. If L/r is not exactly 60, 120, or 200, then interpolation can be exercised to determine the required R_b.

4.1.2. The Maximum Compressive Load

Another controlling value of the $P/P_y - \Delta/\Delta_y$ hysteresis loop is the magnitude of the maximum compressive load. For a member with balanced connection strength, this load is attained at the occurrence of the simultaneous plastification at midspan and at the member ends on the envelope curve. As previously discussed in Chapters II and III, the member with the selected initial plastic rotation angles and with the connection that has larger or equal strength to the balanced strength connection sustains a maximum compressive load that is approximately equal to that given by the modified AISC formula [equation (2.1)] for the given kL/r. Therefore, a load that is equal to or slightly

smaller than that given by equation (2.1) for the given kL/r can be used as the maximum compressive load of the corresponding member with balanced or larger than balanced strength connections.

4.1.3. The Double Plastic Rotation Region

From the equations in Chapter II, the relation between P and the Δ/Δ_y of the DP region of the hysteresis loop can be obtained as

$$\frac{\Delta}{\Delta_y} = \frac{2AE}{P_y L}\left[\frac{L}{2} - \sqrt{\left(\frac{L}{2} - \frac{PL}{2AE}\right)^2 - \left(\frac{M_{pcc} + M_{pcm}}{P}\right)^2}\right] \qquad (4.1a)$$

This equation is simple, and the Δ/Δ_y value can be easily computed for any given value of P. This formula is retained for the semi-graphical construction of the hysteresis loop. Equation (4.1a) can be rearranged in the form

$$\frac{P}{P_y} = \pm \frac{1}{P_y}\left[\frac{M_{pcc} + M_{pcm}}{\sqrt{\left(\frac{L}{2} - \frac{PL}{2AE}\right)^2 - \left(\frac{\frac{AE}{P_y} - \frac{\Delta}{\Delta_y}}{\frac{2AE}{P_y L}}\right)^2}}\right] \qquad (4.1b)$$

where the positive (negative) sign is used for the compression (tension) envelope curve. This form is desirable for the purpose of iterating for the value of P/P_y corresponding to a given value of Δ/Δ_y by assuming a starting value of P. The iteration procedure using equation (4.1b) will converge only for a large positive value of Δ/Δ_y ($\Delta/\Delta_y \gtrsim 2.0$). For

negative or small positive Δ/Δ_y, equation (4.1a) can be used to generate the DP region.

Equation (4.1) also provides a means for comparing the relative P/P_y values of the DP regions for different members at the same Δ/Δ_y. An approximate ratio of these P/P_y values is given by the equation

$$\left(\frac{\frac{P_1}{P_{y1}}}{\frac{P_2}{P_{y2}}}\right)_{\text{approx.}} = \frac{(1 + R_1)}{(1 + R_2)} \frac{Z_1}{Z_2} \frac{L_2}{L_1} \frac{A_2}{A_1} \tag{4.2}$$

where the subscripts 1 and 2 indicate that the subscripted quantities belong to member 1 and member 2, respectively. This equation is also useful in estimating the difference in the normalized energy dissipation for the same interval of Δ/Δ_y of the hysteresis loops of different members.

As an example, this equation will be applied for the parametric study in Section 3.4. The variation only in the cross section or the axis of bending implies $R_1 = R_2$, $\frac{L_2}{L_1} = \frac{r_2}{r_1}$. Equation (4.2) then gives

$$\left(\frac{\frac{P_1}{P_{y1}}}{\frac{P_2}{P_{y2}}}\right)_{\text{approx.}} = \frac{\frac{Z_1}{A_1 r_1}}{\frac{Z_2}{A_2 r_2}} \tag{4.2'}$$

Equation (4.2') (already utilized in Section 3.4) indicates that, at the same Δ/Δ_y on the DP regions, the member with

greater Z/Ar value sustains higher magnitude of P/P_y. The approximate normalized axial load ratio from equation (4.2') for the weak-axis bending of W 8 x 31 and W 14 x 22 members is 1.18. The actual ratio obtained from the hysteresis curve in Figure 3.9 varies from 1.31 at $\Delta/\Delta_y = 12.0$ on the compression side to 1.0 at the tension yield load.

4.1.4. Slope of the E-Region Curve

From the observations in Chapter III, it can be concluded that:

a) the slope of an E region depends on the effective slenderness ratio (kL/r) of the member (Section 3.5),

b) the slope of an E region depends on the value of Δ/Δ_y at the intersection of this region or its extension with the Δ/Δ_y axis (Δ/Δ_y at zero load),

c) the slope of an E region does not depend on the strength ratio R of the member (Section 3.1), and

d) the slope of the ECIP region and that of the ETIP region at the same Δ/Δ_y are approximately the same for any member hysteresis loop.

It is possible to collect the information about the slopes of the E regions of various hysteresis loops and present them in the form of a chart which gives the value of the slope for each pair of given values of kL/r and Δ/Δ_y at zero load. It should be mentioned that when the E region

is linear, the slope and the Δ/Δ_y of the slope are the exact values. However, when the E region is curvilinear, kL/r>60 (high kL/r), two slopes are used to define the E region. The first is the average slope on the compression side of the region and the second is the slope on the tension side of the region. The Δ/Δ_y at zero load is the intersection between these two straight lines.

The data points in Figure 4.2 were collected from a number of hysteresis curves of various effective length coefficients (k). The slope and the Δ/Δ_y at zero load of each data point were collected as described above. Some of the data were taken from the ECIP and some from the ETIP regions. The slope chart as given in Figure 4.2 will be useful in the semi-graphical construction of the hysteresis curves.

4.1.5. Construction of the Hysteresis Curve of a Member with Balanced Strength Connections

One final approximation needs to be introduced to complete the semi-graphical construction of the hysteresis curve of a member with balanced strength connections. As explained in Sections 3.1, the SP region for this type of member is very short for a nearly fixed-ended member and a little longer but virtually the same as the corresponding DP region for a nearly pin-ended member. Therefore, it is assumed that there is no SP region for the member with balanced strength connections or, more precisely, plastic

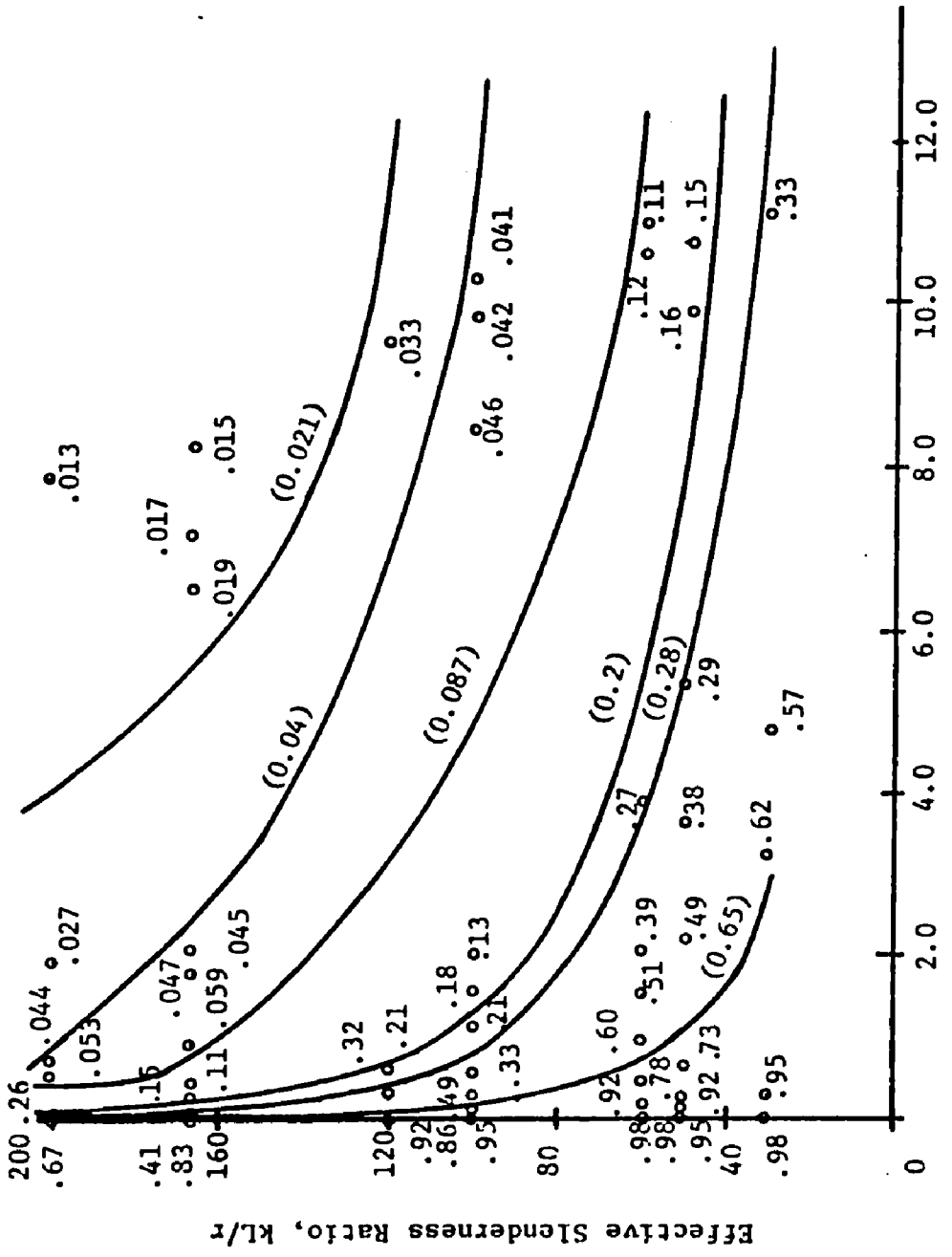


Figure 4.2a Slope of the Elastic Region on the Compression Side of the Normalized Hysteresis Loop

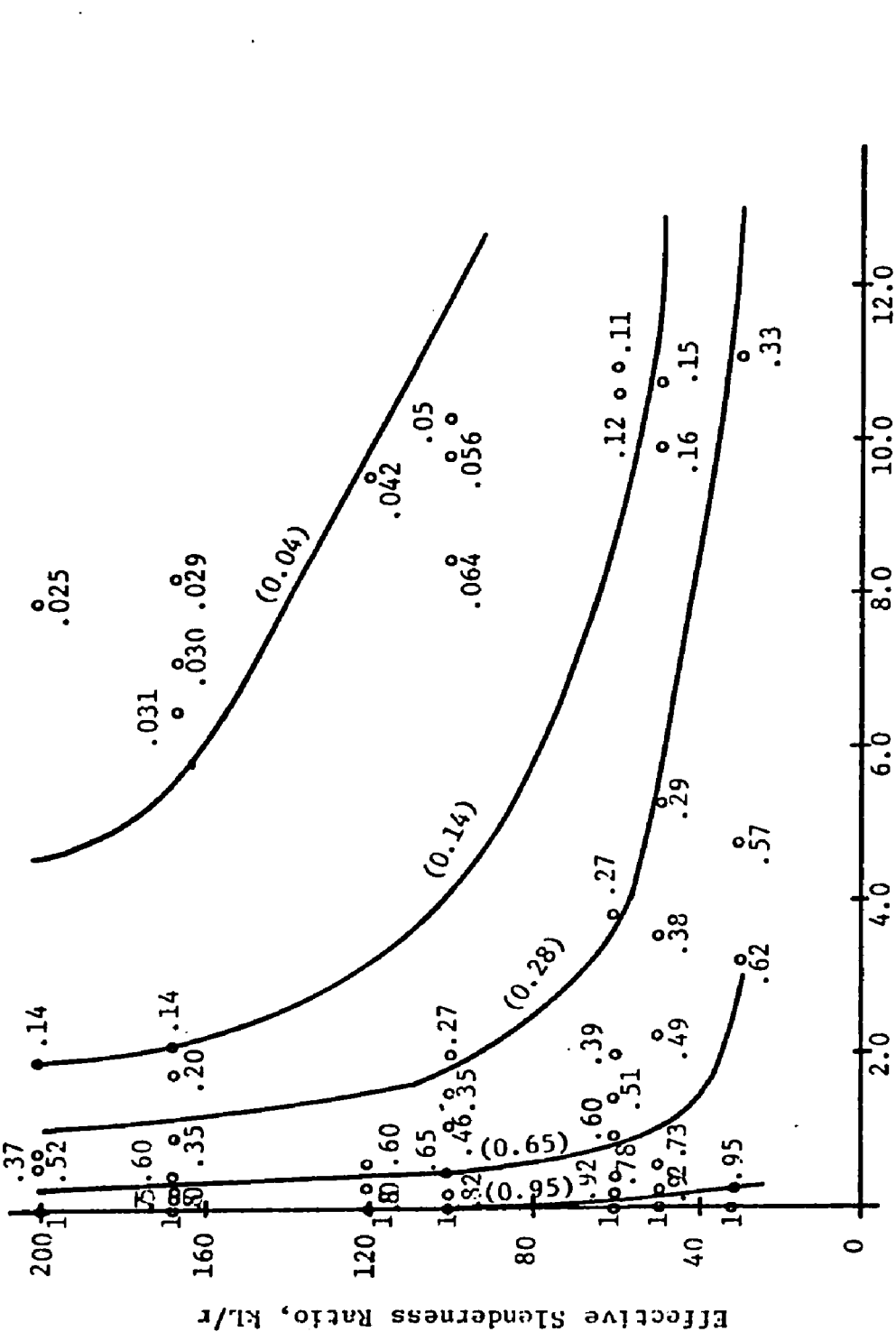


Figure 4.2b Slope of the Elastic Region on the Tension Side of the Normalized Hysteresis Loop

hinges always occur simultaneously at midspan and at the ends for this type of member.

For known member properties and connection stiffness parameter μ, the corresponding value of R_b can be obtained from Figure 4.1, and so all the member and the connection properties are determined. Figure 4.3 shows a hysteresis loop generated by this semi-graphical method for a member with balanced strength connections. For the IE region, path A-B, the initial Δ/Δ_y is a small non-zero value which results from the initial plastic rotation angles. Thus, a straight line is drawn from the origin with the slope obtained from Figure 4.2a for the given value of kL/r and for $\Delta/\Delta_y = 0$. There are two possible shapes of this region:

a) Referring to Figure 4.4a, the line from the origin terminates at point A' where the load equals the maximum compressive load P_{max} given by equation (2.1) for the given kL/r. Then a straight line of constant load is drawn from point A' to point B which is on the CIDP curve (equation 4.1). This shape usually occurs for members with high kL/r values.

b) Referring to Figure 4.4b, the line from the origin terminates at point B which is also on the CIDP curve. This time there is no flat region (A'-B of Figure 4.4a), and the compressive load at point B is equal to or slightly lower than P_{max}. This shape usually occurs for

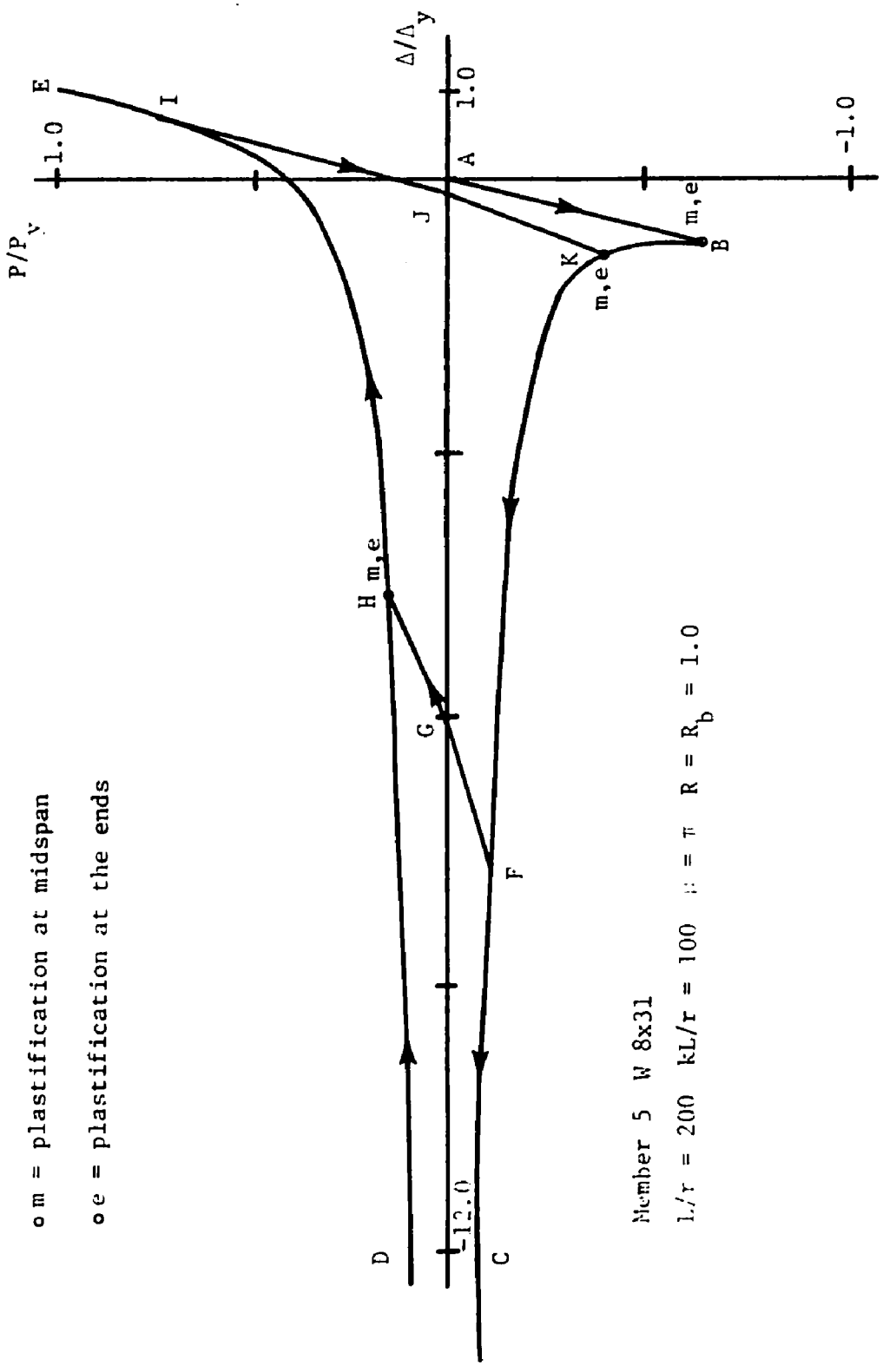


Figure 4.3 Hysteresis Curve for a Member with Balanced Strength Connections Using Semi-Graphical Construction

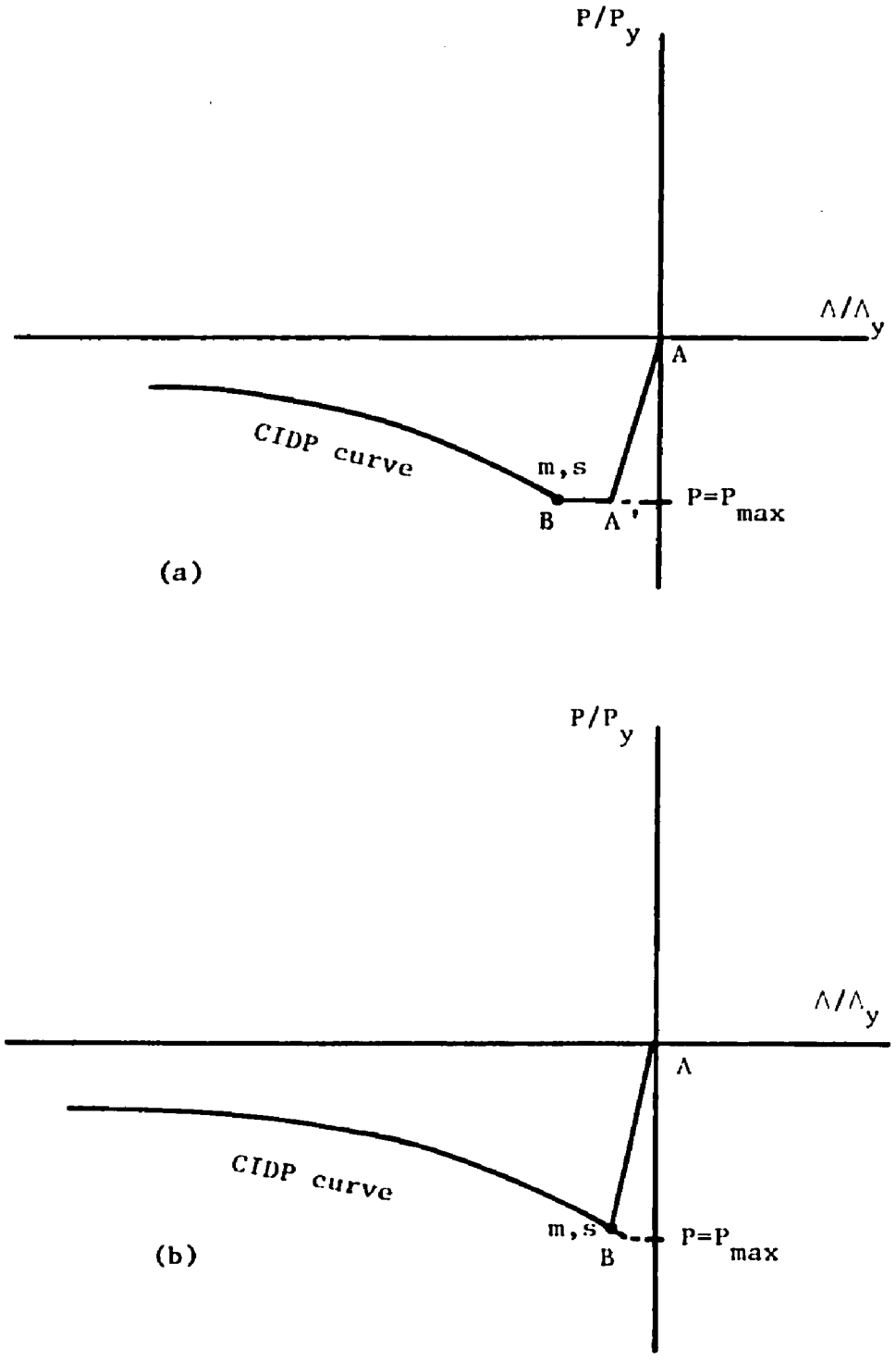


Figure 4.4 The Initial Elastic Region

members with low kL/r values.

The member is assumed to plastify at midspan and at the ends simultaneously when point B is reached. Then the CIDP region (curve B-C of Figure 4.3) can be constructed by using equation (4.1). The TIDP region, curve D-E, can also be constructed from equation (4.1).

If the direction of the relative end displacement is reversed at point F along curve B-C (Figure 4.3), the member behaves elastically along path F-G-H. Path F-G-H is constructed by using one of the two possible ways as follows:

a) For low kL/r members where only one slope is needed for the E region, a trial line is drawn from point F with a trial slope until it intersects the Δ/Δ_y axis at point G. Then the slope corresponding to the kL/r of the member and the Δ/Δ_y at point G is determined from Figure 4.2a. If the trial slope is steeper (lower) than the slope from Figure 4.2, a new trial line with lower (steeper) slope is drawn from point F until it intersects the Δ/Δ_y axis at a new point G. The new trial slope is checked with the slope from Figure 4.2 for the Δ/Δ_y at the new point G. The process of redrawing the line from point F is repeated until the trial slope agrees with the slope from Figure 4.2 for the Δ/Δ_y at zero load. The final line F-G is then extended to meet the tension envelope curve at point H.

b) For high kL/r members where two slopes are

needed for the E region, the same method as used in case a) to get line F-G is repeated. Then, a second straight line G-H with the slope obtained from Figure 4.2b (slope on the tension side) for the given kL/r of the member and the Δ/Δ_y at point G is drawn from point G to meet the tension envelope curve at point H.

At point H, the member is assumed to replastify at the ends and midspan simultaneously. Further increase in tensile load forces the member to stretch along the TIDP region, curve H-E. If the direction of the member relative end displacement is reversed at point I along curve H-E, the member again behaves elastically along path I-J-K. The construction of path I-J-K is analogous to the construction of path F-G-H, but this time the construction starts with the slope on the tension side. At point K, the member is assumed to plastify at midspan and at the ends simultaneously. Further shortening of the member length corresponds to loading along curve K-C, the CIDP region.

Hence, the semi-graphical construction of the hysteresis curve of a member with balanced strength connections has been fully established. This method also will serve as a basis for the following construction of a hysteresis curve of the member with connection strength that is smaller or larger than the balanced connection strength. Figures 4.5 and 4.6 show comparisons of hysteresis curves of members with balanced strength connections using the recommended semi-graphical construction and those

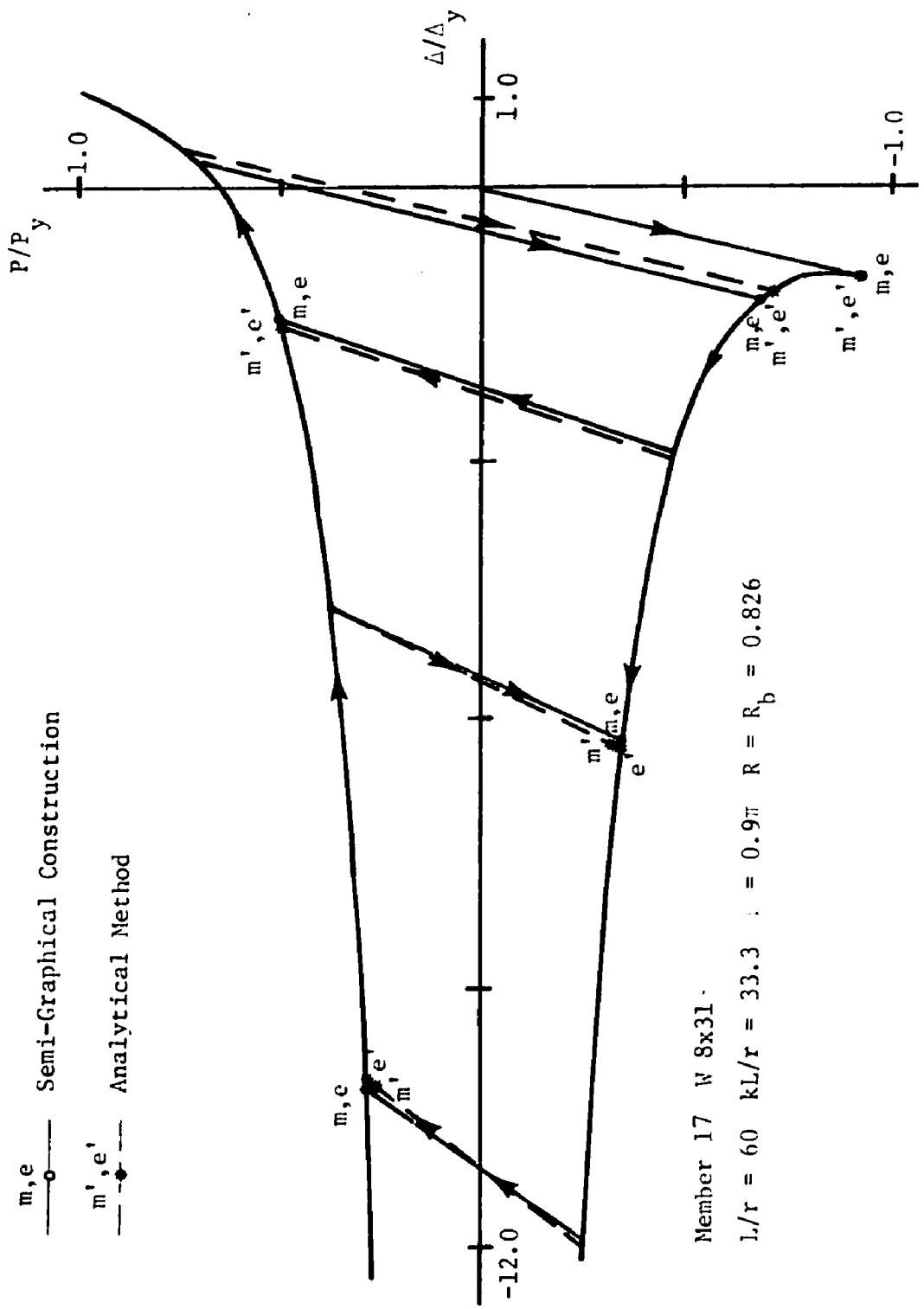


Figure 4.5 Comparison of the Graphical and the Analytical Hysteresis Curves for L/r = 60

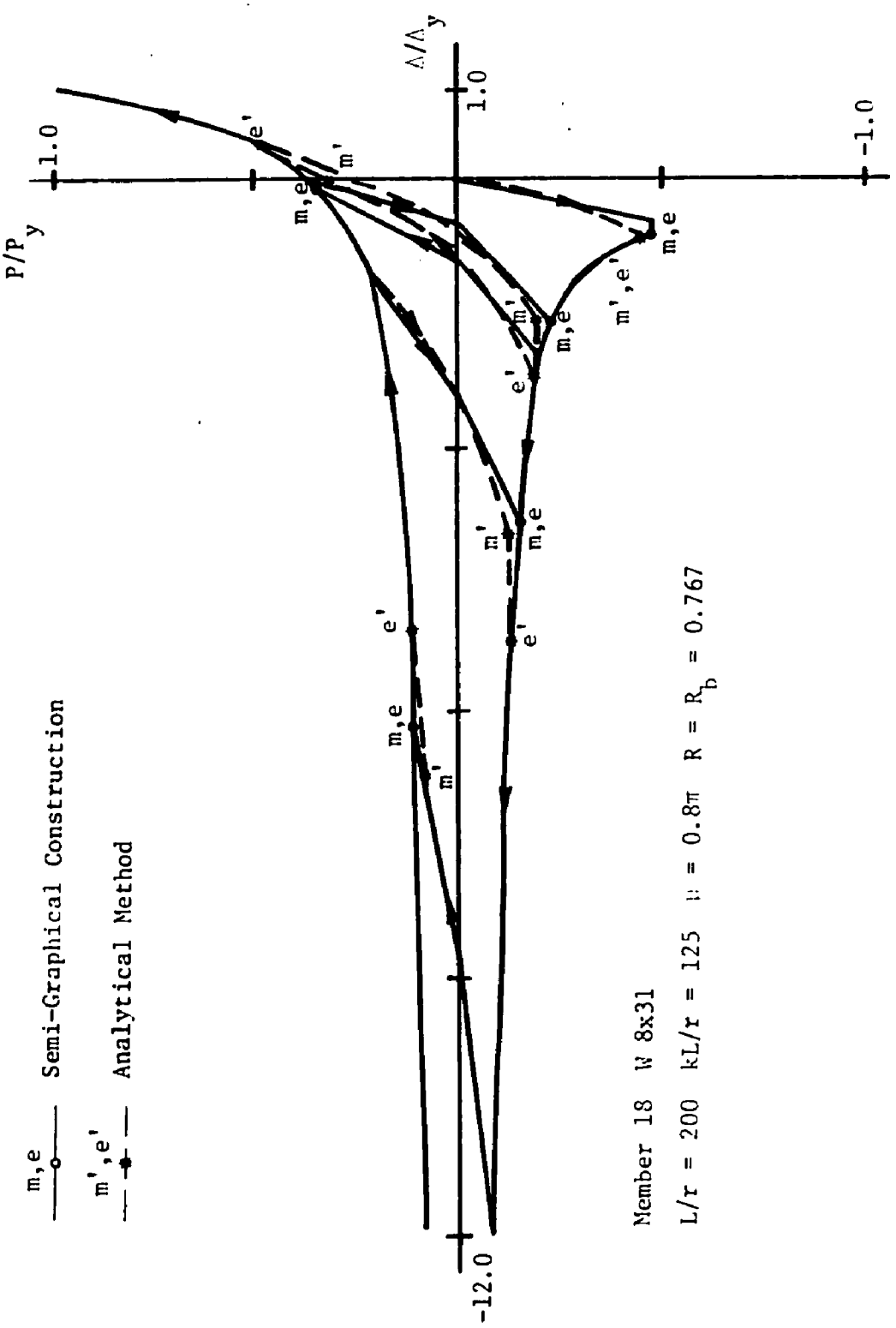


Figure 4.6 Comparison of the Graphical and the Analytical Hysetersis Curves for L/r = 200

computer generated from the equations in Chapter II. It is evident that the agreement is better for the hysteresis curves for members with lower kL/r and higher μ since the elastic region of the semi-graphical construction is more accurate for members with lower kL/r, and the assumption that there is no SP region is more accurate for members with higher μ.

4.2. The Member with Smaller than Balanced Strength Connections

The essential differences between the hysteresis behavior of the member with smaller than balanced strength connections and that of the member with balanced strength connections are explained in this section. All the controlling equations together with complete semi-graphical construction of the hysteresis curve of the member with smaller than balanced strength connections are given. The reference member of a given member with smaller or larger than balanced strength connections is defined here as the member that has the same member properties and connection stiffness as the given member but has the balanced connection strength.

4.2.1. The Compressive Load at the Occurrence of the First and the Second Plastification Along the Compression Envelope Curve

As observed in Section 3.1 in loading the member with

initial imperfection, the magnitude of the compressive loads at the occurrence of the plastic hinges at the connections and at midspan of the member with smaller than balanced strength connections are lower than those of the member with balanced strength connections. The approximate compressive load P_{r1} at the occurrence of plastic hinges at the connections along the compression envelope curve is given by the equation

$$\frac{P_{r1}}{P_{max}} = \frac{3R}{R_b} \; ; \; 0 \leq \frac{R}{R_b} \leq 0.25 \qquad (4.3a)$$

and

$$\frac{P_{r1}}{P_{max}} = \frac{1}{3}\frac{R}{R_b} + \frac{2}{3} \; ; \; 0.25 \leq \frac{R}{R_b} \leq 1.0 \qquad (4.3b)$$

where P_{max} is the maximum compressive load given by equation (2.1) for the kL/r of this member. The comparison of the graphs of P_{r1}/P_{max} against R/R_b using equation (4.3) and the corresponding graphs using the equations in Chapter II is shown in Figure 4.7a for members with $\mu = \pi$ ($R_b = 1.0$) and in Figure 4.7b for members with $\mu = 0.6\pi$ ($R_b \sim 0.3$), respectively. The corresponding approximate and exact values of the load are in good agreement.

After plastification occurs at the connections, further loading along the envelope CISP region causes plastic rotation at the connections until a plastic hinge occurs at midspan. At this stage, the approximate compressive load P_{r2} is given by the equation

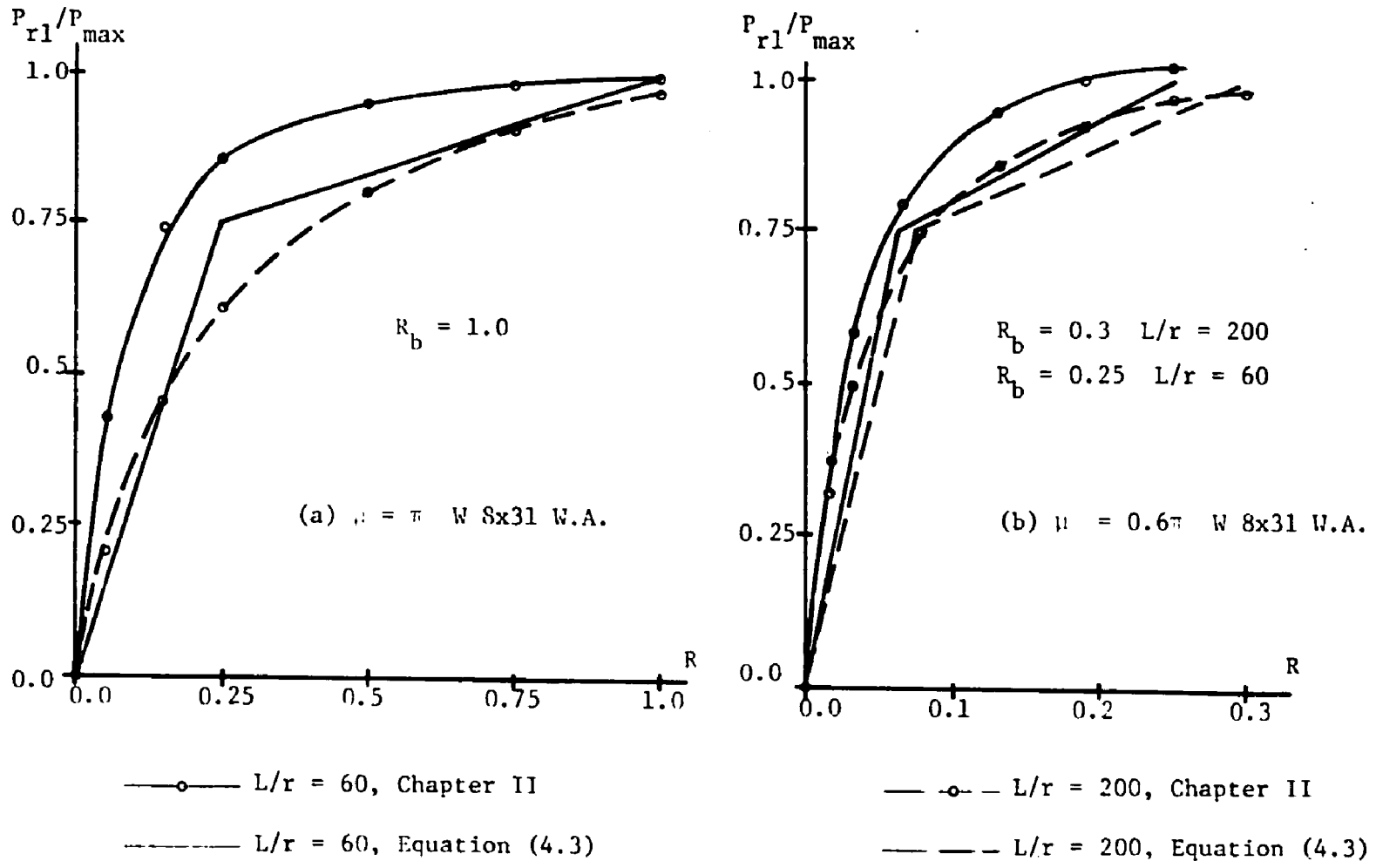


Figure 4.7 Compressive Load at the Occurrence of the Connection Plastic Hinges on the Envelope Curve

$$\frac{P_{r2}}{P_{max}} = \left[1 - \frac{P_{max}\ (\frac{L}{r})}{P_{max}}\right]\frac{R}{R_b} + \frac{P_{max}\ (\frac{L}{r})}{P_{max}} \qquad (4.4)$$

where $P_{max}\ (\frac{L}{r})$ is the maximum compressive load given by equation (2.1) for the member using $\frac{kL}{r} = \frac{L}{r}$. This member behaves exactly the same as the pin-ended member of length L/r when R = 0. As before, the comparison of the graphs of P_{r2}/P_{max} against R/R_b employing equation (4.4) and the corresponding graphs using the equations in Chapter II is shown in Figure 4.8a for members with $\mu = \pi$ and in Figure 4.8b for members with $\mu = 0.6\pi$. Again the corresponding approximate and exact values of the load are in good agreement.

After the plastic hinge occurs at midspan, the CIDP region is governed by equation (4.1).

4.2.2 The Slope and Length of the E-Region Curve

In Section 3.1 it was concluded that change in the connection strength of a member alone does not affect the slope of the E region if the Δ/Δ_y axis intersection of the region remains unchanged. So the chart in Figure 4.2 also provides the slope of the E region for the member with smaller than balanced strength connections for given kL/r and Δ/Δ_y. With regard to the length of the E region with smaller than balanced strength connections, it was observed in Section 3.1 that reduction in the connection strength resulted in a reduction in the length of the E region for

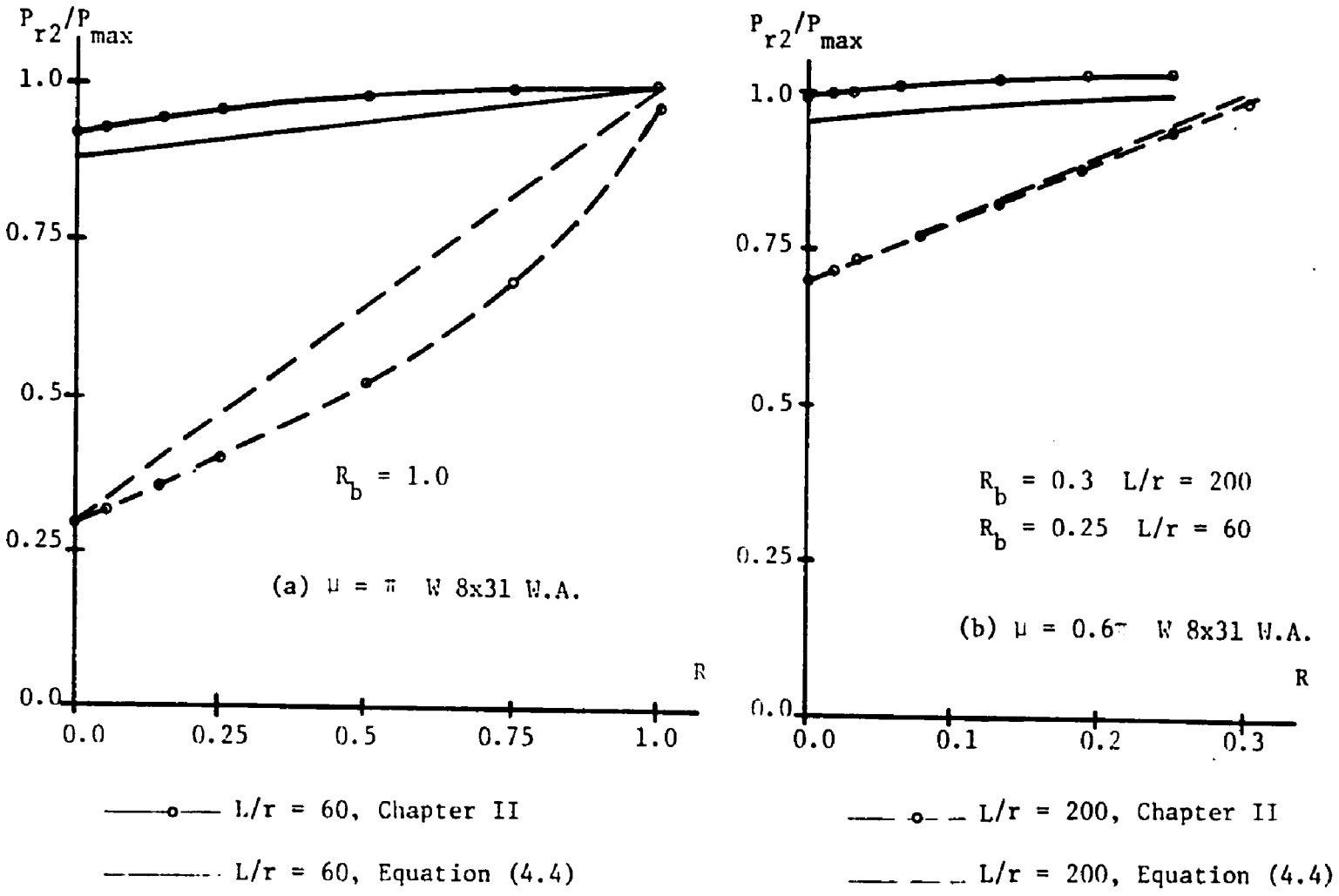


Figure 4.8 Compressive Load at the Occurrence of the Midspan Plastic Hinge at the End of the Envelope CISP Region

the same Δ/Δ_y. This reduction roughly depends on R/R_b, kL/r, and Δ/Δ_y axis intersection. The ECIP-region length with smaller than balanced strength connections and the ECIP-region length with balanced strength connections at the same Δ/Δ_y can be approximately related by the equation

$$\left[\frac{\ell_{c(R)}}{\ell_{c(R_b)}}\right] \underset{\text{approx.}}{=} c_1 \frac{R}{R_b} \quad ; \quad R < R_b \tag{4.5a}$$

where $\ell_{c(R)}$ and $\ell_{c(R_b)}$ denote the ECIP-region length with $R < R_b$ and the ECIP-region length with $R = R_b$ at the same Δ/Δ_y respectively, and

$$\left.\begin{aligned} c_1 &= \frac{1 - c_2}{12.0}\left(\frac{\Delta}{\Delta_y}\right) + c_2 \; ; \; \frac{\Delta}{\Delta_y} \leq 12.0 \\ c_1 &= 1.0 \qquad\qquad ; \; \frac{\Delta}{\Delta_y} > 12.0 \end{aligned}\right\} \tag{4.5b}$$

$$\left.\begin{aligned} c_2 &= \frac{1 - c_3}{40}\left(\frac{kL}{r}\right) + \frac{3c_3 - 1}{2} \; ; \; 20 \leq \frac{kL}{r} \leq 60 \\ c_2 &= c_3 \quad ; \; \frac{kL}{r} < 20 \\ c_2 &= 1 \quad ; \; \frac{kL}{r} > 60 \end{aligned}\right\} \tag{4.5c}$$

and $$c_3 = -1.0\left(\frac{R}{R_b}\right) + 2.0 \tag{4.5d}$$

Δ/Δ_y is the value at the intersection of the region or its extension with the Δ/Δ_y axis.

Analogously the approximate relation between the corresponding ETIP-region lengths with $R < R_b$ and with

$R = R_b$ is given by

$$\left[\frac{\ell_{t(R)}}{\ell_{t(R_b)}}\right]_{approx.} = d_1 \frac{R}{R_b} \quad ; \quad R < R_b \tag{4.6a}$$

where $\ell_{t(R)}$ and $\ell_{t(R_b)}$ denote the ETIP-region length with $R < R_b$ and the ETIP-region length with $R = R_b$ at the same Δ/Δ_y, respectively, and

$$\left.\begin{aligned} d_1 &= \frac{1 - d_2}{12.0}\left(\frac{\Delta}{\Delta_y}\right) + d_2 \; ; \; \frac{\Delta}{\Delta_y} \leq 12.0 \\ d_1 &= 1.0 \qquad\qquad\quad ; \; \frac{\Delta}{\Delta_y} \geq 12.0 \end{aligned}\right\} \tag{4.6b}$$

and $$d_2 = -1.0\left(\frac{R}{R_b}\right) + 2.0 \tag{4.6c}$$

Again Δ/Δ_y is the value at the intersection of the region or its extension with the Δ/Δ_y axis.

The ECIP and the ETIP regions may each possess either one or two slopes depending on the kL/r value of the member and on the length of the region (whether or not it spans both the compression and the tension sides of the hysteresis loop).

4.2.3. The Slope of the Tension Induced Single Plastic Rotation Region

In Section 3.1, it was observed that there is no difference in the hysteresis behavior of members that differ only in the connection stiffness (same L/r, different kL/r)

if all the connections have zero strength. This implies that the TISP regions of these members at the same Δ/Δ_y have the same slope. Also, it was observed that, for the case where $R < R_b$, the slopes of the TISP regions at the same Δ/Δ_y of members that differ only in the connection strength are approximately the same. Therefore, it can be concluded that the slopes of the TISP regions at the same Δ/Δ_y of the members with different connection stiffnesses and strengths are virtually the same provided that all the members have the same L/r and have $R < R_b$. This slope is approximately the same as the slope of the E region at the same Δ/Δ_y of a member with kL/r equal to L/r. This is true because at the same Δ/Δ_y, the TISP region of the member with zero strength connection is the same as the ECIP region of the non-zero strength pin-ended member of length L/r.

A member with a strength ratio much smaller than the balanced strength ratio can have plastification of the connections at the termination of the ECIP region while the member is still subjected to compressive load. Hence, the TISP region includes the compression induced plastic rotation at the connections in addition to the usual tension induced plastic rotation. Similarly, the CISP region that follows the ETIP region may include the tension induced plastic rotation at the connections in addition to the usual compression induced plastic rotation. For this kind of member, two slopes may be required for the TISP

region of semi-graphical construction.

Physically, the occurrence of the plastic hinges at the connections eliminates flexural resistance of the connection to increased moment at the member ends. Hence, the axial stiffness of members with small R ($R < R_b$) and with the same L/r can be expected to be the same at the same Δ/Δ_y along the TISP region.

4.2.4. Physical Constraints of the CIP Region Reversing from the TIP Region

There are two physical constraints of the CIP region reversing from the TIP region which will be useful for the semi-graphical construction of the hysteresis curve introduced in the next section:

a) Referring to curve E-F-K-G-H-L-E of Figure 4.9, if the ECIP region initiates at point E on the CIDP region and if the ETIP region initiates at point G where the member just replastifies at midspan under tensile load, then the corresponding CISP region (curve H-E) must terminate at point E since there is no change in the plastic rotation angle at midspan. Now, suppose the ETIP region initiates at point K on the TISP region (curve F-G), then the ETIP region (curve K-L) must terminate at point L which is on the CISP region (curve H-E) since again, there is no change in the plastic rotation angle at midspan.

b) If the ECIP region initiates at point A where the member just plastifies at midspan along the envelope

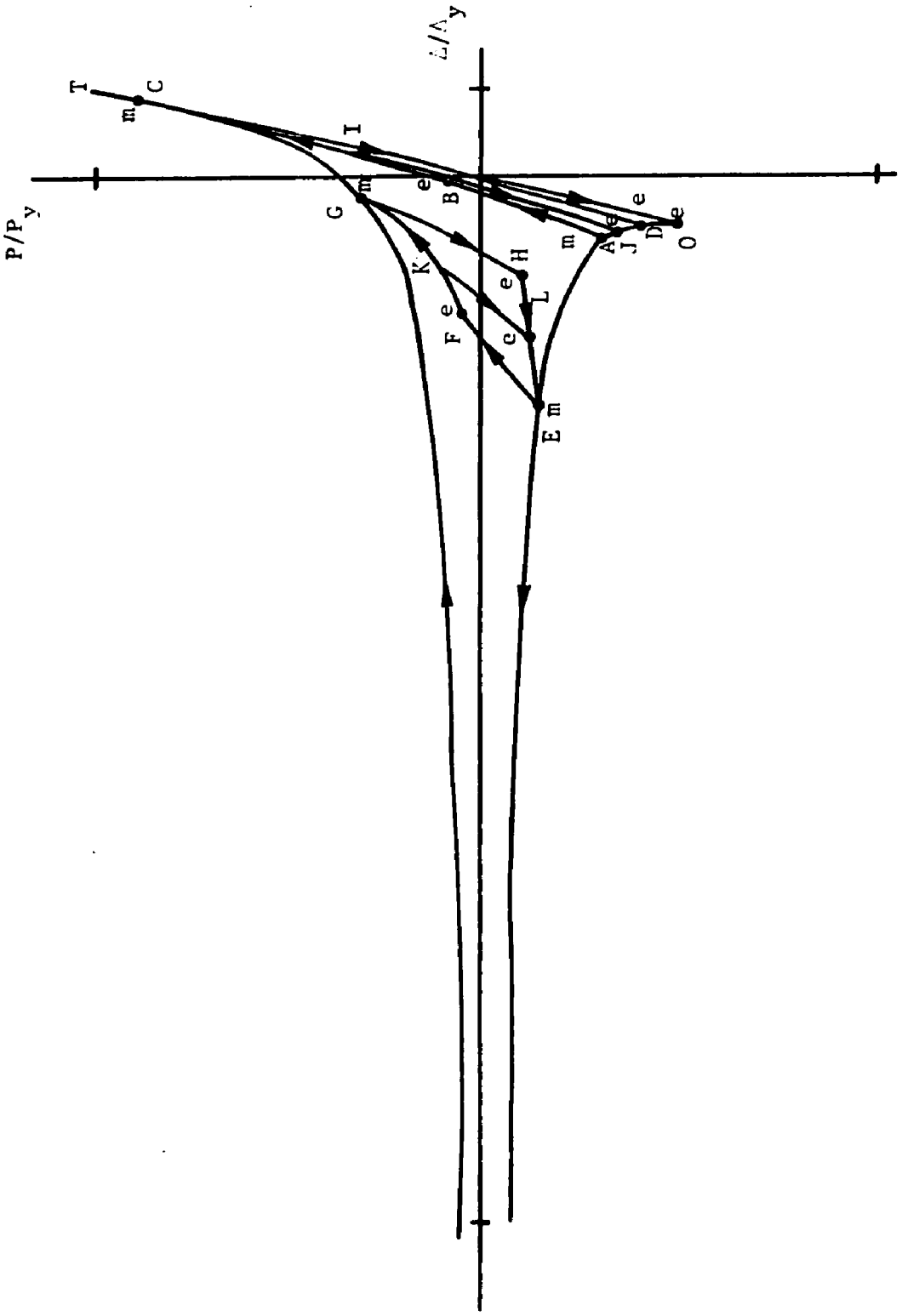


Figure 4.9 Physical Constraints of the Hysteresis Curve of a Member with Smaller than Balanced Strength Connections

CISP region (curve O-A) and if the ETIP region initiates at point C where the member just replastifies at midspan or at any point along curve C-T (T is the tension yield point), then ETIP region is assumed to terminate at some point along the envelope CISP. This assumption is consistent with the restriction that residual plastic rotation angles less than 0.005 radian are restored to 0.005 radian in compression reloading as explained in Chapter II. Also if the ETIP region initiates at point I on the TISP region (curve B-C), this ETIP region (curve I-J) also terminates at some point along the envelope CISP region.

4.2.5. Construction of the Hysteresis Curve for the Member with Smaller than Balanced Strength Connections

Figure 4.10 shows the hysteresis curve of a member with smaller than balanced strength connections generated by semi-graphical construction. Path A-B, the IE region, is a straight line drawn from point A (the origin) with the slope obtained from Figure 4.2a for the given kL/r and for $\Delta/\Delta_y = 0$ to point B. The load at point B where plastic hinges occur at the connections is given by equation (4.3). The value of the load at point C where the member just plastifies at midspan is obtained from equation (4.4), and the corresponding value of Δ/Δ_y can be derived from equation (4.1). A straight line is then drawn from point B to point C to represent the envelope CISP region. Then, the CIDP region (curve C-D) and the TIDP region (curve E-F)

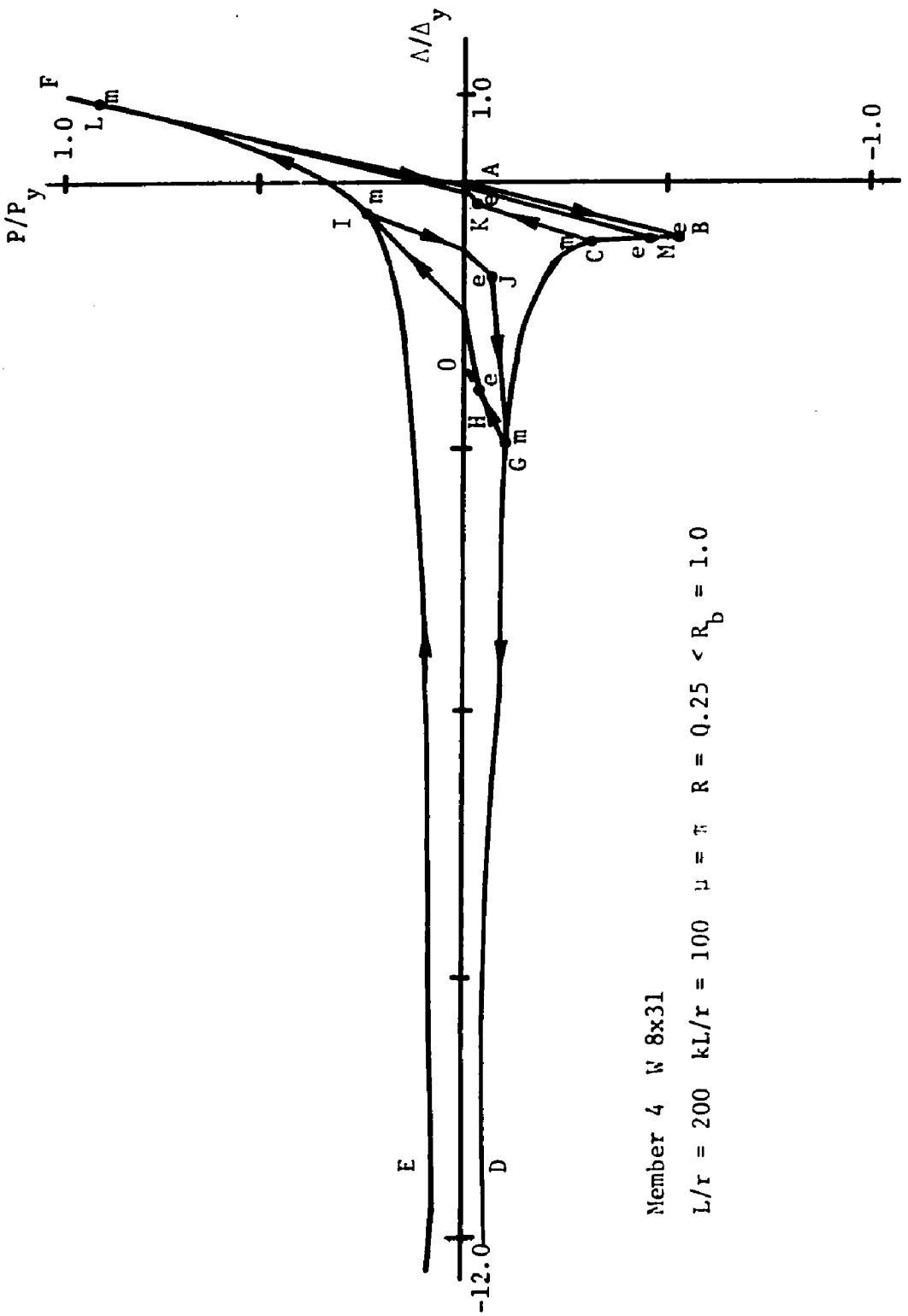


Figure 4.10 Hysteresis Curve for a Member with Smaller than Balanced Strength Connections Using Semi-Graphical Construction

can be constructed by using equation (4.1).

When the direction of the relative end displacement is reversed at point G along curve C-D, elastic behavior (path G-H) prevails. The length of G-H is given by equation (4.5), and so it is necessary to determine the value of $\ell_{c(R_b)}$. This is done by using trial and error method of section 4.1.5 to establish the slope of this region and the Δ/Δ_y at point O which is the zero load point. Then $\ell_{c(R_b)}$ at this Δ/Δ_y is obtained from the hysteresis loop of the reference member and the length of G-H is determined from equation (4.5). Since both the slope and length of G-H are known, point H can be established. Path G-H consists of either one or two straight lines depending on the number of slopes required for this region. At point H, plastic hinges reoccur at the connections.

The TISP region, path H-I, is then constructed by the same trial and error method of matching the slope of a straight line through point H and the Δ/Δ_y at zero load point of this line with the corresponding values from Figure 4.2, but now the slope of the E region of the member with kL/r equal to L/r of this member is used. Path H-I may consist of either one or two straight lines depending on the number of slopes required for this region. Path H-I meets the tension envelope curve at point I where plastification reoccurs at midspan. If the members begin to shorten at point I, the ETIP region, curve I-J, is constructed by a trial and error method similar to that used in the ECIP

region, but this time the value of $\ell_{t(R)}$ (length of path I-J) is given by equation (4.6). The hysteresis loop of the reference member is needed to establish the value of $\ell_{t(R_b)}$ which is used in equation (4.6a). Path I-J consists of either one or two straight lines depending on the number of slopes required. Once the point where plastic hinges occur at the connections is located, point J, a line is drawn from point J to point G to represent the CISP region. At point G, the member plastifies at midspan. Thus, the first physical constraint, discussed in Section 4.2.4a, is utilized. If path I-J is very short, line J-G may intersect paths G-H or H-I. This can happen because of straight lines have been used to approximate the actual curves of the E and the SP regions. In this case, path I-J is extended until line J-G can be drawn without intersecting path G-H or H-I.

Additional constraints were observed in Section 4.2.4b for the small displacement and large tension regions. To utilize these constraints, the above construction of curve G-H-I-J-G is modified to construct curve C-K-L-M-C for the change in direction of the displacement from point C (where the member just plastifies at midspan on the envelope curve). The length of L-M of the ETIP region is not governed by equation (4.6) but, rather, by the constraint described in Section 4.2.4b. So this ETIP region terminates on line B-C which is the envelope CISP region. If a ETIP region initiates anywhere along curve L-F (F is the tension

yield point), that ETIP region also terminates on line B-C. Also, if the ETIP region initiates anywhere along the TISP region (curve H-I or curve K-L), physical constraints described in Sections 4.2.4a and b can be utilized to generate this ETIP region.

This section contains details of the semi-graphical construction of the hysteresis curve for a member with smaller than balanced strength connections. One unavoidable limitation arises from the non-uniformity of the slope of the CISP region. The CISP region, similar to curve J-G, cannot be constructed from the ETIP region, similar to curve I-J, which starts from an arbitrary point between I and F on curve E-F without knowing the location of the starting point of the parent ECIP and TISP regions, point G. However, after the loop G-H-I-J-G and similar loop are constructed some distance apart, interpolation can be used to determine the curve and, thus, override this limitation.

Figures 4.11 and 4.12 illustrate the comparison of the hysteresis curves for these types of members using semi-graphical construction and using the equations of Chapter II. As in Section 4.1.5, the agreement is better for the member with lower kL/r since the E region by semi-graphical construction is more accurate then. When the connection strength is very small, it is difficult to construct curves like the curve G-H-I-J-G of Figure 4.10. For this case, the hysteresis curve can be approximated by the hysteresis curve of a member with zero strength connections.

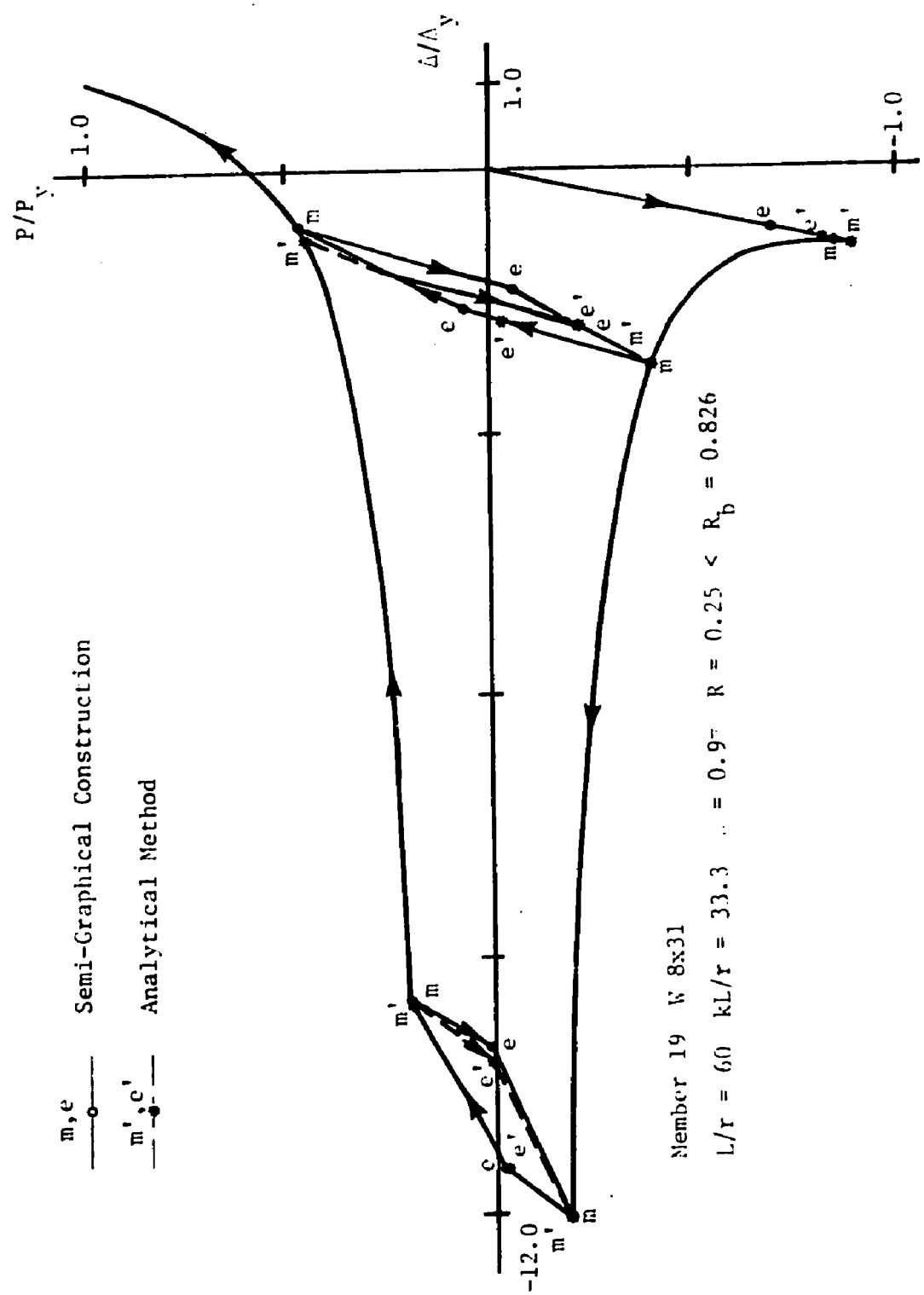


Figure 4.11 Comparison of the Graphical and the Analytical Hysteresis Curves for L/r = 60

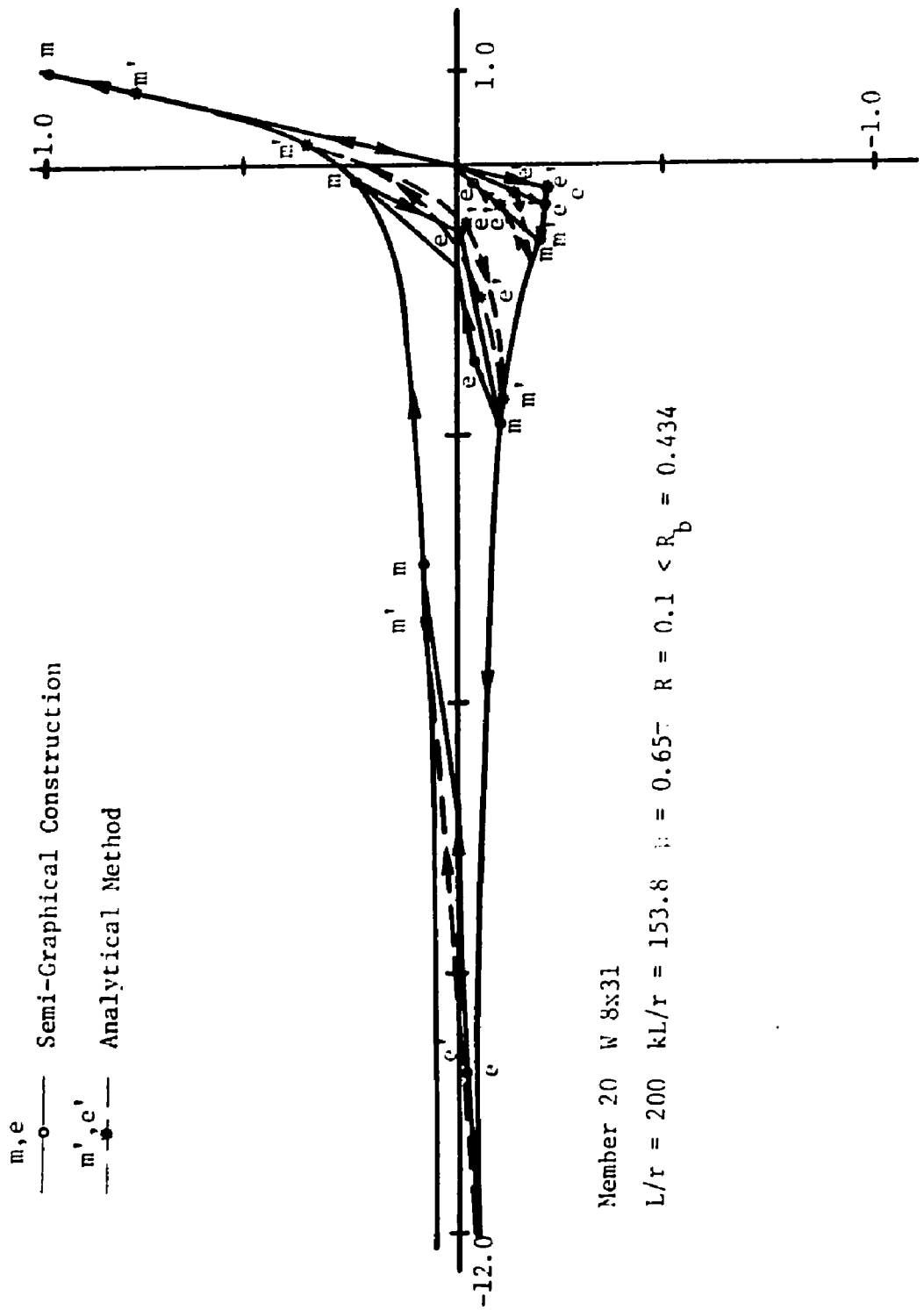


Figure 4.12 Comparison of the Graphical and the Analytical Hysteresis Curves for L/r = 200

4.3. The Member with Greater than Balanced Strength Connections

This section describes the quantitative differences between the hysteresis curve for members with greater than balanced strength connections and that of the reference member, and the semi-graphical construction of the hysteresis curves for members with greater than balanced strength connections.

4.3.1. The Compressive Load at the Occurrence of the First and the Second Plastification along the Compression Envelope Curve

It was concluded in Section 3.1 that there is very little change, if any, in the maximum compressive load carried by a member if the connection strength is equal to or greater than the balanced connection strength. This is because any increase in the connection strength of a member from the balanced connection strength does not affect the occurrence of the plastic hinge at midspan along the compression envelope curve. Further, except for very short members ($L/r \sim 60$ or less), it was the plastification at midspan which produced the maximum compressive load. The occurrence of plastification at the ends varies with the connection strength in a manner that greater connection strength produces a longer envelope CISP region. The empirical equation which approximates the horizontal distance in the hysteresis loop between the point of

occurrence of the plastic hinge at midspan and the point of occurrence of the plastic hinges at the ends is

$$\left(\frac{\overline{\Delta}}{\Delta_y}\right)_c = \left(\frac{\frac{kL}{r}}{125}\right) 8.22*10^{-5}\left(\frac{R}{R_b}\right)^{2.75}\left(\frac{L}{r}\right)^{2.2}\left(\frac{1}{\mu}\right)^{5} \quad ;$$

where $\frac{\frac{kL}{r}}{125} = 1.0$, when $\frac{kL}{r} \geq 125$ (4.7)

This distance, $(\frac{\overline{\Delta}}{\Delta_y})_c$, together with equation (4.1) approximately can locate the point where the plastic hinges occur at the member ends on the compression envelope curve. The DP region is then given by equation (4.1).

4.3.2. The Slope and the Length of the E Region

By the same arguments as given at the beginning of Section 4.2.2, it can be concluded that the chart in Figure 4.2 provides the slope of the E region for a member with greater than balanced strength connections for known kL/r and Δ/Δ_y. According to Section 3.1, the E-region length of the member with greater than balanced strength connections can be assumed to be equal to the E-region length of the reference member at the same Δ/Δ_y. This argument applies to both the ECIP and the ETIP regions.

4.3.3. The Tension Induced Single Plastic Rotation Region

For the case where the connection strength is greater than the balanced connection strength, a change in the

connection strength of a member varies the length of the TISP regions of the corresponding hysteresis loops at the same Δ/Δ_y in such a way that greater connection strength yields longer TISP regions. This TISP region can be very long and nonlinear for a member with small spring stiffness and high kL/r. Therefore, the approximation of this region by a linear region may not yield good results. However, the horizontal distance travelled between the starting and terminating points of this TISP region is approximately equal to $\left(\frac{\overline{\Delta}}{\Delta_y}\right)_t$ which is given by the equation (4.8).

$$\left(\frac{\overline{\Delta}}{\Delta_y}\right)_t = 0.32\ \left(\frac{kL}{r}\right)^{\frac{3}{4}}\ \left(\frac{\Delta}{\Delta_y}\right)^{\frac{4}{5}}\ \frac{\overline{P}}{P_y} \leq \left(\frac{\Delta}{\Delta_y}\right)_s + 1.0 \qquad (4.8)$$

where $\frac{\overline{P}}{P_y}$ is the distance along the P/P_y axis from the starting point of the region (plastic hinge just reoccurs at midspan) to the tension envelope curve at the same Δ/Δ_y. The value of Δ/Δ_y is taken at the Δ/Δ_y-axis intersection of the parent E region and $\left(\frac{\Delta}{\Delta_y}\right)_s$ is the value taken at the starting point of this region. The limiting value of $\left(\frac{\Delta}{\Delta_y}\right)_s$ + 1.0 corresponds to the point where the member becomes straight as the load equals the tension yield load. Equations (4.8) and (4.1) can be used to establish the approximate terminating point of the TISP region (plastic hinges occur at the ends). The details of the construction of this region will be given in Section 4.3.5.

4.3.4. Physical Constraints of the CIP Region Reversing from the TIP Region

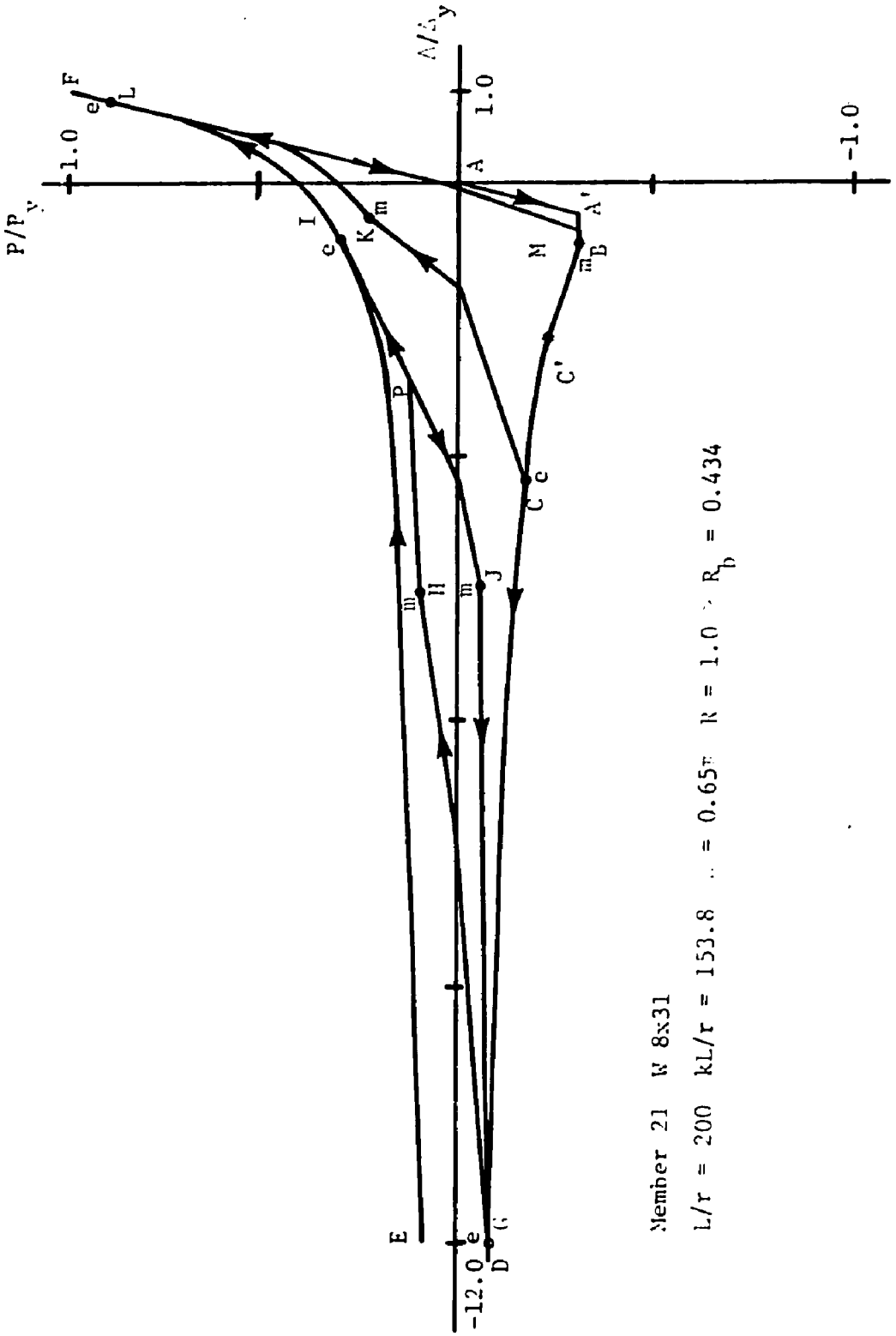
The physical constraints that will be helpful for the semi-graphical construction of the hysteresis curves for these members are completely parallel to those of Section 4.2.4 with the reverse order of the plastic hinges.

a) This section is the same as Section (4.2.4a) except for the changes from all the plastic-hinge actions at midspan to the analogous plastic hinge actions at the ends.

b) This section is the same as Section (4.2.4b) except for the changes from all the plastic-hinge actions at midspan to the analogous plastic-hinge actions at the ends.

4.3.5. Construction of the Hysteresis Curves for the Members with Greater than Balanced Strength Connections

The semi-graphical construction of the hysteresis curves for members with greater than balanced strength connections is parallel to that of the member with smaller than balanced strength connections. A typical hysteresis curve is shown in Figure 4.13. Path A-B, the IE region, is exactly the same as that of the reference member. A plastic hinge develops at midspan at point B. Equation (4.7) gives the value of $(\frac{\overline{\Delta}}{\Delta_y})_c$ which, upon combining with the Δ/Δ_y at



Member 21 W 8x31

L/r = 200 kL/r = 153.8 ... = 0.65π R = 1.0 ... R_b = 0.434

Figure 4.13 Hysteresis Curve for a Member with Greater than Balanced Strength Connections Using Semi-Graphical Construction

point B, yields Δ/Δ_y at point C where plastification occurs at the member ends. The P/P_y at point C can be obtained from equation (4.1), thereby locating point C. Path B-C is constructed by drawing a curve parallel to the CIDP region of the reference member at the same Δ/Δ_y from point C towards B for the distance along the Δ/Δ_y axis of $[(\overline{\frac{\Delta}{\Delta_y}})_c - 1.0]$ to point C'. Then points B and C' are joined by a straight line. If $(\overline{\frac{\Delta}{\Delta_y}})_c$ is less than one, points B and C are joined by a straight line. The CIDP region and the TIDP region, curve C-D and curve E-F, are constructed using equation (4.1).

If the direction of the relative end displacement is reversed at point G along curve C-D, the ECIP region (path G-H) prevails. The construction of path G-H involves the same trial and error procedure as in Section 4.1.5 of drawing a line from point G until its slope and its Δ/Δ_y at zero load agree with Figure 4.2 for the given kL/r. The length of path G-H is the same as the length of the ECIP region at the same Δ/Δ_y of the reference member. Hence, point H, where the plastic hinge reoccurs at midspan, is established and path G-H can consist of either one or two straight lines depending on the member kL/r value.

Curve H-I, the TISP region, is constructed with the help of equation 4.8. The values of $(\overline{\frac{\Delta}{\Delta_y}})_t$ and of Δ/Δ_y at point H can be used to give Δ/Δ_y value of point I which is the point of reoccurence of plastic hinges at the ends.

The P/P_y value at point I is then obtained by using equation (4.1). Path H-I is drawn by one of the two possible ways as follows:

a) Point H and point I are joined by a straight line if this line does not intersect curve E-F at any other point, otherwise

b) a curve is drawn from point H parallel to curve E-F as far as necessary to point P where a straight line P-I can be drawn without intersecting curve E-F at any other point.

To take advantage of the physical constraints mentioned in Section 4.3.4a, the ETIP region is assumed to start at point I. The construction of path I-J of the ETIP region is similar to that of path G-H. A straight line is drawn between point J and point G for the CISP region. Also similar to Section 4.2.5, another physical constraint (Section 4.3.4b) can be used to construct the curve C-K-L-M-C. The construction of this curve is different from the construction of curve G-H-I-J-G in the ETIP region since the length of L-M is controlled by the physical constraint. Path L-M must terminate at point M on curve A'-B-C and in this case, point M and point B are the same point. The additional constraints discussed in Sections 4.3.4a and b can be utilized to generate the ETIP region that initiates anywhere along the TISP region (curve H-I or curve K-L). If the ETIP region initiates anywhere along curve L-F (F is the tension yield point), this ETIP region also terminates on

path A'-B-C.

The limitation in regard to the lack of ability of this method to provide the CISP region for the ETIP region which occurs at an arbitrary point along curve E-F and the technique to overcome this limitation are the same as discussed in Section 4.2.5. The comparison of the hysteresis curves for members with greater than balanced strength connections using semi-graphical construction and using the equations in Chapter II is shown in Figures 4.14 and 4.15. As in the first two cases, the agreement is better for the member with lower kL/r due to the better accuracy of the E region by the semi-graphical construction. The agreement is also better for greater connection stiffness since the SP regions are shorter.

4.4 Conclusions

In Section 4.1, the hysteresis behavior of the member with balanced strength connections together with semi-graphical construction were discussed in detail. The various equations and graphs presented also provide information about the quantitative influence of different parameters on the hysteresis behavior. By introducing the concept of the reference member, the hysteresis curve of the corresponding member with smaller or greater than balanced strength connections can be compared with the reference hysteresis curve. This lead to information (equations and graphs) about the quantitative influence of the parameters on the hysteresis

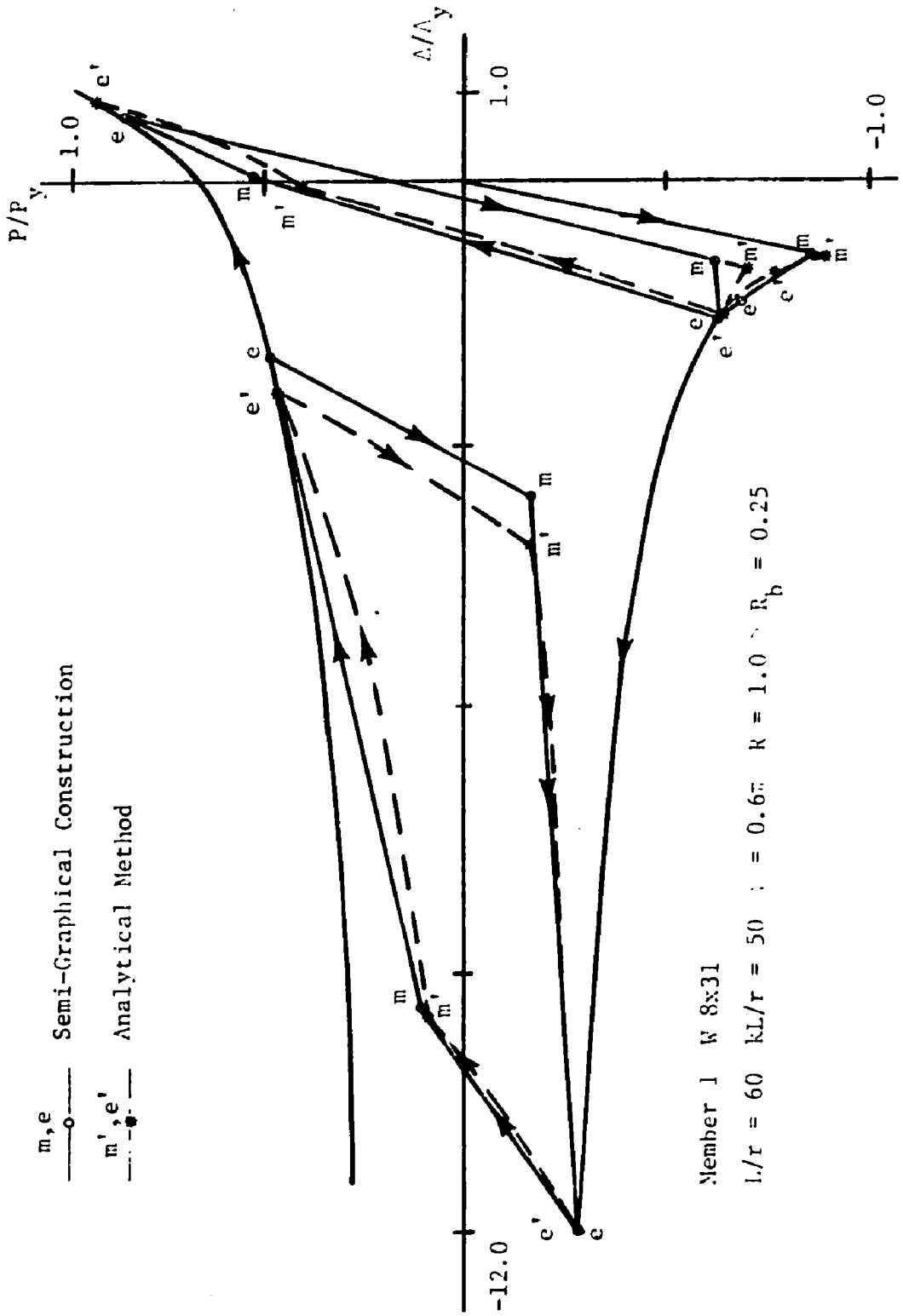


Figure 4.14 Comparison of the Graphical and the Analytical Hysteresis Curves for L/r = 60

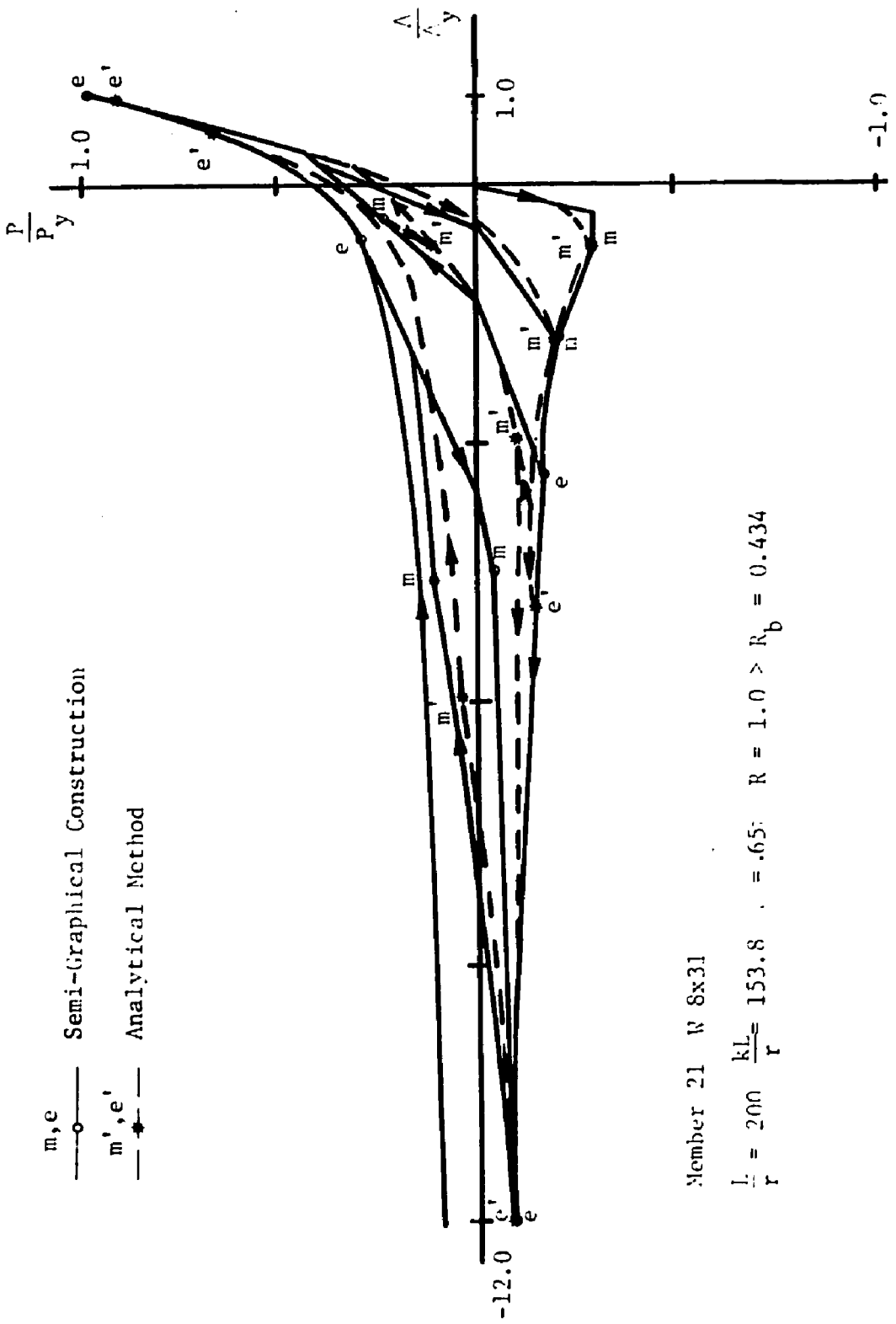


Figure 4.15 Comparison of the Graphical and the Analytical Hysteresis Curves for L/r = 200

behavior as well as the semi-graphical construction of these types of hysteresis curves as explained in Sections 4.2 and 4.3.

In the next chapter the results of this study of the member behavior will be re-evaluated in a form useful for practical application.

CHAPTER V

APPLICATIONS OF RESULTS

Chapters III and IV described the influence of different parameters on the hysteresis characteristics in detail both qualitatively and quantitatively. With such knowledge, one is in a position to make conclusions regarding some practical applications of the results obtained. For primarily axial-load-carrying members which can be satisfactorily represented by the model used in this study, conclusions can be made about the member and connection (system) properties that optimize the hysteresis behavior based on selected objective functions. The important load-resisting characteristics of this type of member are the compressive load capacity, the tensile load capacity, and the energy dissipation.

In a practical design of structure, a member length is usually governed by the geometric requirement and cannot vary. Consequently it is reasonable to find system properties that will optimize these objective functions for members of a given length. It also seems appropriate to utilize members using the same cross section because the cross-sectional effect on the hysteresis behavior can be conveniently concluded from Section 3.4. Hence, members using the same cross section and having the same

length will be investigated for the optimum system properties. By using the same cross section, the tensile load capacities are the same for different system properties since they are all equal to the tensile yield load of the selected cross-sectional area.

5.1. Compressive Load Capacity

As a recapitulation of the influence of system properties on the member compressive load capacity, three dimensional plots of the normalized load capacity against R and k are given in Figures 5.1 and 5.2 for W 8x31 members with L/r = 60 and 200, respectively. Figure 5.1 indicates that

(a) For a fixed k, one gains load capacity by strengthening the connections up to the balanced connection strength. Additional connection strength beyond that has virtually no effect on the load capacity.

(b) For a fixed R, stiffening the connections increases the load capacity. The rate of increase is greater in the strong connection region, i.e., the region where the connection strength is greater than the balanced connection strength.

(c) The increase in the load capacity is more rapid along the balanced strength curve than those in both (a) and (b). This suggests that the system is more efficient in compressive load capacity along the balanced strength curve than along other corresponding constant R

S.C. = strong connection region

B.C. = balanced strength curve

W.C. = weak connection region

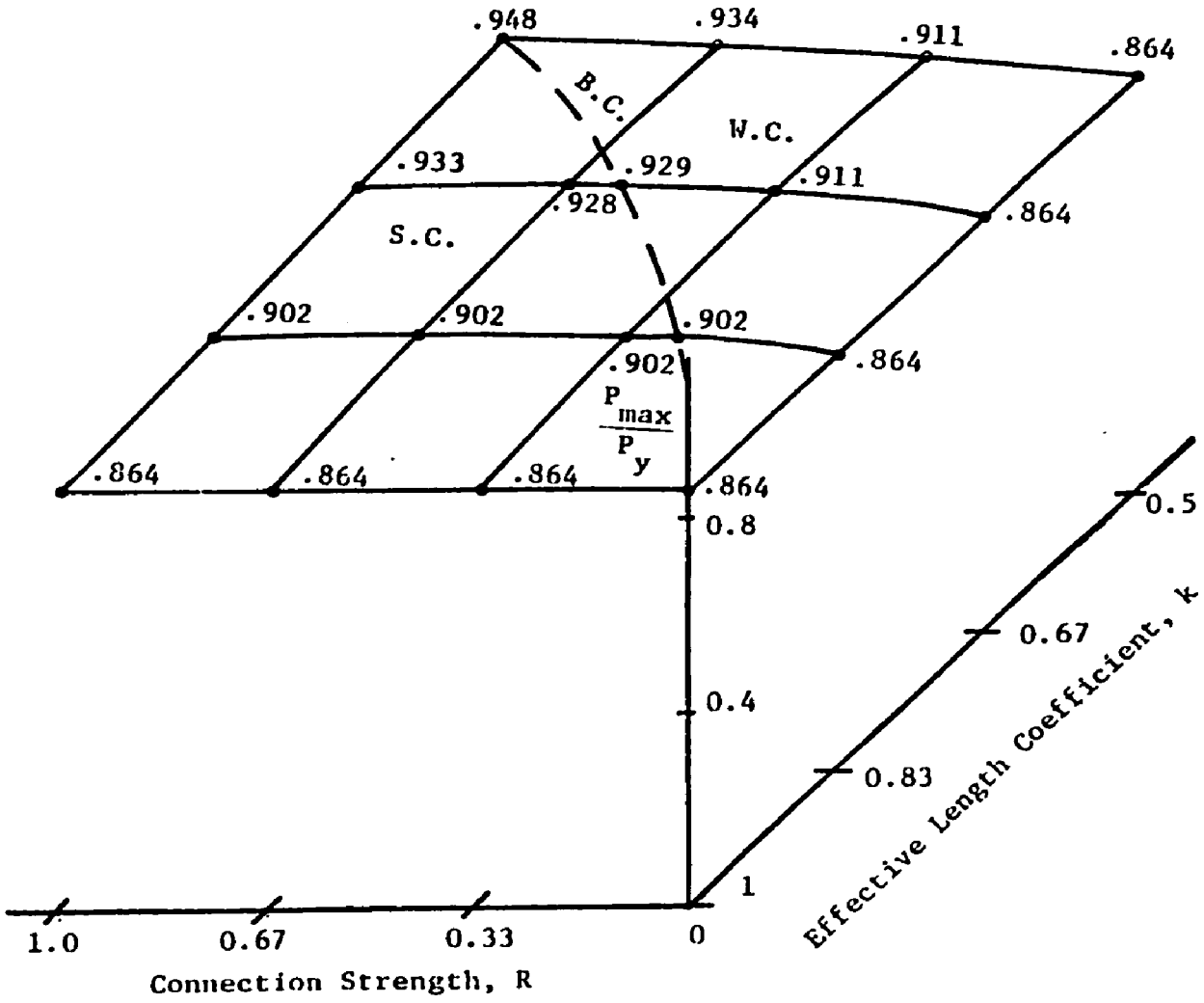


Figure 5.1 Normalized Compressive Load Capacity of W 8x31 Members with L/r = 60

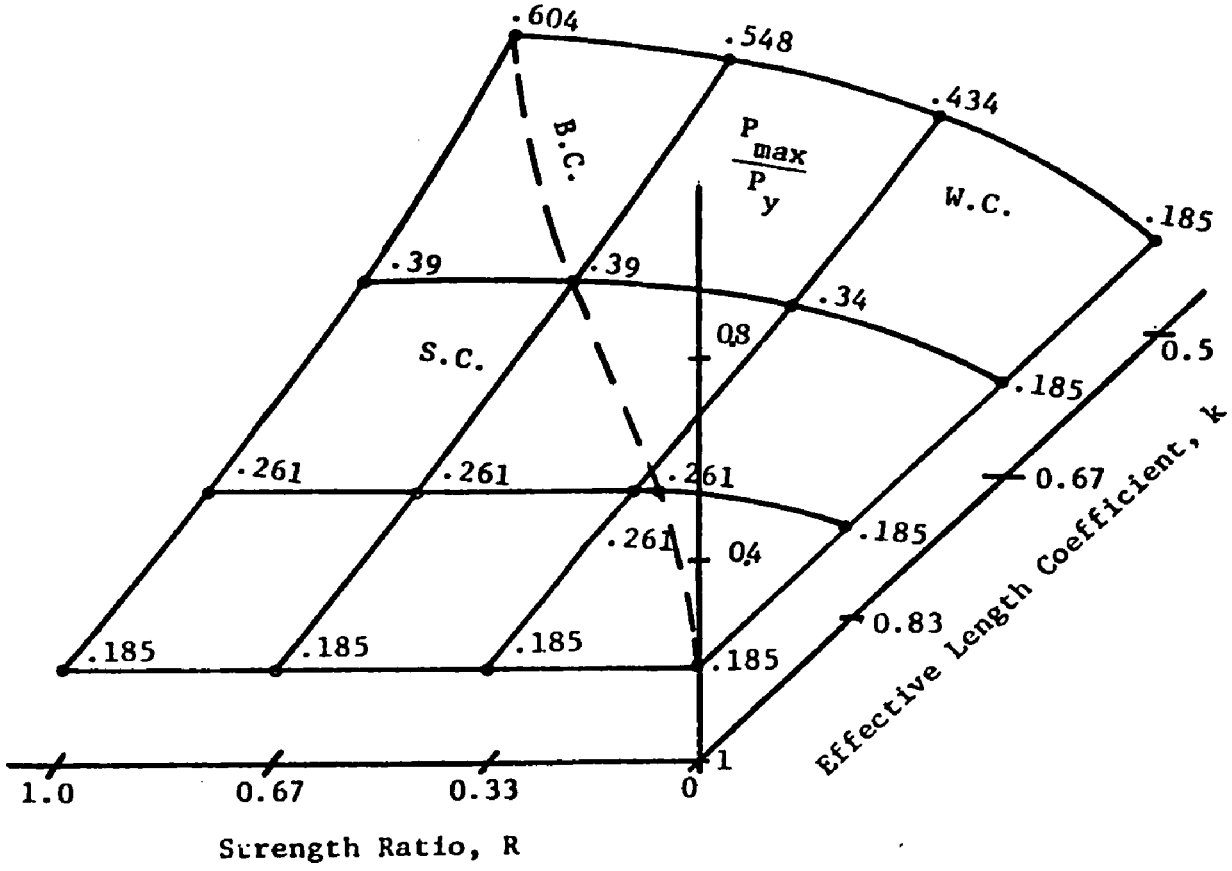


Figure 5.2 Normalized Compressive Load Capacity of W 8x31 Members with L/r = 200

or k curves. Therefore, the system properties along the balanced strength curve are desirable with respect to the maximum compressive load.

Figure 5.2 also reveals similar characteristics as those of Figure 5.1. The difference is mainly in the magnitude of the rate of increase in the load capacity which is greater in Figure 5.2. From these results and the results of section 3.4, one can readily anticipate that similar plots for members of different cross sections and with different L/r would demonstrate analogous results as above. Therefore, it can be concluded that the system properties along the balanced strength curve optimize the member compressive load capacity.

It is evident from Section 3.5 that the load capacity of a member with balanced strength connections is approximately equal to the load capacity of a pin-ended member of equal effective slenderness ratio (both members with initial Θ_p = 0.005 radian). Also, from Figure 2.5, the load capacities of pin-ended members with Θ_p = 0.005 radian are practically the same as those given by equation 2.1. So the AISCx1.7 curve essentially gives complete information about the balanced-strength-member load capacities. For example, the balanced strength curve in Figure 5.2 is approximately the AISCx1.7 curve between kL/r values of 100 and 200. Similar curves of members with different L/r can be approximated by the AISCx1.7 curve in an analogous manner. The AISCx1.7 curve also

yields the compressive load capacities of members of different cross sections and different axes of bending according to Section 3.4.

One of the most important information from the AISCx1.7 curve (Figure 2.5) is the manner in which the load capacity varies with respect to k since this can aid the designer in selecting the optimal system properties. As an example for a member with L/r = 200, varying k from 1.0 to 0.90 (kL/r from 200 to 180) is not as efficient as varying k from 0.6 to 0.5 (kL/r from 120 to 100) since the chord slope is steeper for kL/r from 120 to 100.

5.2. Member Energy Dissipation

Analogous to the compressive load capacity, three dimensional plots of normalized dissipated energy against R and k are given in Figures 5.3 and 5.4 for W 8x31 members with L/r = 60 and 200, respectively. The normalizing value in each case is the dissipated energy of the corresponding pin-ended member. The dissipated energy is defined as the area of the P/P_y - Δ/Δ_y plot enclosed by the loop similar to O-A-B-C-D-O'-O in Figure 5.5. OAB is the compression envelope curve, and Δ/Δ_y at B is 5.0. D is the tension yield point. The absolute dissipated energy is equal to the dissipated energy times $P_y\Delta_y$. The following conclusions can be deduced from Figures 5.3 and 5.4:

(a) For a fixed k, strengthening the connections

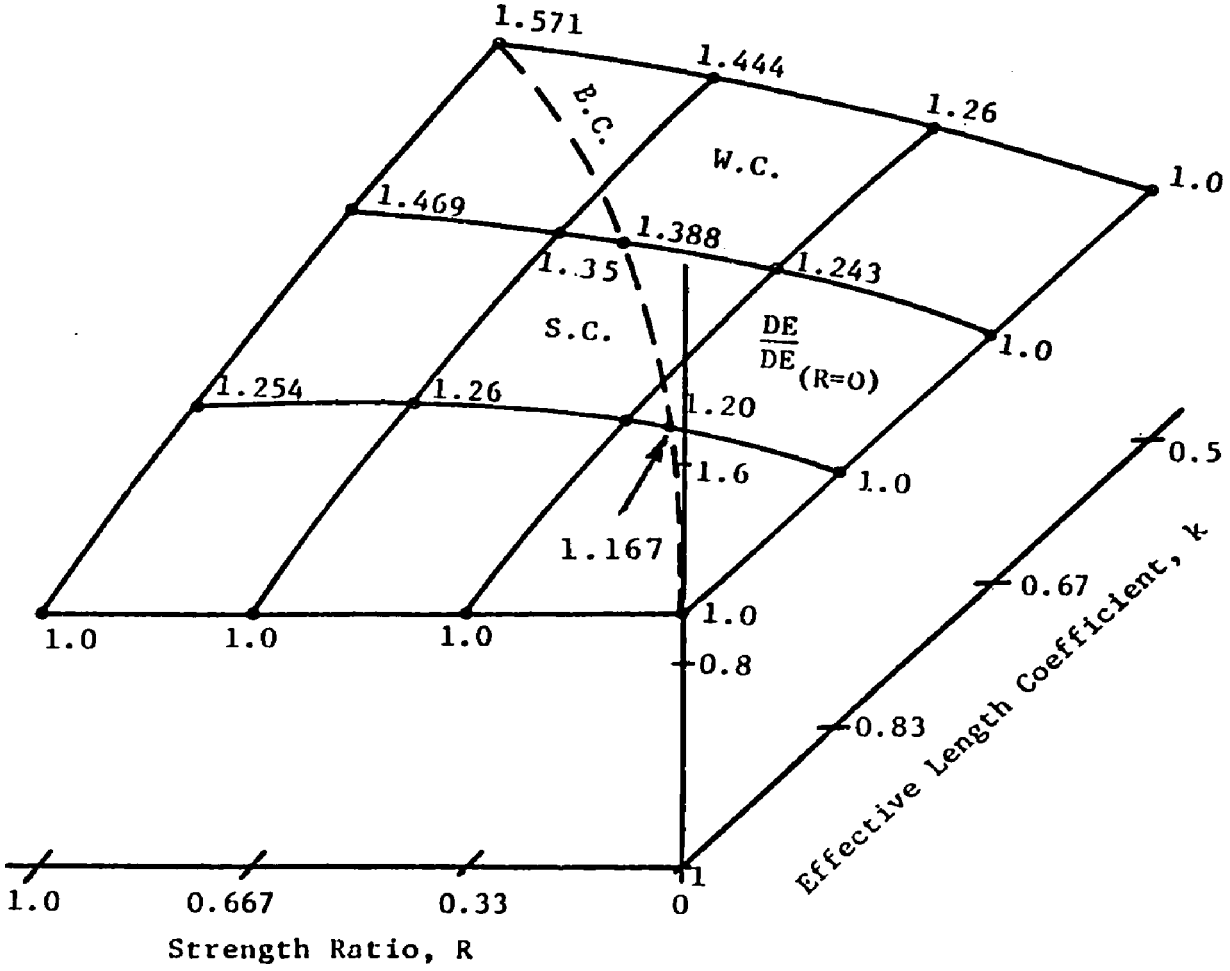


Figure 5.3 Normalized Dissipated Energy of W 8x31 Members with L/r = 60

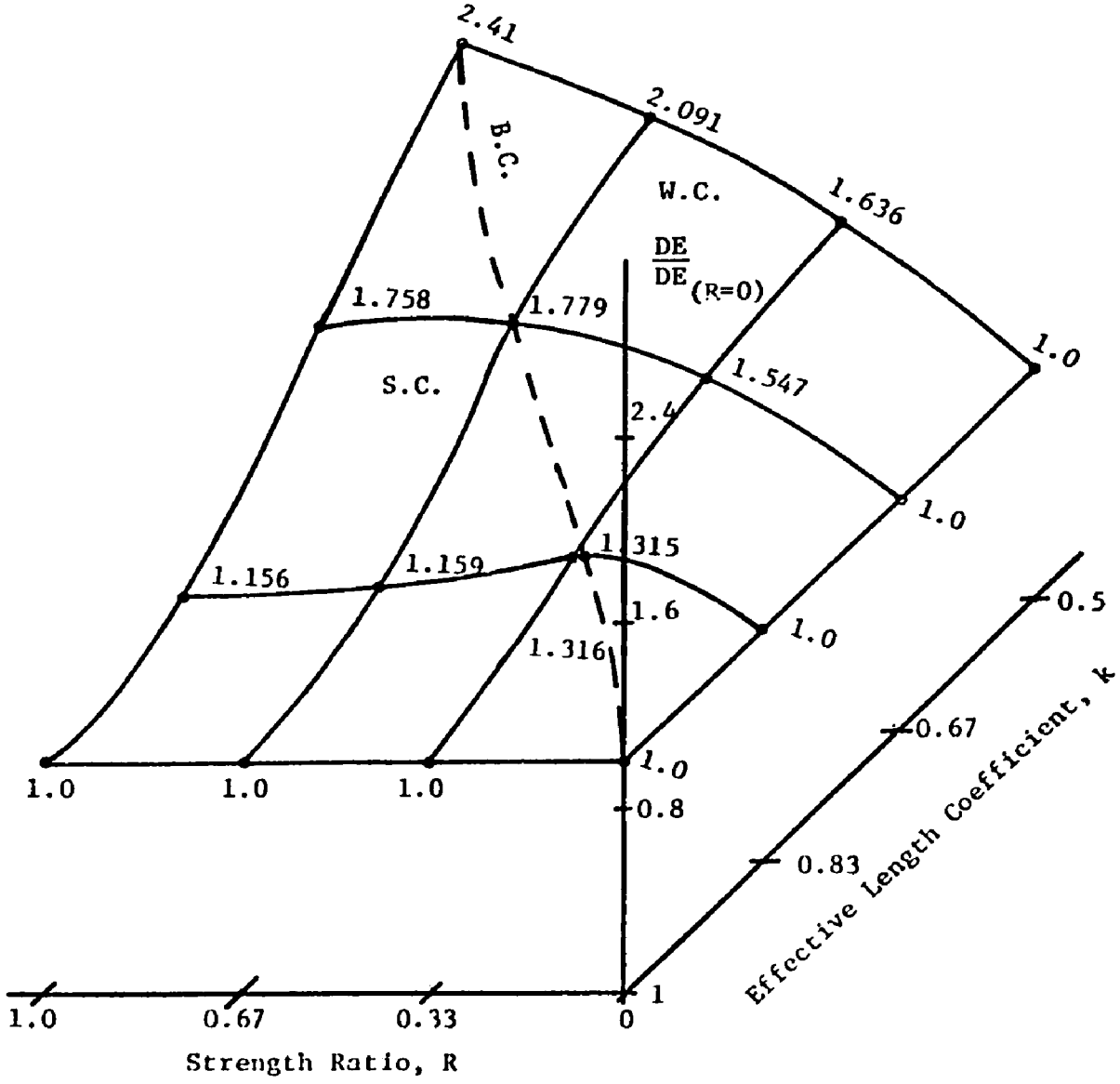


Figure 5.4 Normalized Dissipated Energy of W 8x31 Members with L/r = 200

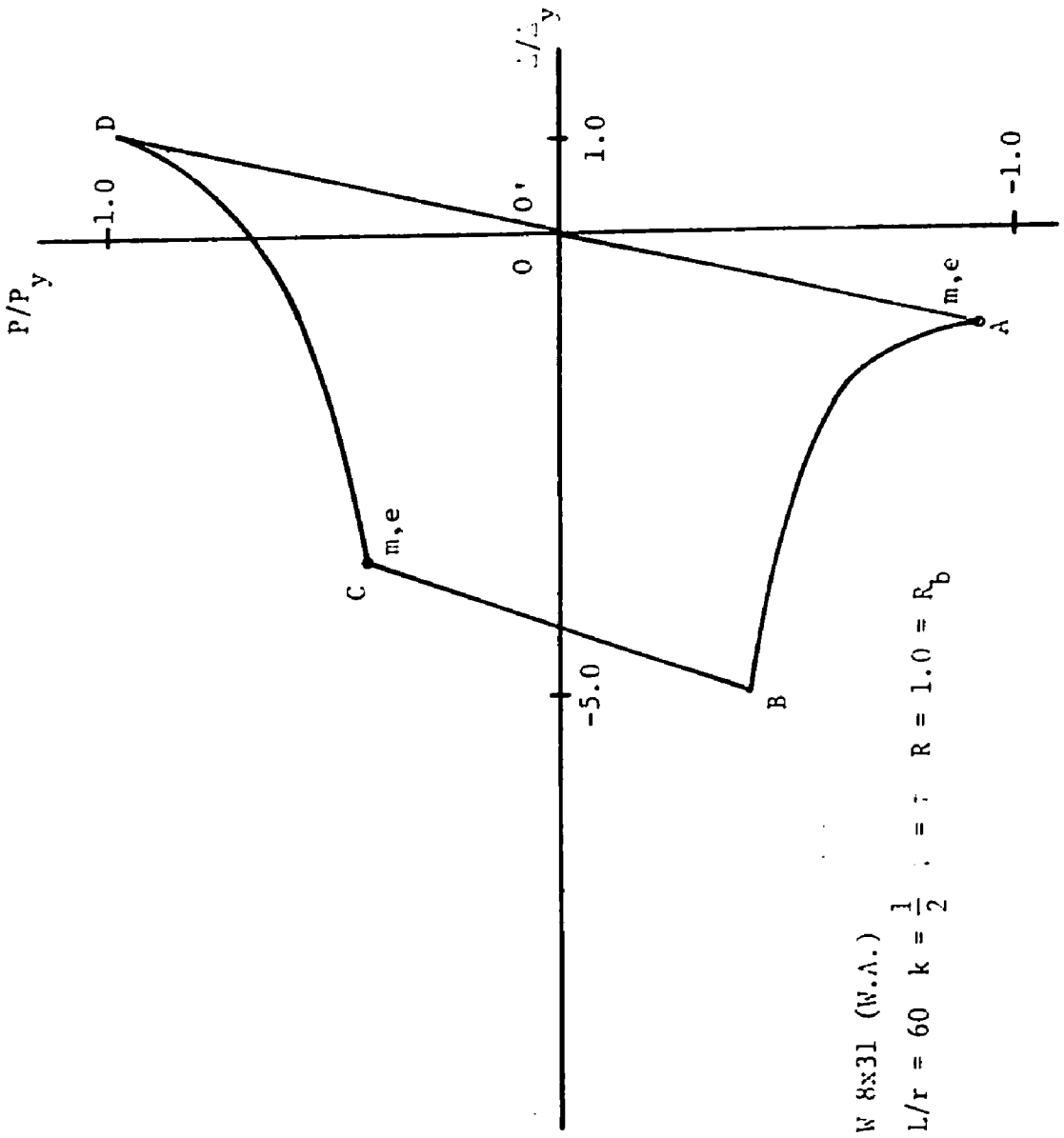


Figure 5.5 Dissipated Energy of the Hysteresis Loop for $\Delta/\Delta_y = 5.0$

leads to an increase in the dissipated energy up to the balanced connection strength. Further increase in the connection strength beyond the balanced strength results in either a slight increase or a slight decrease in the dissipated energy. The decrease is more pronounced for a more slender member (Figure 5.4).

(b) For a fixed R, stiffening the connections increases the dissipated energy. The rate of increase is greater in the strong connection region.

(c) The increase in the dissipated energy is more rapid along the balanced strength curve than those in both (a) and (b). This again suggests that the system is more efficient with respect to energy dissipation along the balanced strength curve than along other corresponding constant R or k curves. It is also evident that the rate of increase of the normalized dissipated energy is greater for the more slender member. One can anticipate again that similar characteristics prevail for members of different length and cross section and hence, conclude that the system properties along the balanced strength curve optimize the member dissipated energy.

The possibility of using a single curve to yield complete information about the energy dissipation of all the balanced strength members (similar to the case for compression load capacity) is explored here. Figure 5.6 shows the comparison of the normalized dissipated energies of W 8x31 members (L/r = 60 and 200) along the

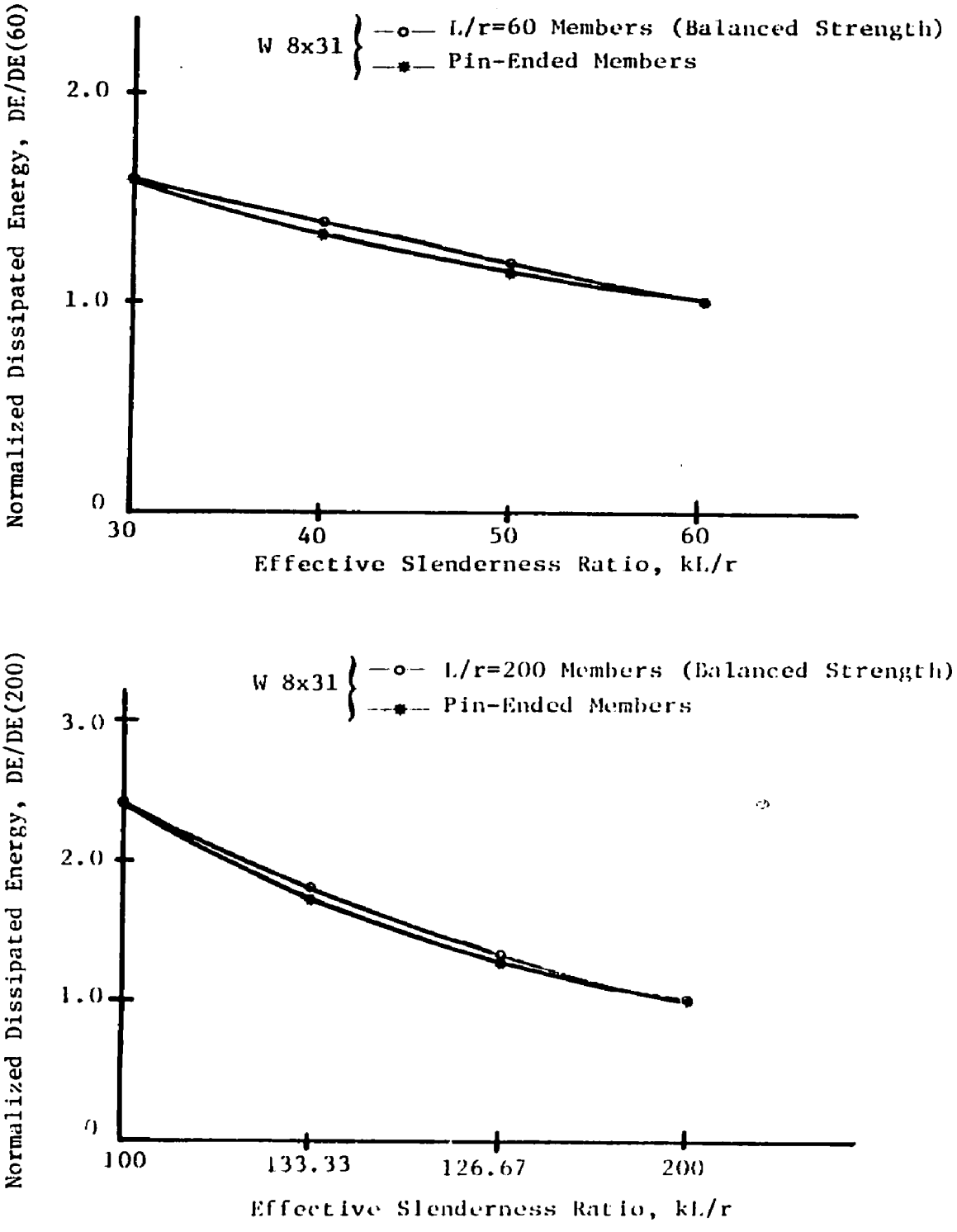


Figure 5.6 Comparisons of the Normalized Dissipated Energy

balanced strength curves with those of the pin-ended members of the same effective slenderness ratio. The differences in the normalized dissipated energy are practically insignificant in both cases. Hence, it can be concluded that the dissipated energy curve of pin-ended members with L/r ranging from 0-200 (practical design range) such as shown in Figure 5.7 provides the complete information about the dissipated energy characteristics of all the balanced strength members. The same conclusion can also be drawn from Section 3.5. It should be noted that as L/r approaches zero, the corresponding dissipated energy for $(\frac{\Delta}{\Delta_y})_B = 5.0$ (Figure 5.5) approaches the value eight which corresponds to the elasto-plastic axial behavior of a member of nearly zero length. It can also be concluded by referring to Section 3.4 that analogous dissipated energy curve for members of different cross sections and different axes of bending will have similar shape to that of W 8x31 members with slightly different coordinate values.

Similar to the compressive load capacity, the instantaneous slope and the chord slope of the curve in Figure 5.7 are valuable in helping the designer to select the most efficient system properties for the geometric requirement. It should be kept in mind that although Figure 5.7 can be used to give the approximate dissipated energy for a balanced strength member (by entering L/r = kL/r of that member), the absolute dissipated energy is equal to the dissipated energy from Figure 5.7 times

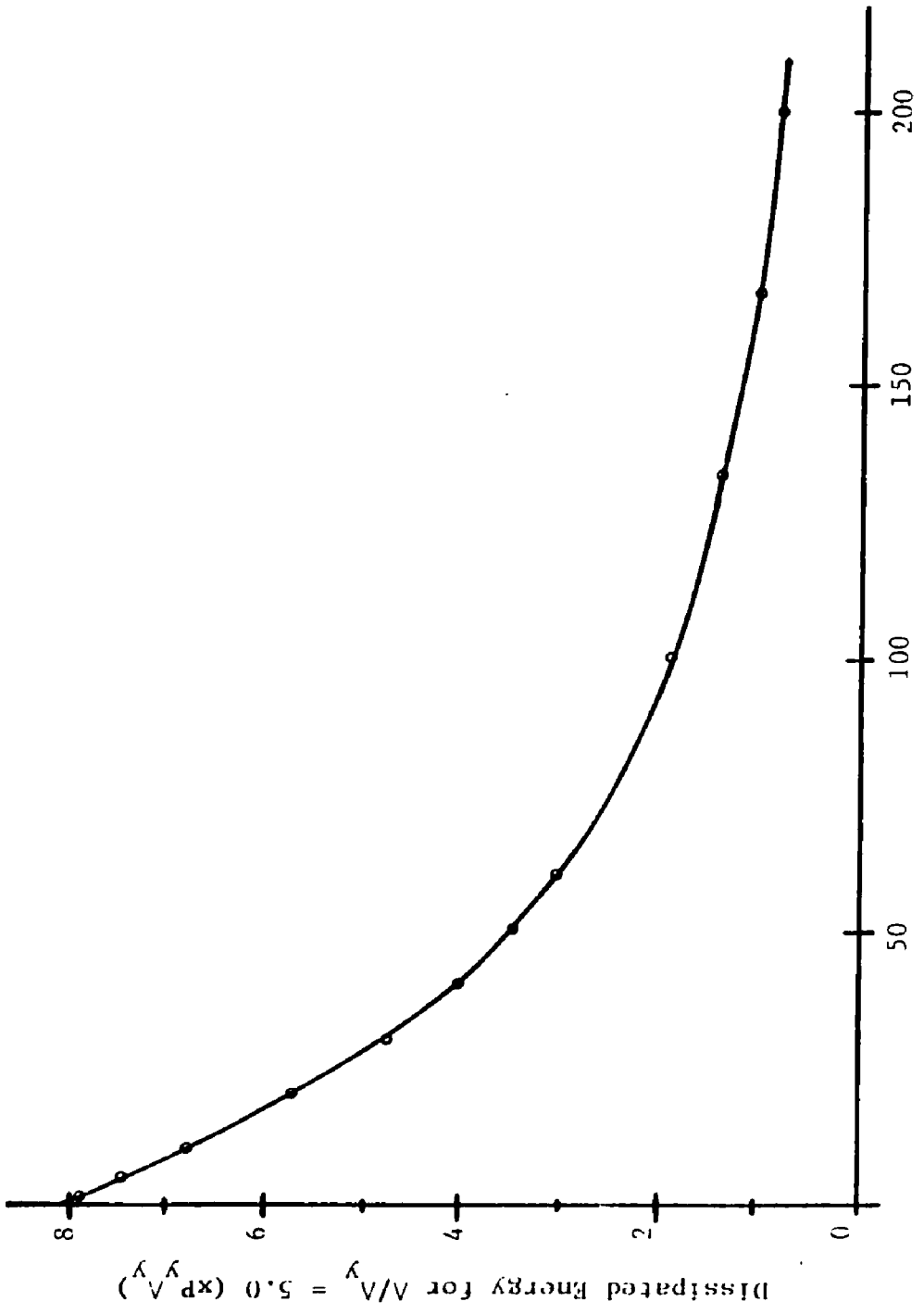


Figure 5.7 Dissipated Energy for W 8x31 Pin-Ended Members

$P_y\Delta_y$. The values of Δ_y are different for members of different slenderness ratios.

5.3. Angles of Rotation at Midspan and at the Ends

For a member to undergo the hysteresis cycle, it must be ductile enough to sustain large angles of rotation at both the midspan and the ends. In order to get an idea of the magnitude of these angles of rotation, the angle between the tangent of the elastic section adjacent to the plastic hinge and the horizontal axis is obtained at both the ends and the midspan [$(\theta_e + \theta_{1p})$ and θ_{2p} of Figure 2.8]. Figure 5.8 shows the contour curves of $(\theta_e + \theta_{1p})$ and Figure 5.9 the contour curves of θ_{2p} of W 8x31 members at $\Delta/\Delta_y = 12.0$ plotted against L/r and R. The reason for leaving out the stiffness parameter μ is that the member is usually in the DP region at such a high Δ/Δ_y value. Consequently, there is no difference in the rotation angles for members with different μ but with the same L/r as explained in Section 3.2.

It is evident from Figures 5.8 and 5.9 that there are only minor variations in the magnitude of both rotation angles with respect to the strength and slenderness ratio. This is because the angle between chord AB (Figure 2.8) and the horizontal axis is approximately constant for all the members at $\Delta/\Delta_y = 12.0$. Since the sine of this angle (about 10°) is assumed to be equal to the angle itself [equation (2.7)], then

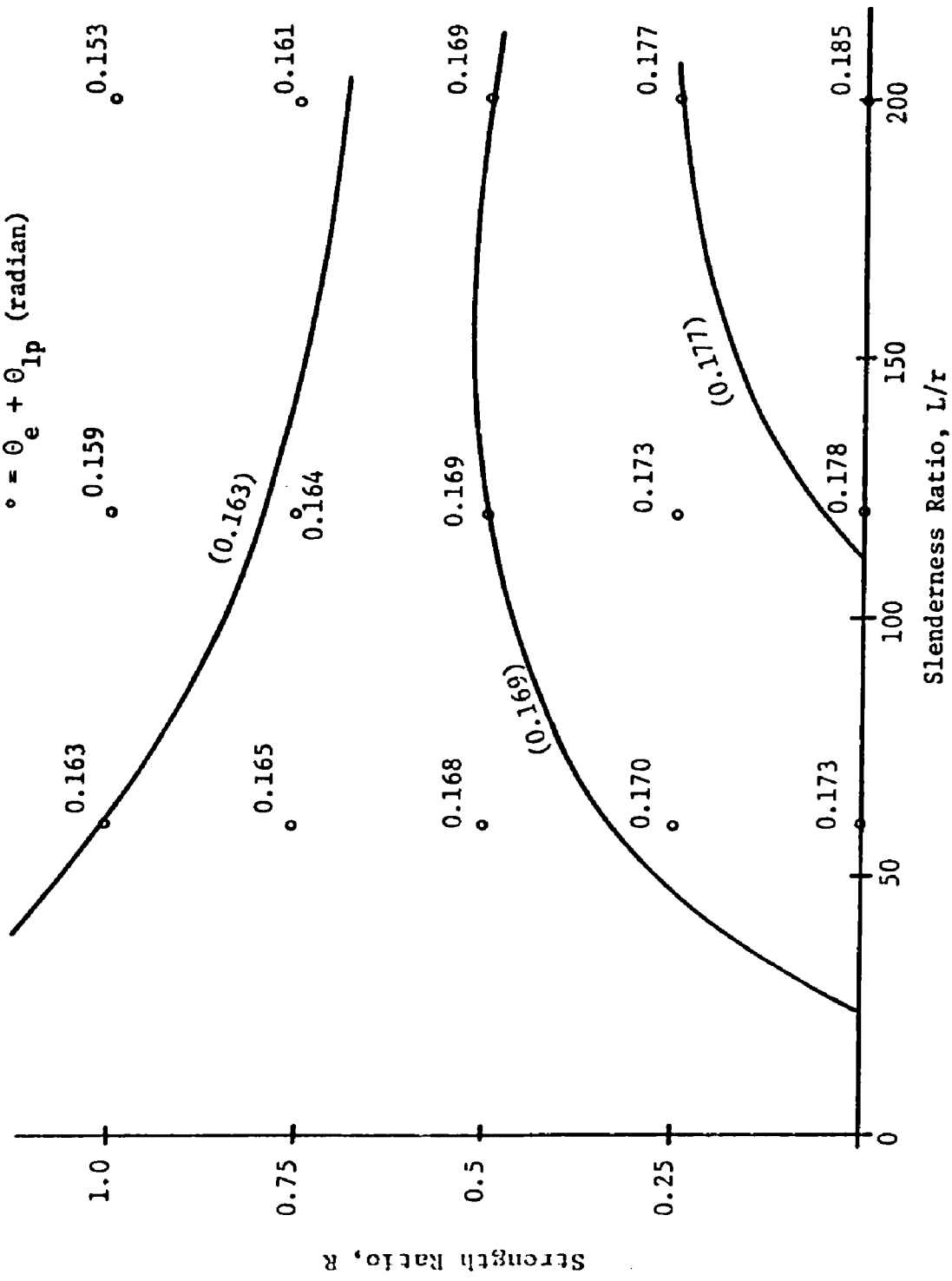


Figure 5.8 Angles of Rotation at the Ends of W 8x31 Members at Δ/Δ_y = 12.0

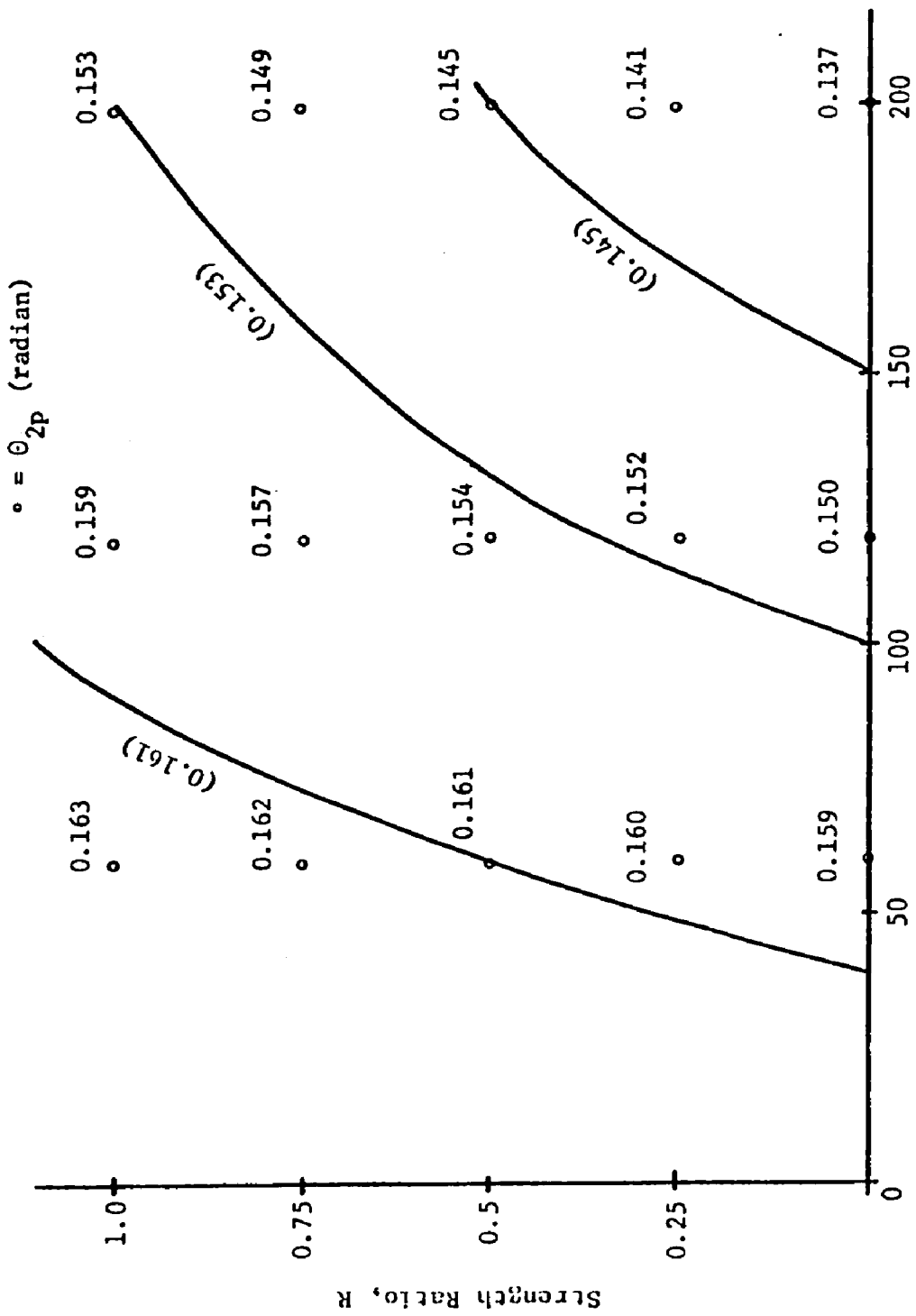


Figure 5.9 Angles of Rotation at Midspan of W 8x31 Members at Δ/Δ_y = 12.0

$$\theta_e + \theta_{1p} + \theta_1 = \theta_{2p} + \theta_2 = \frac{Y_m}{\ell} \sim \text{constant}$$

This conclusion can also be obtained from equation (4.1a) which can take another form as

$$\frac{\Delta}{\Delta_y} = \frac{2AE}{P_Y}\left[\frac{1}{2} - \sqrt{\left(\frac{1}{2} - \frac{P}{2AE}\right)^2 - \left(\frac{Y_m}{L}\right)^2}\right]$$

The term P/2AE is small compared with $\frac{1}{2}$ for large Δ/Δ_y in the DP region (elastic shortening is small relative to the member length). Thus, different members must have approximately equal Y_m/L in order to achieve equal Δ/Δ_y. Equal Y_m/L implies approximately equal Y_m/ℓ.

At $\Delta/\Delta_y = 12.0$ on the DP region, the magnitudes of θ_1 and θ_2 are small (<0.03 radian) compared with those of $(\theta_e + \theta_{1p})$ and θ_{2p}. Therefore, the variations in θ_1 and θ_2 of different members due to the variations in M_1 and M_2 are small relative to the values of $(\theta_e + \theta_{1p})$ and θ_{2p} which results in only minor variations of both rotation angles. The change of cross section and the bending about different axes also have only small effects on these rotation angles.

From Workman's study[12], the seventh story of his ten-story single bay braced frame subjected to modified El Centro earthquake accelerogram has a girder maximum ductility ratio of about one and the bracing ductility ratio of about five. The yield rotation for anti-symmetrical bending of this girder is 0.00375 radian. For the

members studied in this dissertation, the connection rotation is about 0.1 radian for $\Delta/\Delta_y = 5.0$. This is about 26 times greater than yield rotation of the girder for Workman's frame as mentioned above. In other words, this may be an example where the end rotation of the rigidly connected columns and girders in braced frames may be much smaller than the rotation at the connections of the bracing members.

5.4. Conclusions

The results of the studies in this chapter lead to two important conclusions for primarily axial-load-carrying members which can be satisfactorily represented by the utilized model. First, for a given member length and cross section properties, the balanced strength member optimizes the important load-resisting characteristics of compressive load capacity and hysteretic energy dissipation. Secondly, from the studies in Sections 3.5, 5.1, and 5.2, it is evident that these (normalized) hysteretic characteristics of a balanced strength member can be adequately represented by those of a pin-ended member of the same kL/r and same cross section. Therefore, the information as presented in Figures 2.5 and 5.7 for pin-ended members with slenderness ratios in practical design range can provide the designer with essential hysteretic characteristics of all balanced strength members with the

same cross section. The tensile load capacities for members of the same cross section are equal.

It should be noted again that the dissipated energies from Figure 5.7 need different denormalizing factors (P_y Δ_y) for different members. Also that the variations in the cross section and in the axis of bending have only minor effects on these characteristics.

CHAPTER VI

SUMMARY AND CONCLUSIONS

This dissertation is concerned with the study of the hysteresis behavior of axially loaded steel members with rotational end restraints. Symmetrical rotational end springs were used to simulate the end restraints of a member due to gusset plates or other connected structural members. The analytical solution of this physical member was given in Chapter II using approximate expression for curvature and in Appendix A (partially) using exact expression for curvature. The approximate model was introduced because the exact expression for curvature model is too complicated to be used for a more thorough study of the member behavior.

The parameters that were varied in this study are the connection flexural strength, the connection flexural stiffness, the member slenderness ratio, and the member cross-sectional properties. Chapter III presented the qualitative observations of the parametric influences on the hysteresis behavior. In Chapter IV, quantitative influences of the parameters were deduced and used as a basis for semi-graphical construction of the hysteresis curves. This semi-graphical construction provides a means for generating approximate hysteresis curve as well as for

elucidating the parametric influences. Practical applications of the results of this study were concluded in Chapter V.

From the results of this study of primarily axially loaded members which assumed symmetrical rotational end restraints, an elasto-plastic moment-curvature relationship with plastic moment modified due to axial force, no local and lateral-torsional buckling, and no strain hardening, the following conclusions can be drawn:

1) The balanced-strength-connection concept introduced in this discourse proves to be very significant. A member with balanced strength connections is more efficient with respect to the important properties of a primarily axial-force-carrying member than members of the same length and same cross-sectional properties with non-balanced strength connections. These properties are the compressive load and the energy dissipation capacities. A balanced-strength-connected member also serves as a reference for the corresponding member with smaller or greater than balanced strength connections in the semi-graphical hysteresis-curve construction.

2) As it is evident from the studies in Chapters III and V, the normalized hysteresis curve (P/P_y - Δ/Δ_y plot) of any balanced strength member can be adequately represented by the curve of a pin-ended member of the same cross section and with the same effective slenderness ratio.

Hence, for the purpose of studying the hysteresis characteristics of a balanced strength member, a pin-connected member with equivalent slenderness ratio can be used. The denormalized properties of the balanced strength members are obtained by reapplication of the appropriate normalizing values.

3) Increase in the connection strength above the balanced strength does not significantly influence the compressive load capacity and the energy dissipation of the member. However, in so doing, the member will plastify and replastify first at midspan and hence, have larger plastic rotation angle at midspan and smaller plastic rotation angles at the ends compared to those of the balanced strength member at the same Δ/Δ_y (DP region).

4) Decrease in the connection strength from the balanced strength reduces the compressive load capacity and the dissipated energy of the member considerably. The member will also plastify and replastify first at the ends and hence, have plastic-rotation-angle characteristics reversed from those mentioned in 3).

5) Variation in the connection stiffness affects the connection balanced strength as well as the hysteresis behavior up to plastification of the member ends. Thereafter, the plastic hinges release the rotational end restraints and further incremental load resisting characteristics depend primarily on the geometry of the deformed

member.

6) Variation in the cross-sectional properties, such as Z/A, or the axis of bending has little influence on the member hysteresis behavior provided that local and lateral-torsional buckling do not occur.

Concluding Remarks

The purpose of this dissertation was to perform a parametric study of this physical member and lucidly demonstrate the influence of each parameter on the member hysteretic characteristics as well as to develop information for practical application. As a result, several assumptions were introduced to simplify the analytical solution to a level that is practically suitable for these purposes. A more elaborate analysis could include:

a) the spread of plastification which incorporates the bilinear or curvilinear moment-curvature relationships (partial yielding of the cross sections),

b) the localized strain hardening of the member subjected to large deformation, and

c) unequal springs at the member ends resulting in an unsymmetrical member.

The physical member and connections employed in this study were intended to be a simulation of the bracing member and the connections (gusset plates) when the rotation of the joints can be neglected. This model also can serve to simulate an axially loaded member with rigid

connections when the flexural restraints from other connected members can be adequately represented by rotational end springs. Additional studies are needed to acquire a complete understanding of the hysteretic characteristics of a primarily axial-load-carrying member under arbitrary combined active bending and axial actions.

APPENDIX A

MODEL 1: HYSTERESIS BEHAVIOR WITH EXACT EXPRESSION FOR CURVATURE

The governing equations for the member behavior under the applied load using the exact expression for curvature and the corresponding method of solution are given in this appendix. The derivations in this appendix are closely related to some previous works. Timoshenko and Gere[45] introduced the elastica which is the post-buckling solution of axially-loaded pin-ended members using exact expression for curvature. In his study, the member was assumed to always remain elastic. More recently Higginbotham and Hanson[29] and Nilforoushan[30] used the same approach and added the concept of plastic hinge under combined axial and bending action to study the inelastic hysteresis behavior of axially-loaded pin-ended members. These analyses involve elliptic integrals and, therefore, need an iterative type solution.

While most of the assumptions employed in this study are the same as those utilized by Higginbotham and Hanson[29] and Nilforoushan[30], this analysis is more complicated as a result of the additional end restraints introduced. Therefore, one can expect that this analysis should also involve the elliptic integrals and also need

an iterative type solution. In the following derivation, the connections are assumed to be nonrigid . The connection and the member are assumed to have equal flexural strength (equal plastic moment). Such a member always plastifies and replastifies first at midspan. The complete derivation for the general case where the connections may have smaller flexual strength than the member was not attempted. This is due to the many possible different member configurations under the applied load which require different sets of governing equations.

A.1. Compressive Loading

The sign convention used in this derivation is as shown in Figure A.1. By using the exact expression for curvature ($\Phi = \frac{d\theta}{ds}$) for the member in Figure A.1, the differential equation of the deflection curve is

$$EI \frac{d\theta}{ds} = -M = -Py - M_1 \qquad (A.1)$$

where

$$M_1 = -k_\theta \theta_e$$

Differentiating equation (A.1) with respect to s and using the relation

$$\frac{dy}{ds} = \sin\theta \qquad (a.2)$$

yields

$$EI \frac{d^2\theta}{ds^2} = -P\sin\theta \qquad (A.3)$$

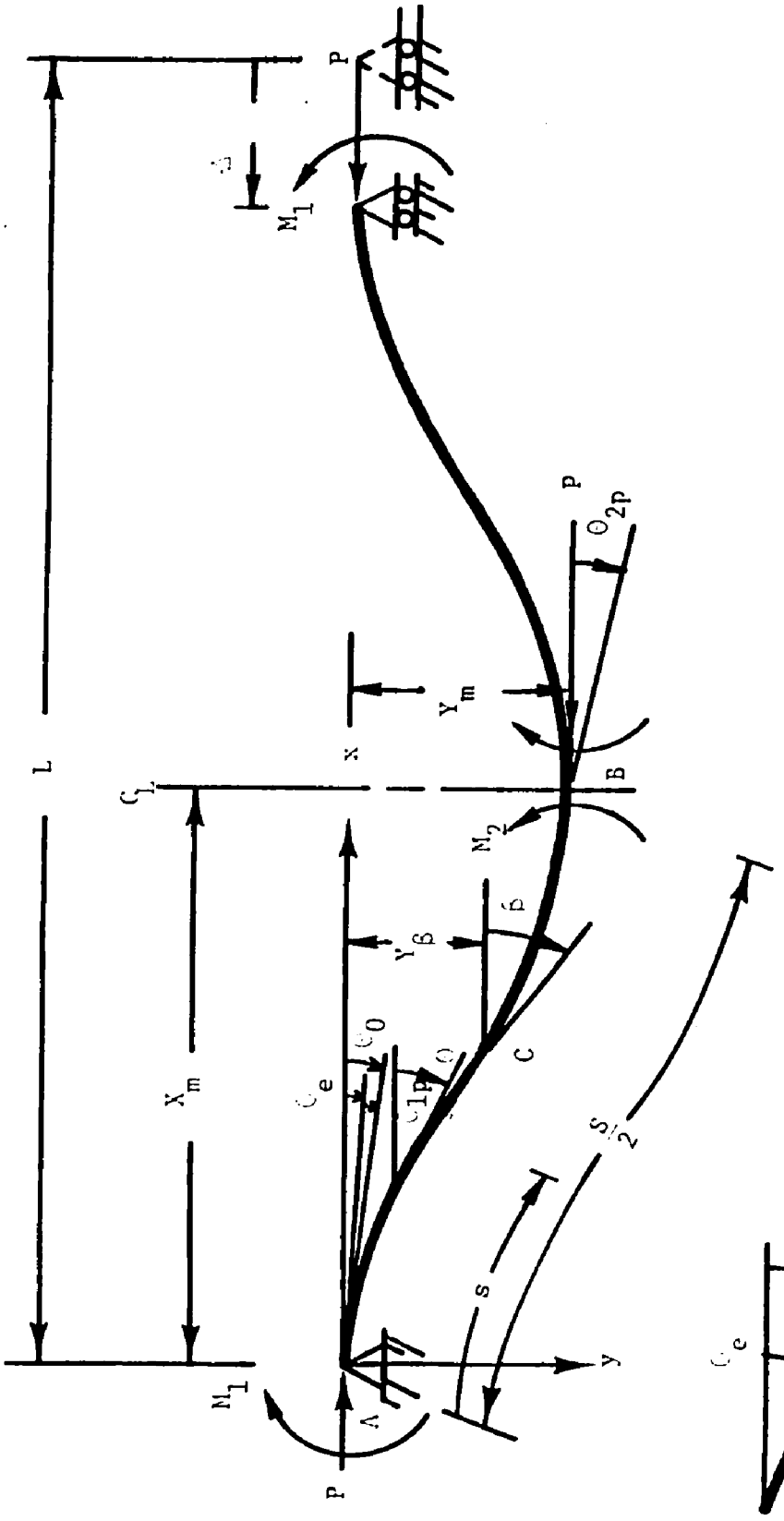


Figure A.1 Member Subjected to Compressive Loading

Both sides of equation (A.3) are multiplied by $d\theta$ and integrated to give

$$\frac{EI}{2}\left(\frac{d\theta}{ds}\right)^2 = P\cos\theta + Q' \qquad (A.4)$$

where Q' is the constant of integration. By letting $K^2 = \frac{P}{EI}$ and $Q = \frac{Q'}{EI}$, equation (A4) can be transformed into

$$\frac{1}{2}\left(\frac{d\theta}{ds}\right)^2 = K^2\cos\theta + Q' \qquad (A.5)$$

Further derivation of the governing equations depends on the characteristic of the point of inflection and can be subdivided into two cases.

A.1.1. Case I: - Inflection Point Within the Member Length

Derivation

The member containing contraflexure points is shown in Figure A.1. Applying the boundary conditions at the inflection point (C) that $\theta = \beta$ and $\frac{d\theta}{ds} = 0$ to equation (A.5) gives

$$Q = -K^2\cos\beta$$

The result after substituting this value of Q in equation (A.5) can be arranged in the form

$$ds = \pm \frac{d\theta}{K(2\cos\theta - 2\cos\beta)^{1/2}} \qquad (A.6)$$

where the positive sign governs the deflection curve from A to C, and the negative sign from C to B in Figure A.1. Integrating both sides of equation (A.6) from A to B yields

$$\frac{S}{2} = \int_{\Theta_0}^{\beta} \frac{d\Theta}{K\,(2\cos\Theta - 2\cos\beta)^{1/2}} + \int_{\beta}^{\Theta_{2p}} \frac{-d\Theta}{K\,(2\cos\Theta - 2\cos\beta)^{1/2}} \qquad (A.7)$$

where S is the deformed length of the member. The right-hand side of equation (A.7) can be transformed into standard elliptic integrals. The relation $\cos\Theta = 1-2\sin^2\frac{\Theta}{2}$ is used for both Θ and β in equation (A.7) to render

$$\frac{S}{2} = \int_{\Theta_0}^{\beta} \frac{d\Theta}{2K\,(\sin^2\frac{\beta}{2} - \sin^2\frac{\Theta}{2})^{1/2}} - \int_{\beta}^{\Theta_{2p}} \frac{d\Theta}{2K\,(\sin^2\frac{\beta}{2} - \sin^2\frac{\Theta}{2})^{1/2}} \qquad (A.8)$$

By allowing

$$\sin\frac{\beta}{2} = q \qquad (A.9a)$$

$$\sin\frac{\Theta}{2} = q\,\sin\phi \qquad (A.9b)$$

and noting that as Θ possesses the value Θ_0, β, and Θ_{2p}, ϕ has the values χ, $\frac{\pi}{2}$, and ψ, respectively where

$$\chi = \sin^{-1}\frac{\sin\frac{\Theta_0}{2}}{\sin\frac{\beta}{2}} \qquad (A.10a)$$

and

$$\psi = \sin^{-1}\frac{\sin\frac{\Theta_{2p}}{2}}{\sin\frac{\beta}{2}} \qquad (A.10b)$$

Equation (A.9b) is differentiated to give

$$d\Theta = \frac{2q\cos\phi d\phi}{(1-q^2\sin^2\phi)^{1/2}} \qquad (A.11)$$

Substituting $d\Theta$ from equation (A.11) together with the identity

$$(\sin\frac{\beta}{2} - \sin\frac{\Theta}{2})^{1/2} = q\cos\phi \qquad (A.12)$$

and making proper changes in the limits of integration in equation (A.8) yields

$$\frac{S}{2} = \frac{1}{K}\int_{\chi}^{\frac{\pi}{2}} \frac{d\phi}{(1-q^2\sin^2\phi)^{1/2}} - \frac{1}{K}\int_{\frac{\pi}{2}}^{\psi} \frac{d\phi}{(1-q^2\sin^2\phi)^{1/2}} =$$

$$\frac{1}{2}\ (L-\frac{PL}{AE})$$

as the deformed half-member length is also given by $\frac{S}{2} = \frac{1}{2} * (L-\frac{PL}{AE})$, or

$$\frac{S}{2} = \frac{1}{K}\ [2F(q) - F(q,\chi) - F(q,\psi)] = \frac{1}{2}\ (L-\frac{PL}{AE}) \qquad (A.13)$$

where F(q) and F(q,*) represent elliptic integrals of the first kind.

The vertical deflection y can be derived from equations (A.2) and (A.6) as

$$dy = \frac{\pm\ \sin\Theta\ d\Theta}{K(2\cos\Theta - 2\cos\beta)^{1/2}} \qquad (A.14)$$

where the positive and negative signs correspond to the same portions of the member as before. Integrating both sides of equation (A.14) from A to B and using the relation

$\sin\Theta = 2\sin\frac{\Theta}{2}\,(1-\sin^2\frac{\Theta}{2})^{1/2}$ together with the same changes of variables as used for equations (A.9), (A.10), (A.11), and (A.12) yields

$$Y_m = \frac{2q}{K}\,(\cos\chi + \cos\psi) \qquad (A.15)$$

where Y_m = vertical deflection at the midspan. From the development of equation (A.15), it can be shown that

$$Y_\beta = \frac{2q}{K}\cos\chi \qquad (A.16a)$$

where Y_β = vertical deflection at the point of inflection. It is evident from the moment equilibrium of portion AC that $Y_\beta = -M_1 = \frac{k_\Theta \Theta_e}{P}$, and so

$$\frac{k_\Theta \Theta_e}{P} = \frac{2q}{K}\cos\chi \qquad (A.16b)$$

Additional equations can be obtained from bending moment conditions if plastification occurs. That is,

$$k_\Theta \Theta_e = M_{pcm} = -M_1 \qquad (A.16c)$$

for plastification at the member ends, and

$$\frac{2q}{K}\cos\psi = \frac{M_{pcm}}{P} \qquad (A.17)$$

for plastification at midspan, where M_{pcm} is given by equation (2.10). Geometry of the member in Figure (A.1) also yields

$$\Theta_0 = \Theta_e + \Theta_{1p} \qquad (A.18)$$

where Θ_0 is the angle between the tangent of the elastic curve at point A and the horizontal axis. In order to

obtain the horizontal distance x, equation (A.6) and the relation

$$\frac{dx}{ds} = \cos\Theta \tag{A.19}$$

can be solved to give

$$dx = \frac{\pm\cos\Theta d\Theta}{K(2\cos\Theta - 2\cos\beta)^{1/2}} \tag{A.20}$$

Integrating equation (A.20) along path AB and using the procedure utilized to get equation (A.13), results in

$$X_m = \frac{2}{K}\left[2E(q) - E(q,\chi) - E(q,\psi)\right] - \frac{S}{2} \tag{A.21}$$

where E(q) and E(q,*) represent elliptic integrals of the second kind, and X_m is the horizontal projection of the deformed half member. The relative end displacement Δ can then be obtained from the equation

$$\Delta = 2\left(\frac{L}{2} - X_m\right) \tag{A.22}$$

Solution

The presence of the elliptic integrals prevents a closed-form solution to these equations since the quantities q, χ, and ψ have to be known before the integrals can be evaluated. Hence, an iterative procedure is required to solve these equations. It is most convenient to select the axial load P as the independent variable and to use the knowledge that when the member is elastic, the angle Θ_0 increases as the compressive load P increases while Θ_{1p} and Θ_{2p} remain constant in the method of solution.

A value of P is selected, and a corresponding value of Θ_0 can be assumed. After Θ_e is obtained from equation (A.18), equation (A.16b) can be solved to give

$$\beta = \cos^{-1} \left(\cos\Theta_0 - \frac{k^2{}_0\Theta^2{}_e}{2PEI}\right) \qquad \text{(A.16b')}$$

Once β is known, q, χ, and ψ can be evaluated from equations (A.9a), (A.10a), and (A.10b), respectively. Equation (A.13) then gives a check on the assumed value of Θ_0. If

$$\frac{S}{2} = \frac{1}{K} \left[2F(q) - F(q,\chi) - F(q,\psi)\right]$$

is not equal to the exact value $\frac{1}{2}\left(L-\frac{PL}{AE}\right)$, pick a new value of Θ_0 and rework the above calculation. This process is repeated until the two values of $\frac{S}{2}$ are equal or satisfactorily close to each other. The final correct values of q, χ, and ψ are substituted in equations (A.15) and (A.21) to yield Y_m and X_m. Equation (A.22) then gives the value of Δ. For the next data point, the same iteration procedure is applied to the new selected values of P and Θ_0 such that $P_{new} > P_{old}$ and $\Theta_{0new} > \Theta_{0old}$. In this model where the connections have equal flexural strength to the member, and the connection is nonrigid, plastic hinge will occur and reoccur first at midspan. So this iterative method is valid until the bending moment at midspan, M_2, is equal to the modified plastic moment as given by equation (2.10).

The member then deforms plastically as P decreases and Θ_0 increases, so $P_{new} < P_{old}$ and $\Theta_{0new} > \Theta_{0old}$ are

selected. Θ_e and β are obtained from equations (A.18) and (A.16b') as before, but Θ_{2p} becomes an unknown. Equations (A.9a) and (A.10a) give the values of q and χ and equation (A.17) is solved for ψ. A similar check on the correctness of the assumed Θ_0 is again given by equation (A.13). The process is repeated with a revised value of Θ_0, if necessary, until the two values of $\frac{S}{2}$ from equation (A.13) agree. Y_m, X_m, and Δ can then be obtained from the same set of equations as before. This procedure is repeated for the new data points until the bending moment at the member ends, M_1, attains its modified plastic moment value.

After the second plastification develops at the member ends, decreasing load along the double plastic rotation region is accompanied by increasing Θ_0; therefore $P_{new} < P_{old}$ and $\Theta_{0new} > \Theta_{0old}$ are chosen. This time Θ_{1p} is also an unknown while equation (A.16c) provides the value of Θ_e. Similar iteration procedure as the one used for the single plastic rotation region can be utilized to obtain the required results.

A.1.2. Case II: - Inflection Point Outside the Member Length

Derivation

When the relative displacement of the member ends changes direction after some plastic rotation has occured, the reduction in magnitude of M_2 is greater than that of M_1 as the compressive load decreases. So along this elastic post-compression induced plastic rotation region, the

inflection point moves towards point B in Figure A.1. Equations (A.13), (A.15), (A.16a and b), (A.21), and (A.22) govern this member behavior until the inflection point is at point B. The method of solution for this portion of the hysteresis loop is also the same as that of the elastic region of Case I, but P and trial Θ_0 for each new data point are chosen such that $P_{new} < P_{old}$ and $\Theta_{0new} < \Theta_{0old}$.

Once the inflection point is at point B, further decrease in the load results in the deformed half member without a contraflexure point within its length as shown in Figure A.2. However, the half member can be assumed to extend to point D in Figure A.2 which is an imaginary inflection point. This point of inflection is significant for the purpose of converting the derived integrals into the standard elliptic integrals.

For the half member with the extension part as shown in Figure A.2, equations (A.1-A.6) remain valid but with

$$ds = \frac{d\Theta}{K(2\cos\Theta - 2\cos\beta)^{1/2}} \qquad (A.6')$$

Upon integrating from A to B, equation (A.6') yields

$$\frac{S}{2} = \frac{1}{K}\int_{\Theta_0}^{\Theta_{2p}} \frac{d\Theta}{(2\cos\Theta - 2\cos\beta)^{1/2}} = \frac{1}{2}\left(L-\frac{PL}{AE}\right) \qquad (A.23)$$

because the deformed half-member length is also equal to $\frac{1}{2}\left(L-\frac{PL}{AE}\right)$. By performing the changes of variables as those utilized in Case I, equation (A.23) can be changed into

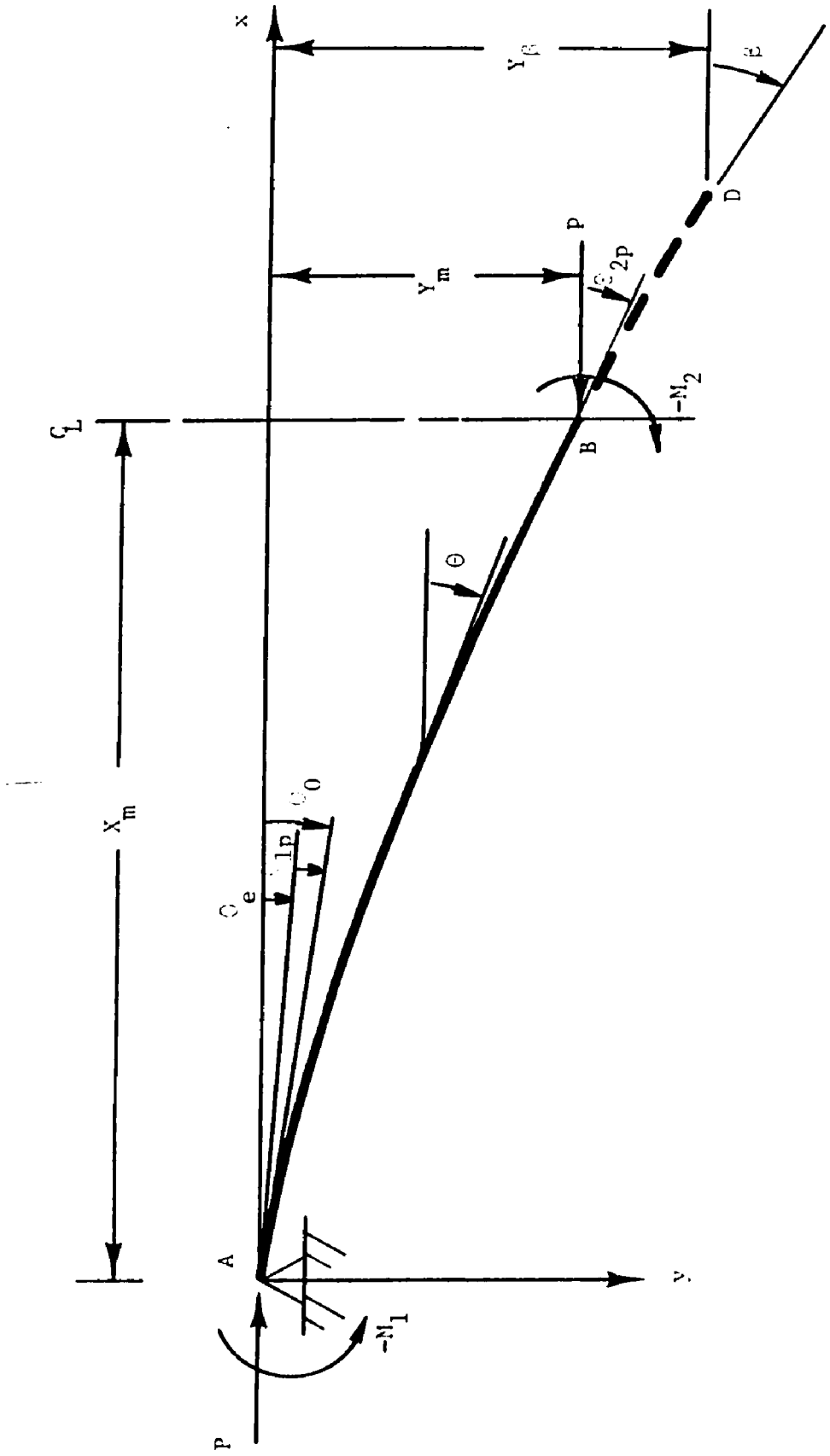


Figure A.2 Half Member with Inflection Point Outside Its Length

$$\frac{S}{2} = \frac{1}{K}\,[F(q,\psi) - F(q,\chi)] = \frac{1}{2}\,(L - \frac{PL}{AE}) \qquad (A.24)$$

The derivation of the vertical deflection y, the horizontal distance x, and the axial displacement Δ are analogous to those of Case I, and the corresponding results are

$$Y_m = \frac{2q}{K}\,(\cos\chi - \cos\psi) \qquad (A.25)$$

$$Y_\beta = \frac{2q}{K}\,(\cos\chi) = \frac{k_\theta \theta_e}{P} \qquad (A.16b)$$

$$X_m = \frac{2}{K}\,[E(q,\psi) - E(q,\chi)] - \frac{S}{2} \qquad (A.26)$$

and $$\Delta = 2\,(\frac{L}{2} - X_m) \qquad (A.22)$$

Solution

The method of solution for this set of equations is quite similar to that of the elastic region of Case I. The main difference is that in this case, as the load decreases, θ_0 also decreases. So the values $P_{new} < P_{old}$ and $\theta_{0new} < \theta_{0old}$ should be selected. θ_{1p} and θ_{2p} are constant known values because this is an elastic region. The values of θ_e, β, χ, and ψ can be obtained from equations (A.18), (A.16b'), (A.10a) and (A.10b), respectively. This time equation (A.24) provides a similar check for the correctness of the assumed θ_0 as equation (A.13) did in Case I. θ_0 is revised until the two values of $\frac{S}{2}$ from equation (A.24) agree. Then solving equations (A.25), (A.26), and (A.2), gives the values of Y_m, X_m, and Δ, respectively. This procedure is repeated to get new data

points until the compressive load decreases to zero magnitude.

A.2. Zero Load Configuration Derivation

When the applied load decreases to zero magnitude, bending moments still exist in the member due to Θ_e. This remaining Θ_e results from the difference in residual plastic rotation angles Θ_{1p} and Θ_{2p}. In the absence of the applied load, the half member has constant moment and curvature throughout its length. The differential equation of the deflection curve is

$$EI \frac{d\Theta}{ds} = k_\Theta \Theta_e \qquad (A.27)$$

Rearranging equation (A.27) and integrating both sides along the half member in Figure A.3 yields

$$\frac{S}{2} = \frac{EI}{k_\Theta \Theta_e} (\Theta_{2p} - \Theta_0) = \frac{L}{2} \qquad (A.28)$$

The vertical deflection y and the horizontal distance x can be obtained by integration of the basic governing equations (A.2) and (A.19) to give

$$Y_m = \frac{EI}{k_\Theta \Theta_e} (\cos\Theta_0 - \cos\Theta_{2p}) \qquad (A.29)$$

and

$$X_m = \frac{EI}{k_\Theta \Theta_e} (\sin\Theta_{2p} - \sin\Theta_0) \qquad (A.30)$$

the axial displacement Δ is given by equation (A.22).

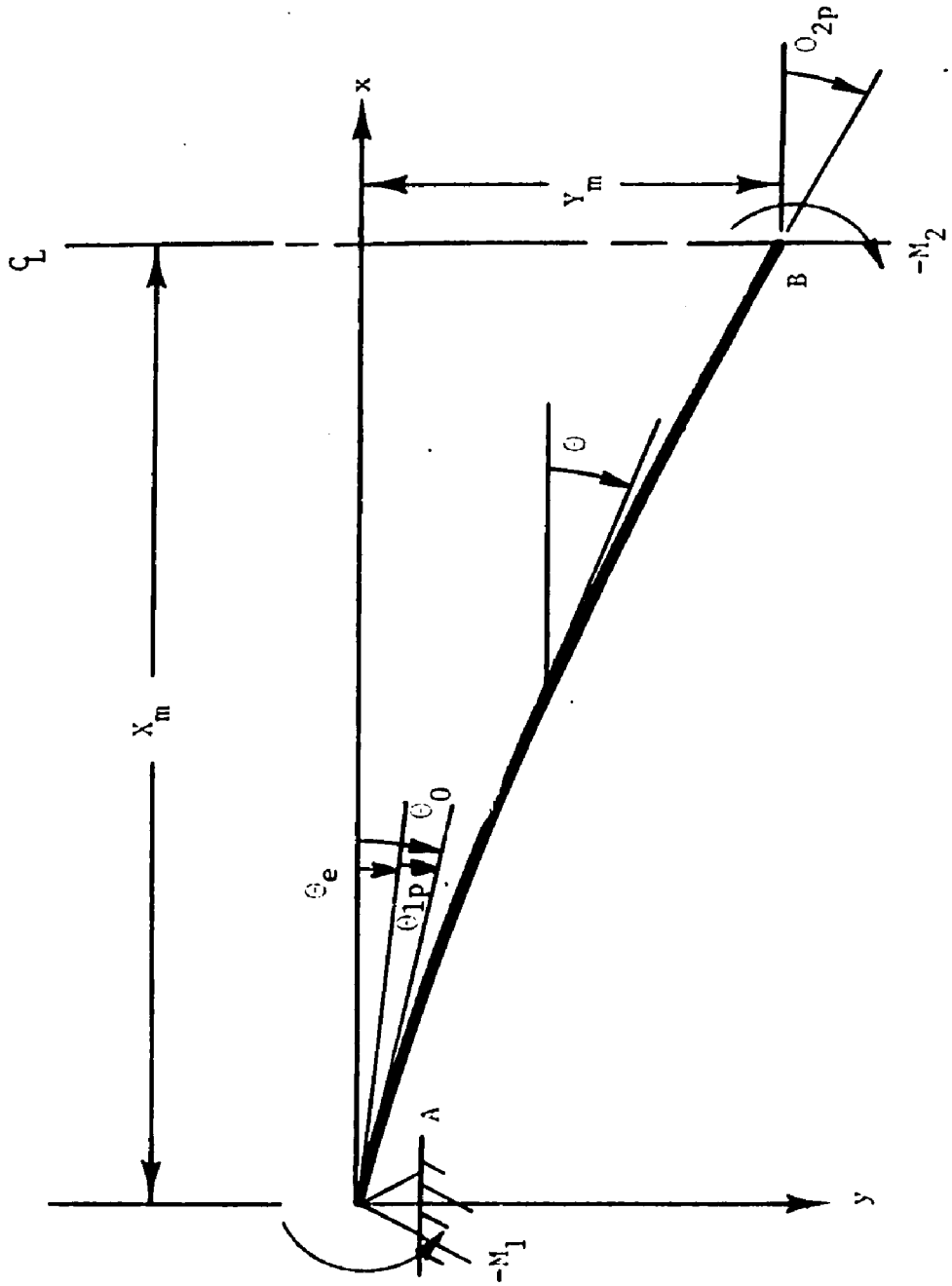


Figure A.3 Zero Load Configuration of the Half Member

Solution

This set of equations has a closed-form solution. By knowing the values of θ_{1p} and θ_{2p} because the member is elastic, equations (A.18) and (A.28) are solved for θ_e. Then Y_m, X_m, and Δ can be determined from equations (A.29), (A.30), and (A.22), respectively.

A.3. Tensile Loading

When a non fixed-ended member with the connections that have flexual strength equal to that of the member is subjected to small tensile load, there is no point of contraflexure in the half member or the extended part to the right of it (see Figures A.1 and A.2). This is evident from the moment equilibrium condition of the half member (AB) shown in Figure A.4. If the half member is assumed to extend to the left side (Figure A.4), there can also be no inflection point because the tensile load magnitude is small enough to make the moment due to this load too small to balance the connection restraining moment. Such a configuration is shown in Figure A.4. Increase in the magnitude of tensile load increases the corresponding bending moment introduced by the load and makes it possible to balance the connection restraining moment. So the inflection point can occur in the extended portion to the left side of the half member. Analogous to the compression-loading case, this point of contraflexure is particularly important for the conversion of the integrals in the

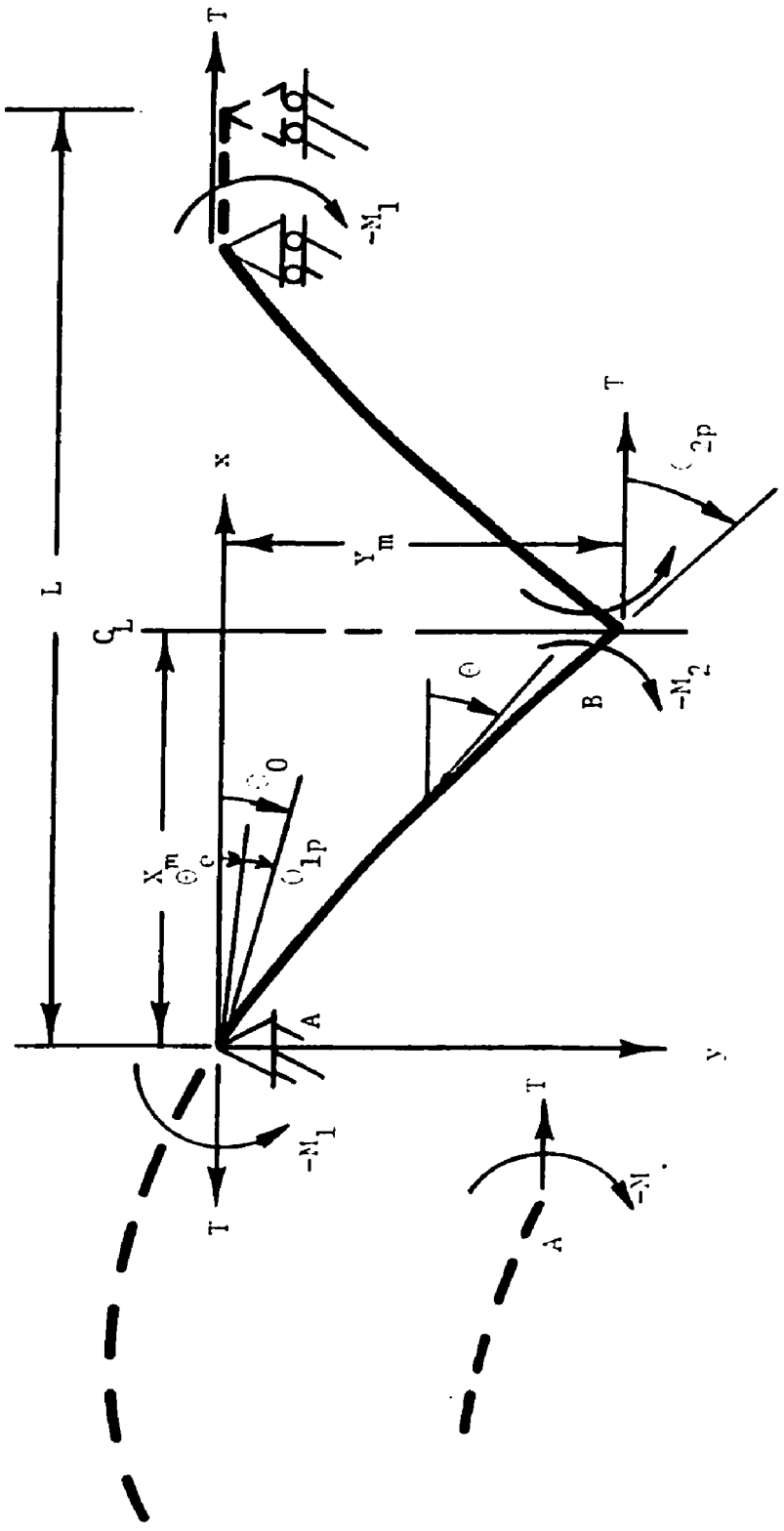


Figure A.4 Member Subjected to Tensile Loading

governing equations of the member behavior into the standard elliptic integrals.

The governing equations of the member behavior under tensile load are derived by procedure similar to that for the member under compressive load. Equations (A.1)-(A.4) are valid, and with the introduction of T = -P (for T, tension is positive, and so T is positive for this case), equation (A.4) can be changed to

$$\frac{EI}{2}\left(\frac{d\Theta}{ds}\right)^2 = -T\cos\Theta + Q' \qquad (A.31)$$

Further derivation of the governing equations depends on the characteristic of the inflection point.

A.3.1. Case I: - No Inflection Point

Derivation

As described above, it is possible that a member subjected to small tensile load may not have an inflection point as shown in Figure A.4. This configuration has controlling equations with the integrals that cannot be converted into the standard elliptic integrals. The constant Q' of equation (A.31) is evaluated at point A where $\Theta = \Theta_0$ and $\frac{d\Theta}{ds} = \frac{k_\Theta \Theta_e}{EI}$ to give

$$Q' = T\cos\Theta_0 + \frac{k_\Theta^2 \Theta_e^2}{2EI}$$

Equation (A.31), after the substitution of Q', can be rearranged as

$$ds = \frac{d\theta}{K\left(-2\cos\theta + 2\cos\theta_0 + \frac{k_\theta^2\theta_e^2}{TEI}\right)^{1/2}} \qquad (A.32)$$

where $K^2 = \frac{T}{EI}$. Upon integration, equation (A.32) yields

$$\frac{S}{2} = \int_{\theta_0}^{\theta_{2p}} \frac{d\theta}{K\left(-2\cos\theta + 2\cos\theta_0 + \frac{k_\theta^2\theta_e^2}{TEI}\right)^{1/2}}$$

$$= \frac{1}{2}\left(L + \frac{TL}{AE}\right) \qquad (A.33)$$

since $\frac{S}{2}$ also equals $\frac{1}{2}\left(L + \frac{TL}{AE}\right)$.

Y and x can be obtained from equations (A.2), (A.19), and (A.32). The results after integration are

$$Y_m = \int_{\theta_0}^{\theta_{2p}} \frac{\sin\theta d\theta}{K\left(-2\cos\theta + 2\cos\theta_0 + \frac{k_\theta^2\theta_e^2}{TEI}\right)^{1/2}}$$

$$= \frac{1}{K}\left[\left(-2\cos\theta_{2p} + 2\cos\theta_0 + \frac{k_\theta^2\theta_e^2}{TEI}\right)^{1/2} - \frac{k_\theta\theta_e}{(TEI)^{1/2}}\right] \qquad (A.34)$$

and

$$X_m = \int_{\theta_0}^{\theta_{2p}} \frac{\cos\theta d\theta}{K\left(-2\cos\theta + 2\cos\theta_0 + \frac{k_\theta^2\theta_e^2}{TEI}\right)^{1/2}} \qquad (A.35)$$

Δ is given by equation (A.22).

Solution

The integrals in this case have to be evaluated numerically since they cannot be transformed into the standard elliptic integrals. θ_{1p} and θ_{2p} are known

constants since this is an elastic region. Is it also obvious that Θ_0 decreases as T increases. So for each load increment, the values $T_{new} > T_{old}$ and $\Theta_{0new} < \Theta_{0old}$ are chosen. Θ_e is obtained from equation (A.18). Equation (A.33) gives a comparison of the exact value of $\frac{S}{2}$ $[\frac{1}{2}$ $(L + \frac{TL}{AE})]$ with the value obtained by using the trial Θ_0. Θ_0 is reselected if necessary, until the two values of $\frac{S}{2}$ from equation (A.33) coincide. Then, Y_m, X_m, and Δ can be obtained from equation (A.34), (A.35), and (A.22), respectively. This procedure is repeated for additional data points until the tensile load is large enough to introduce an inflection point on the extended portion to the left of the half member.

A.3.2. Case II: - Inflection Point Outside the Member Length

Derivation

The half member tensile load with the fictitious inflection point in the extended portion AE is shown in Figure A.5. Evaluating the constant Q' of equation (A.31) at point E where $\Theta = \beta$ and $\frac{d\Theta}{ds} = 0$ gives

$$Q' = T\cos\beta$$

Therefore

$$ds = \frac{d\Theta}{K\ (-2\cos\Theta + 2\cos\beta)^{1/2}} \qquad (A.36)$$

Upon integration, equation (A.36) yields

$$\frac{S}{2} = \frac{1}{K} \int_{\Theta_0}^{\Theta_{2p}} \frac{d\Theta}{(-2\cos\Theta + 2\cos\beta)^{1/2}} = \frac{1}{2}\ (L+\frac{TL}{AE}) \qquad (A.37)$$

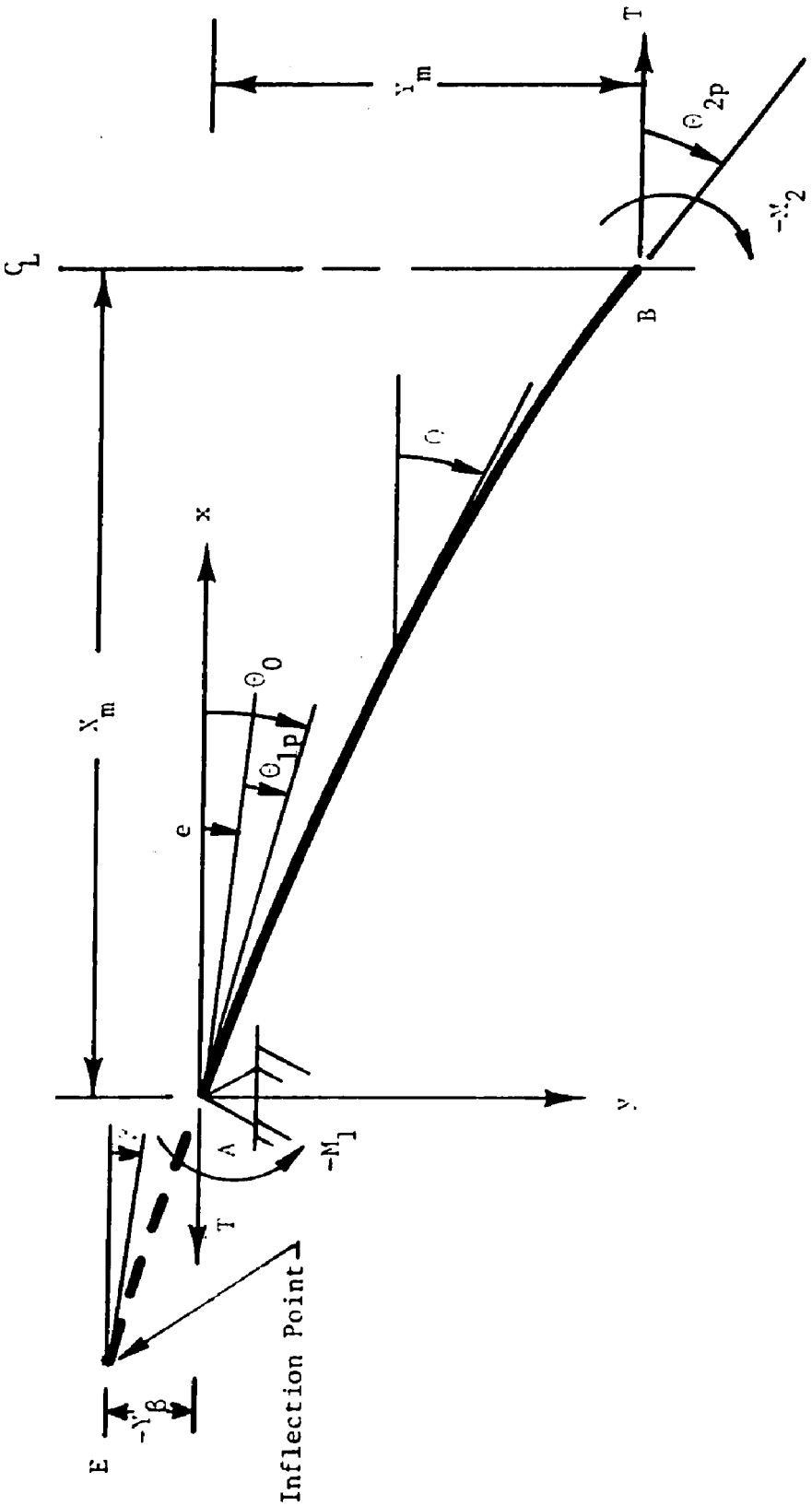


Figure A.5 Half Member with Inflection Point Outside Its Length

Let

$$\cos \frac{\beta}{2} = m$$

$$\cos \frac{\Theta}{2} = m \cos\xi$$

and notice that as Θ assumes the values β, Θ_0, and Θ_{2p}, ξ assumes the values $\frac{\pi}{2}$, ζ, and η, respectively, where

$$\zeta = \cos^{-1} \frac{\cos\frac{\Theta_0}{2}}{\cos\frac{\beta}{2}} \qquad \text{(A.38a)}$$

and

$$\eta = \cos^{-1} \frac{\cos\frac{\Theta_{2p}}{2}}{\cos\frac{\beta}{2}} \qquad \text{(A.38b)}$$

Performing the above changes of variables in equation (A.37) produces

$$\frac{S}{2} = \frac{1}{K} \int_{\frac{\pi}{2}}^{\zeta} \frac{d\xi}{(1-m^2\cos^2\xi)^{1/2}} - \frac{1}{K} \int_{\frac{\pi}{2}}^{\eta} \frac{d\xi}{(1-m^2\cos^2\xi)^{1/2}} \qquad \text{(A.39)}$$

By allowing $\xi = \frac{\pi}{2} - \rho$ ($d\xi = -d\rho$) and noticing that as ξ equals $\frac{\pi}{2}$, ζ, and η, the corresponding values of ρ are 0, $\frac{\pi}{2}-\zeta$, and $\frac{\pi}{2}-\eta$; equation (A.39) can be transformed to give

$$\frac{S}{2} = \frac{1}{K} \left[F(m,\tfrac{\pi}{2} - \zeta) - F(m,\tfrac{\pi}{2} - \eta)\right] = \frac{1}{2} \left(L+\frac{TL}{AE}\right) \qquad \text{(A.40)}$$

The deflection y is derived in a manner analogous

to that for the member under compressive load with the above changes of variables. The results are

$$Y_m = \frac{2m}{K} (\sin\eta - \sin\zeta) \tag{A.41}$$

and

$$Y_\beta = \frac{-2m}{K} \sin\zeta = \frac{-k_\Theta \Theta_e}{T} \tag{A.42}$$

Similar derivation for the horizontal distance x yields

$$X_m = \frac{S}{2} - \frac{2}{K} [E(m, \frac{\pi}{2} - \zeta) - E(m, \frac{\pi}{2} - \eta)] \tag{A.43}$$

and Δ is given by equation (A.22).

Solution

In this region, the reappearance of the contra-flexure point makes it possible to transform the integrals into the standard elliptic integrals and thus eliminates the necessity of numerical integration. By knowing that Θ_0 decreases as T increases, incremental values of T and Θ_0 are chosen such that $T_{new} > T_{old}$ while $\Theta_{0new} < \Theta_{0old}$. Θ_e can be determined from equation (A.18) since Θ_{1p} and Θ_{2p} are still known constants. Solving equation (A.42) yields

$$\beta = \cos^{-1} (\cos\Theta_0 + \frac{k_\Theta^2 \Theta_e^2}{2\ TEI})$$

Then equations (A.38a and b) give the values of ζ and η. Equation (A.40) can be used to check whether the chosen Θ_0 is correct. If the two values of $\frac{S}{2}$ from equation (A.40) are not equal, the calculation is repeated with a revised value of Θ_0 until both values of $\frac{S}{2}$ agree. Then y_m, X_m, and Δ can

be obtained from equations (A.41), (A.43), and (A.22), respectively. This procedure is repeated for the new data points until the point of inflection moves to point A. This stage corresponds to zero elastic rotation angle and hence, zero moment ($M_1 = 0$) at the member ends. Any increase in tensile load magnitude will change the direction of Θ_e and M_1 and reintroduce the inflection point within the member length.

A.3.3. Case III: - Inflection Point Within the Member Length

Derivation

The controlling equations of Case II are also valid in this case up to equation (A.36) which changes slightly to

$$ds = \pm \frac{d\Theta}{K\ (-2\cos\Theta + 2\cos\beta)^{1/2}} \qquad (A.36')$$

where the negative sign governs the portion AF and the positive sign governs the portion FB in Figure A.6. By integrating equation (A.36') from A to B the half length of the member is given by

$$\frac{S}{2} = \frac{1}{K} \int_{\Theta_0}^{\beta} \frac{-d\Theta}{(-2\cos\Theta + 2\cos\beta)^{1/2}} + \frac{1}{K} \int_{\beta}^{\Theta_{2p}} \frac{d\Theta}{(-2\cos\Theta + 2\cos\beta)^{1/2}} \qquad (A.44)$$

By the same process of changes of variables as in Case II, equation (A.44) can be converted into

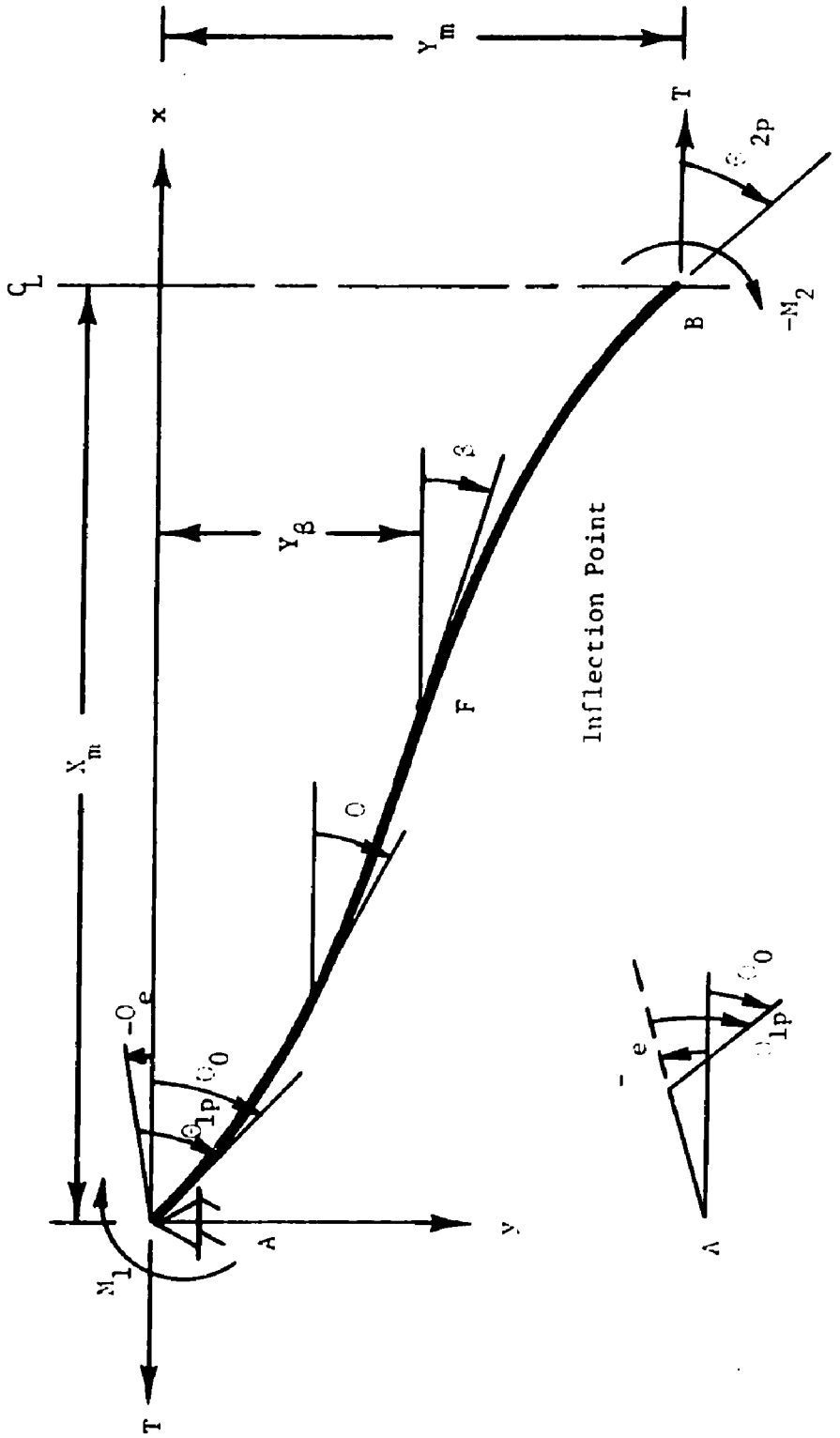


Figure A.6 Half Member with Inflection Point Within Its Length

$$\frac{S}{2} = \frac{1}{K} \cdot [2F(m) - F(m, \frac{\pi}{2} - \zeta) - F(m, \frac{\pi}{2} - \eta)]$$

$$= \frac{1}{2} (L + \frac{TL}{AE}) \qquad (A.45)$$

The vertical deflection y and the horizontal distance x are obtained by solving equations (A.2), (A.19) and (A.36') using appropriate integrals and changes of variables as used in Case II. The results including the plastic hinge conditions are:

$$Y_m = \frac{2m}{K} (\sin\zeta + \sin\eta) \qquad (A.46)$$

$$Y_\beta = \frac{2m}{K} (\sin\zeta) = \frac{-k_\theta \theta_e}{T} \qquad (A.47a)$$

$$k_\theta \theta_e = M_{pcm} \qquad (A.47b)$$

if plastic hinges occur at the member ends

$$\frac{2m}{K} \sin\eta = M_{pcm} \qquad (A.48)$$

if plastic hinge occurs at midspan, and

$$X_m = \frac{S}{2} + \frac{2}{K} [-2E(m) + E(m, \frac{\pi}{2} - \zeta) + E(m, \frac{\pi}{2} - \eta)] \qquad (A.49)$$

The axial displacement Δ is given by equation (A.22).

Solution

The method of solution in this case is similar to that of Case II. The main difference is that θ_e is always negative in this case. Since θ_0 decreases as T increases, $T_{new} > T_{old}$ and $\theta_{0new} < \theta_{0old}$ are selected. θ_{1p} and θ_{2p} are known constants as long as the member is still elastic. Equations (A.18) and (A.47a) can be solved for θ_e and β. Then ζ and η are obtained from equations (A.38a and b).

Equation (A.45) gives a check for the correctness of the selected Θ_0 in a manner similar to the check of Case II. The process is repeated with a new value of Θ_0, if necessary, until the correct results are obtained. Then equations (A.46), (A.49), and (A.22) give the value of Y_m, X_m, and Δ, respectively. As mentioned earlier, a nonfixed-ended member that has connection flexural strength equal to the member flexural strength always plastifies or replastifies first at midspan. So this procedure is repeated for additional data points until plastification redevelops at the midspan.

After the midspan plastic hinge occurs, Θ_{2p} becomes an unknown. The method of selection of the new T and Θ_0 used above is still valid. The above process for determining the values of Θ_e, β, and ζ is repeated here while equation (A.48) gives the value of η. Equation (A.45) yields the same check on the value of $\frac{S}{2}$ for the assumed Θ_0. After this computation is repeated for each revised value of Θ_0 until the correct values of Θ_0, β, ζ, and η are obtained, equations (A.46), (A.49), and (A.22) can be solved for Y_m, X_m, and Δ. This procedure is repeated for new data points until plastic hinges reoccur at the member ends.

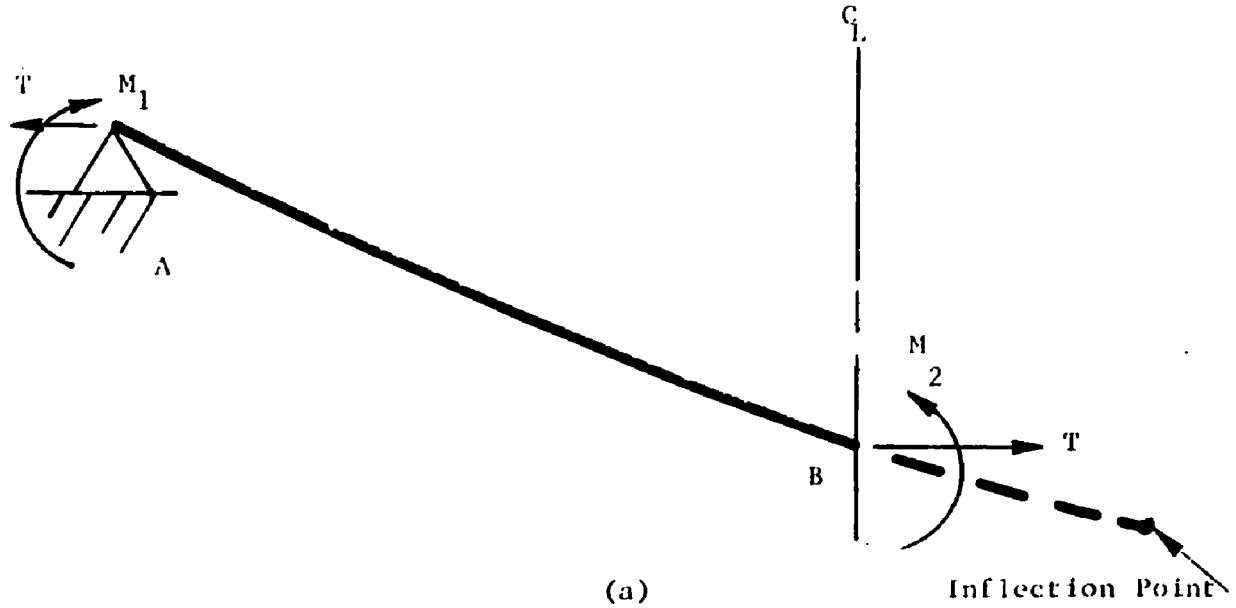
In the double plastic rotation region under tensile load, $T_{new} > T_{old}$ and $\Theta_{0new} < \Theta_{0old}$ are still chosen because increasing load is accompanied by decreasing Θ_0. Θ_e is given by equation (A.47b) while Θ_{1p} becomes an unknown which can be determined from equation (A.18). Except for the differences in obtaining Θ_e and Θ_{1p}, the rest of the

iteration procedure for the correct value of θ_0 and the computation of the values of Y_m, X_m, and Δ are the same as those utilized in the preceding single plastic rotation region under tensile load.

A.4. Other Possible Equilibrium Configurations

It is evident from the above derivations that the solutions of this exact expression for curvature model are quite involved. Furthermore, these derivations are not complete. There are other possible equilibrium configurations of the member under the applied load. These configurations, although employing the same fundamental governing equations as used above, have different forms of the final equations. Additional member equilibrium configurations are shown in Figure A.7. Figure A.7a demonstrates the half-member configuration along the elastic post-tension induced plastic rotation region under tensile load, whereas Figure A.7b demonstrates the configuration along the same region under small compressive load.

If the connections are allowed to have smaller flexural strength than the member, the sequence of the member equilibrium configurations can be different from the above sequence for the equal flexural strength case. This difference is the direct consequence of the reduction in the plastic moment capacity of the connections. Examples of half-member configuration for this type of member are shown in Figure A.8. The configuration in Figure



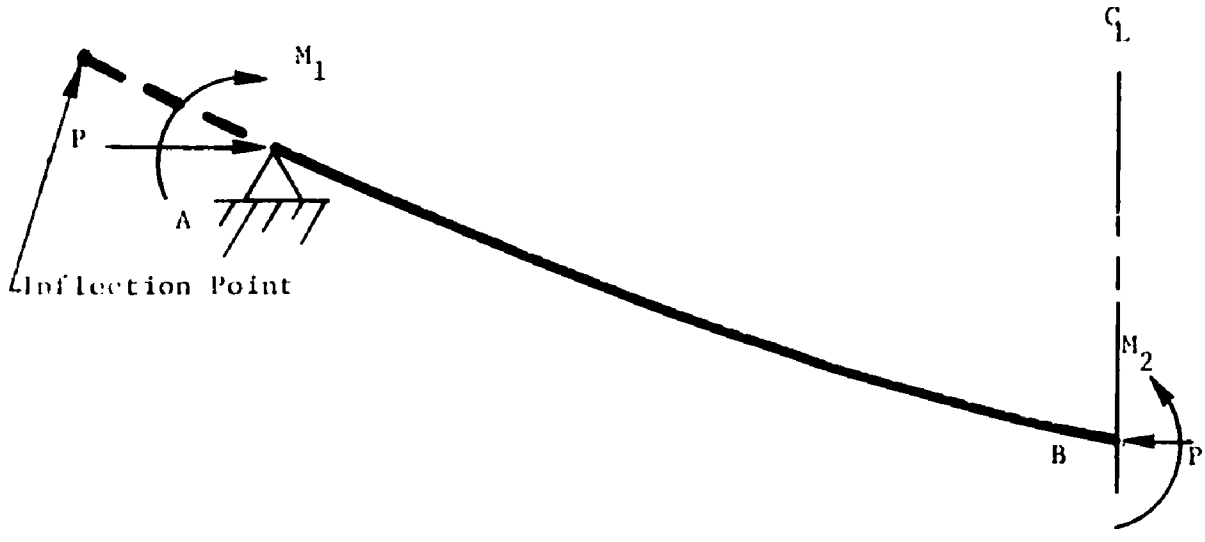


Figure A.7 Additional Member Equilibrium Configurations

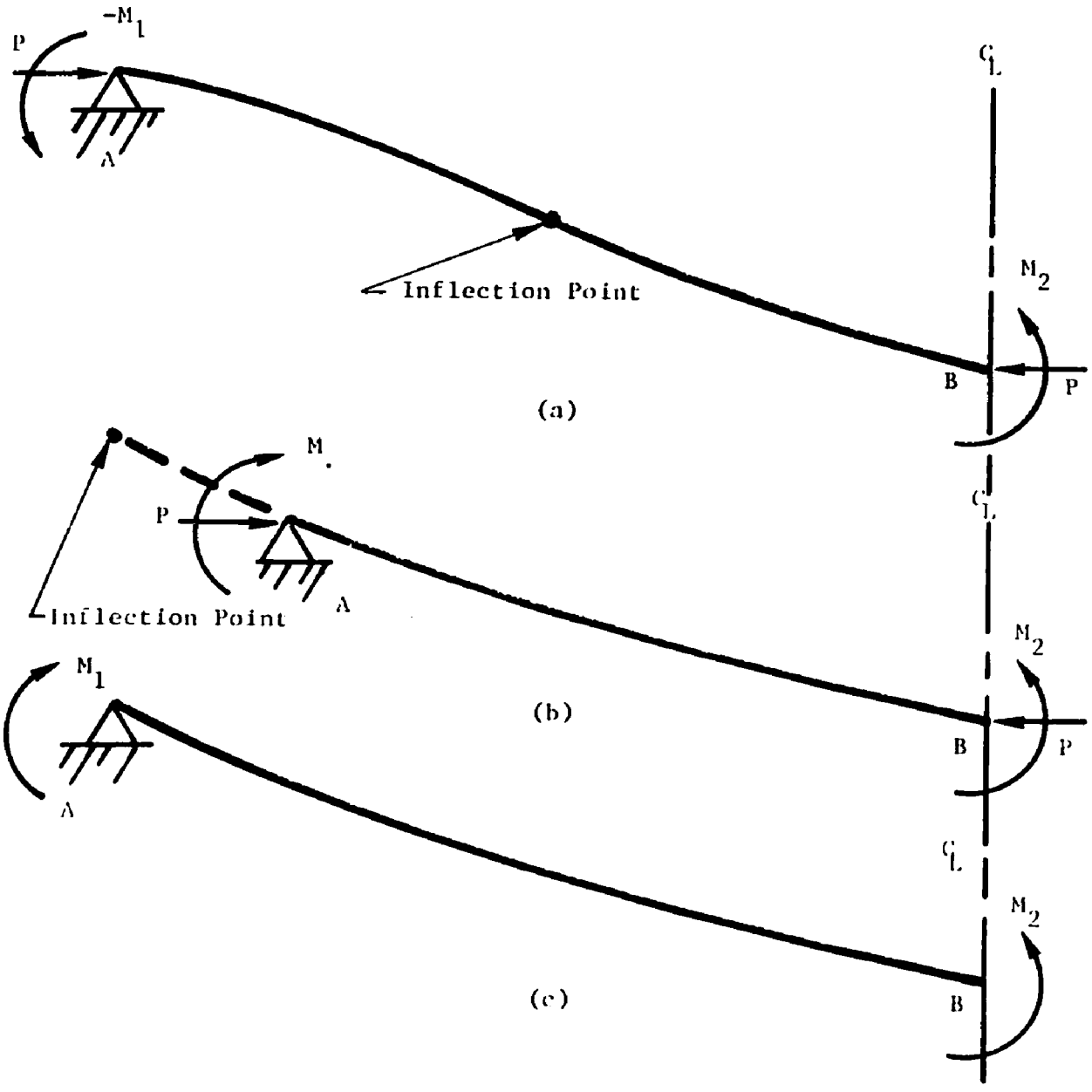


Figure A.8 Equilibrium Configurations of the Member with Connections that Have Smaller Flexural Strength than the Member

A.8a is similar to that of Figure A.1 and is also valid for the initial elastic, the single plastic rotation, and the double plastic rotation regions under compressive load. But the elastic post-compression induced plastic rotation under compressive load configuration and the following zero load configuration as shown in Figures A.8b and c are different from those of the equal strength case (Figures A.2 and A.3).

The derivation of the remaining governing equations and the corresponding method of solution were not completed due to increasing complexity and the number of possible member configurations.

REFERENCES

1. Housner, G. W., "Limit Design of Structures to Resist Earthquakes," Proceedings, World Conference on Earthquake Engineering, Berkeley, California, June, 1956.
2. Berg, G. V., "The Analysis of Structural Response to Earthquake Forces," Ph.D. Thesis, The University of Michigan, Ann Arbor, Michigan, 1958.
3. Newmark, N. M., "A Method of Computation for Structural Dynamics," Journal of the Engineering Mechanics Division, ASCE, Vol. 85, No. EM3, July, 1959, pp. 67-94.
4. Penzien, J., "Dynamic Response of Elasto-Plastic Frames," Journal of the Structural Division, ASCE, Vol. 86, No. ST7, July, 1960, pp. 81-94.
5. Iwan, W. D., "The Dynamic Response of Bilinear Hysteretic Systems," Ph.D. Thesis, California Institute of Technology, Pasadena, California, 1961.
6. Clough, R. W., Benuska, K. L., and Wilson, E. L., "Inelastic Earthquake Response of Tall Buildings," Proceedings, Third World Conference on Earthquake Engineering, Auckland and Wellington, New Zealand, 1965.
7. Giberson, M. F., "The Response of Nonlinear Multi-story Structures Subjected to Earthquake Excitation,"

Ph.D. Thesis, California Institute of Technology, Pasadena, California, May, 1967.

8. Jennings, P. C., "Earthquake Response of a Yielding Structure," Journal of the Engineering Mechanics Division, ASCE, Vol. 91, No. EM4, August, 1965, pp. 41-68.

9. Kaldjian, M. J. and Fan, W. R. S., "Earthquake Response of a Ramberg-Osgood Structure," Journal of the Structural Division, ASCE, Vol. 94, No. ST10, October, 1968, pp. 2451-2465.

10. Goel, S. C. and Berg, G. V., "Inelastic Earthquake Response of Tall Steel Frames," Journal of the Structural Division, ASCE, Vol. 94, No. ST8, August, 1968, pp. 1907-1934.

11. Hanson, R. D. and Fan, W. R. S., "The Effect of Minimum Cross Bracing on the Inelastic Response of Multistory Buildings," Proceedings, Fourth World Conference on Earthquake Engineering, Santiago, Chile, January, 1969.

12. Workman, G. W.,"The Inelastic Behavior of Multistory Braced Frame Structures Subjected to Earthquake Excitation," Ph.D. Thesis, The University of Michigan, Ann Arbor, Michigan, September, 1969.

13. Goel, S. C. and Hanson, R. D., "Seismic Behavior of Multistory Braced Steel Frames," Journal of the Structural Division, ASCE, Vol. 100, No. ST1, January, 1974, pp. 79-95.

14. Popov, E. P. and Pinkney, R. B., "Cyclic Yield Reversal in Steel Building Joints," Journal of the Structural Division, ASCE, Vol. 95, No. ST3, March, 1969, pp. 327-353.

15. Popov, E. P. and Stephen, R. M., "Cyclic Loading of Full-Size Steel Connections," Earthquake Engineering Research Center, Report No. EERC-70-3, University of California, Berkeley, California, July, 1970.

16. Almuti, A. M. and Hanson, R. D., "Static and Dynamic Cyclic Yielding of Steel Beams," Journal of the Structural Division, ASCE, Vol. 99, No. ST6, June, 1973, pp. 1273-1285.

17. Bertero, V. V., Popov, E. P., and Krawinkler, H., "Beam-Column Subassemblages Under Repeated Loading," Journal of the Structural Division, ASCE, Vol. 98, No. ST5, May, 1972.

18. Feder, D. K. and Lee, G. C., "Residual Stresses in High Strength Steel," Report No. 269.2, Fritz Engineering Laboratory, Lehigh University, Bethlehem, Pa., March, 1959.

19. Tall, L., "Recent Developments in the Study of Column Behavior," Report No. 249.21, Fritz Engineering Laboratory, Lehigh University, Bethlehem, Pa., September, 1963.

20. McFalls, R. K. and Tall, L., "A Study of Welded Columns Manufactured from Flame-Cut Plates," Report No. 321.1, Fritz Engineering Laboratory, Lehigh University,

Bethlehem, Pa., June, 1967.

21. Bijlaard, P. P., Fisher, G. P., and Winter, G., "Eccentrically Loaded End-Restrained Columns," Transactions, ASCE, Vol. 120, 1955.

22. Galambos, T. V. and Ketter, R. L., "Columns Under Combined Bending and Thrust," Journal of the Engineering Mechanics Division, ASCE, Vol. 85, No. EM2, April, 1959.

23. Chen, W. F. and Santathadaporn, S., "Curvature and the Solution of Eccentrically Loaded Columns," Journal of the Engineering Mechanics Division, ASCE, Vol. 95, No. EM1, February, 1969.

24. Lay, M. G. and Galambos, T. V., "End-Moment End-Rotation Characteristics for Beam-Columns," Report No. 205A.36, Fritz Engineering Laboratory, Lehigh University, Bethlehem, Pa., May, 1962.

25. Fukumoto, Y. and Galambos, T. V., "Inelastic Lateral-Torsional Buckling of Beam-Columns," Journal of the Structural Division, ASCE, Vol. 93, No. ST2, April, 1966.

26. Birnstiel, C., Harstead, G. A., and Leu, K. C., "Inelastic Behavior of H-Columns Under Biaxial Bending," New York University, N. Y., November, 1967.

27. Chen, W. F. and Santathadaporn, S., "Review of Column Behavior under Biaxial Loading," Journal of the Structural Division, ASCE, Vol. 94, No. ST.12, December, 1968.

28. Sharma, S. S. and Gaylord, E. H., "Strength of Steel Columns with Biaxially Eccentric Load," Journal of the Structural Division, ASCE, Vol. 95, No. ST.12, December, 1969.

29. Higginbotham, A. B. and Hanson, R. D., "Axial Hysteretic Behavior of Steel Members," Journal of the Structural Division, ASCE, Vol. 102, No. ST7, July, 1976.

30. Nilforoushan, R. "Seismic Behavior of Multistory K-Braced Frame Structures," Ph.D. Thesis, The University of Michigan, Ann Arbor, Michigan, November, 1973.

31. Kahn, L. F. and Hanson, R. D., "Inelastic Cycles of Axially Loaded Steel Members," Journal of the Structural Division, ASCE, Vol. 102, No. ST5, Proc. Paper 12111, May, 1976.

32. Wakabayashi, M., "The Behavior of Steel Frames with Diagonal Bracing Under Repeated Loading," Proceedings of the U.S.-Japan Seminar on Earthquake Engineering, Sendai, Japan, 1970.

33. Wakabayashi, M., Nonaka, J., Koshiro, O., and Yamamoto, N., "An Experiment on the Behavior of a Steel Bar Under Repeated Axial Loading," Disaster Prevention Research Institute Annuals, Kyoto University, 14A, pp. 371-381, 1971, (in Japanese).

34. Nonaka, T., "An Elastic-Plastic Analysis of a Bar Under Repeated Loading," International Journal of Solid Structures, Vol. 9, 1973, pp. 569-580.

35. Igarashi, S., Inoue, K., Asano, M. and Ogawa, K., "Restoring Force Characteristics of Steel Diagonal Bracings," Proceedings, Fifth World Conference on Earthquake Engineering, Rome, Italy, 1973.

36. Shibata, M., Nakamura, T., Yoshida, N., Morino, S., Nonaka, T., and Wakabayashi, M., "Elasto-Plastic Behavior of Steel Braces Under Repeated Axial Loading ," Proceedings, Fifth World Conference on Earthquake Engineering, Rome, Italy, 1973.

37. Nonaka, T., "An Analysis for Large Deformation of an Elastic-Plastic Bar Under Repeated Axial Loading," Research Report, Disaster Prevention Research Institute, Kyoto University, Uji City, Kyoto Prefecture, Japan, 1974.

38. Morino, S., "An Experimental Study on the Hysteretic Behavior of Steel Braces Under Repeated Loading," IABSE Final Report on the Symposium on "Resistance and Ultimate Deformability of Structures Acted Upon by Well Defined Repeated Loads," Vol. 14, Lisboa, 1973, pp. 31-37.

39. Shibata, M., Lecturer, Osaka Institute of Technology, Private Communication, September, 1974.

40. Maugh, L. C., Statically Indeterminate Structures, John Wiley & Sons, Inc., New York, 1946, pp. 126-131.

41. Hoff, N. J., The Analysis of Structures, John Wiley & Sons, Inc., New York, 1956, pp. 103-112.

42. Bresler, B. and Lin, T. Y., Design of Steel Structures, John Wiley & Sons, Inc., New York, 1960, pp. 614-616.

43. Specification for the Design, Fabrication & Erection of Structural Steel for Buildings [with Supplements 1 (1970), 2 (1971), and 3 (1974)], American Institute of Steel Construction, New York, N. Y., 1969.

44. Massonnett, C. E. and Save, M. A., Plastic Analysis and Design, Volume One - Beams and Frames, Blaisdell Publishing Company, New York, 1965, pp. 128-135.

45. Timoshenko, S. P. and Gere, J. M., Theory of Elastic Stability, McGraw-Hill Book Company, New York, 1961, pp. 76-82.